

POLITECNICO DI TORINO

Master's degree in Mechatronic engineering

Master Thesis

**Kinematic and dynamic analysis of
a machine for additive
manufacturing**



Supervisor:
prof. Federico Colombo

Author:
Vito BORRELLI

July 2018

Summary

Table of contents

Summary	ii
1 General introduction	1
1.1 Additive manufacturing	1
2 Description of molten plastic deposit machines	6
2.1 Available machine for additive manufacturing	6
2.1.1 SLA	7
2.1.2 CLIP	8
2.1.3 DLP	8
2.1.4 MJM	9
2.1.5 BJ	9
2.1.6 SLS	10
2.1.7 LOM	11
2.2 Machine for fuse plastic deposit- FDM	11
3 Print specifications	17
3.1 Velocity and precision of the delta printer	17
3.2 Velocity limit for material deposit	21
4 Parallel machines	24
4.1 Classification of PKM	27
4.2 Two degree of freedom PKM	28
4.3 Three degree of freedom PKM	28
4.4 Four and five degree of freedom PKM	29
4.5 Six degree of freedom PKM	29
4.6 Other classification scheme	30
5 Delta Robot	32
5.1 Description	32
5.2 Geometry and assumptions	35

5.3	Degree of freedom	38
5.4	Workspace	39
6	Kinematic of the Delta robot	40
6.1	Direct Kinematic	40
6.2	Inverse Kinematic	46
6.3	Jacobian	47
6.4	Resolution variation along X Y plane	49
6.5	Workspace	54
7	Model	56
7.1	Numerical data used for simulation	57
7.2	Simmechanics model	59
7.2.1	Reference frame and translation	64
7.2.2	Path checking	73
7.3	Lagrangian model	74
7.3.1	Generalized coordinates	77
7.3.2	Kinetic Co-energy	78
7.3.3	Potential energy	78
7.3.4	Lagrangian	79
7.3.5	Generalized Forces	80
7.3.6	Constraint equations	81
7.3.7	Dynamic equations of the 3D printer	86
7.4	Comparison between Matlab and dynamic equations	87
7.4.1	straight line on X-Y plane	87
7.4.2	Circular path X-Y plane	89
7.4.3	Acceleration on Z axis	90
7.4.4	Lissajous curve on X-Y plane	92
7.4.5	Random curve on X-Y plane	93
7.4.6	Circular curve on the edge of workspace	95
7.4.7	Evaluation of the data obtained	96
8	Motor	97
8.1	Force and acceleration required	99
8.1.1	Friction consideration	103
8.1.2	Timing pulley	104
8.1.3	Stepper motors size	105
	Bibliography	108

Chapter 1

General introduction

1.1 Additive manufacturing

The additive manufacturing is

”a process of joining materials to make objects from 3D model data, usually layer upon layer, as opposed to subtractive manufacturing methodologies. Synonyms: additive fabrication, additive processes, additive techniques, additive layer manufacturing, layer manufacturing, and free-form fabrication ” [8.1]

as defined by the American standardization organization ASTM.

Additive manufacturing it’s a generic term used to represent all the technologies and techniques that permits to obtain a solid piece without the use of molds or presses that characterized the 19 century production systems.

Respect to a classical machining processing, that usually subtract material from a raw piece in order to obtain the final product (ex CNC’s), the AM builds a solid object from a series of layers, each one placed directly on top of the previous one. This result in several benefits as the minimization of the wasted products, lighter pieces and more complex form and shapes that lead, in some case, to geometries that cannot be created with SM methodologies.

The main fields in which the additive manufacturing has already took place are basically application not suited for large scale production that needs large customization or single prototypes.

Mainly the types of companies that have already adopted AM are divided into three fields:

- **Automotive field**

Used for functional prototyping, to manufacture custom tooling or complex



Figure 1.1: Complex lattice geometry piece

part produced in particular for low volume production as happened for luxury brands, custom jigs, fixtures and for design validation.

One of this industries is Volkswagen that "produces 93% of all externally manufactured tools in-house. The transition to 3D printing saved Volkswagen Autoeuropa 91% in tool development costs and reduced development time by 95%" ¹.

This led to a lower cost and production time thanks the possibility to produce in locus the self-engineered tool printed ad-hoc for custom vehicles. Other examples can be found in Bentley motors production plant that use additive manufacturing to fabricate custom interior, as bezels or the large diffusion of AM in car racing sports that, thanks to the use of lightweight alloy (ex. titanium) and hollow geometries permits to drastically reduce weight saving the mechanical resistance.

- **Medical application**

Thanks to the 3D data obtained with TAC or RM exam, additive manufacturing gives the possibility to reproduce the damaged organ or the trauma, making doctors more aware about the entity of the damage or the better strategy to use. Another benefit is the ability to generate internal mesh inside a prosthesis recreating a porous structure, allowing the bone to grow inside the implant. The prosthesis implant can also be adapted to each patient in order to have a less invasive surgery. Today the main use of this technology are in the orthodontics field and in acoustic aids production for which "AM accounts for 99% of those that are placed in the ear" ²

¹<https://ultimaker.com/en/stories/43969-volkswagen-autoeuropa-maximizing-production-efficiency-with-3d-printed-tools-jigs-and-fixtures>

²T. S. Douglas, Additive manufacturing: From implants to organs, South African Med. J., vol.

- **Aerospace industry**

That use the AM in order to decrease the weigh maintaining an high coefficient of security. One of the first industry in this field to adopt AM is Boeing Inc. that has manufactured with this technique more than 200 different parts for 10 aircraft platforms ³ or General Electric, one of the major supply of jet engine, which was capable of manufacture 25% and 5 times more durable fuel injector substituting the existing model made of more than 20 welded parts ⁴.

The AM is a relatively young field: the first 3d printer has been invented in 1988 while the first AM machine came out in '81, but only recently, from 2010, the trend has been ramping up ⁵ thanks to the drop in both material and machine cost, a more mature technology and the end of Fused Deposition Modeling (FDM) printing process patent that expired in 2009 ⁶.

The figure 1.2 has been taken from " Get Ready for Industrialized Additive Manufacturing " ⁷ and confirm the trend antecedently predicted by the "Manufacturing Engineering Media SME"⁸ publication that gives an idea of the grow in revenues for products and services produced using AM technique .

104, no. 6, p. 408, 2014.

³Boeing.com , Boeing Launches New Manufacturing Venture, September 3, 2002.

⁴Davidson, 3-D Printing Could Remake U.S. Manufacturing, June 10, 2013, 3.

⁵Google Ngram at books.google.com/ngrams/graph?content=additive+manufacturing&case_insensitive=on&year.

⁶<https://techcrunch.com/2016/05/15/how-expiring-patents-are-ushering-in-the-next-generation-of-3d-printing/>

⁷Daniel Kpper , Wilderich Heising , Gero Corman , Meldon Wolfgang , Claudio Knizek , and Vladimir Lukic

⁸<http://www.sme.org/MEMagazine/Article.aspx?id=80916>

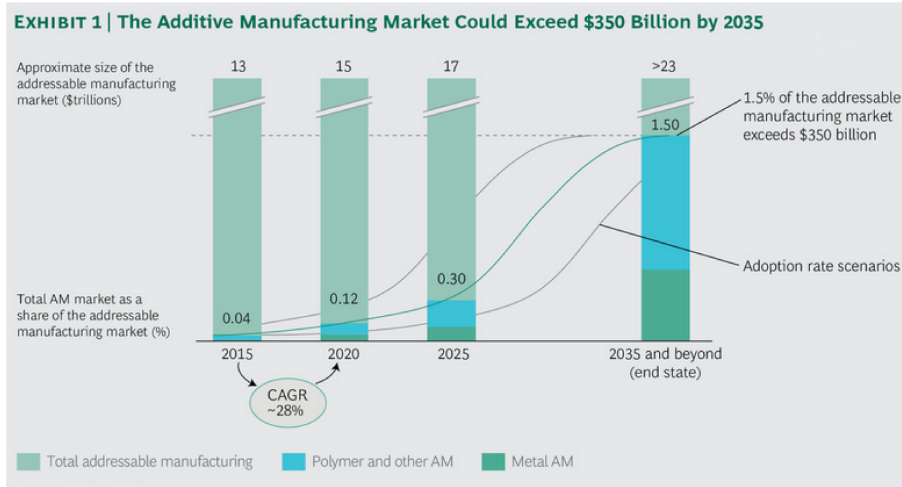


Figure 1.2: Industrial grow over year for services and parts produced using additive manufacturing technique in million of dollars

This trend is increasing year after year, with a compound annual growth rate of the 28%.

Many authors thinks that "AM must be viewed as a transformative technology. It will transform the way many items are manufactured. It will transform traditional business models. It will transform established supply chains. Lastly, it will transform the economics of where, how and when things are made"⁹.

This revolution is clearly visible in makers contest, where 3D printers transforms simple sketch on CAD software to functional prototypes in just few hours without the need of leave our houses.

While additive manufacturing progressed a lot from the begin of the century, many problem remains to be addressed as: the poor part accuracy, the high cost per kilogram of raw material and it's availability, inadequate repeatability of the machines and the mechanical strength of the final product that suffers of high residual stress due to shrinkage in materials. Most important, the lack of qualification and certification methodologies for the processes, makes the engineering of the final product an experimental analysis. A lot of work and researches are guided by the scope of

⁹Pearce, Joshua M.; Morris Blair, Christine; Laciak, Kristen J.; Andrews, Rob; Nosrat, Amir; Zelenika-Zovko, Ivana (2010). "3-D Printing of Open Source Appropriate Technologies for Self-Directed Sustainable Development". Journal of Sustainable Development

increase the throughput^{10 11 12} of this machine and generate fine features down to 50 μm ^{13 14}.

This kind of immaturity is visible in the "Technology readiness levels" (TRL) widely accepted as a way of measuring the maturity of applications or technologies. Divided in 9 levels in which levels 1 mean basic principles observed and level 9 represent the actual system proven in operational environment (competitive manufacturing in the case of key enabling technologies - or in space) the current state of additive manufacturing process for plastic is placed between levels 4 and 5¹⁵.

¹⁰Rate limits of additive manufacturing by fused filament fabrication and guidelines for high-throughput system design Go, Jamison ; Schiffres, Scott N. ; Stevens, Adam G. ; Hart, A. John Additive Manufacturing, August 2017, Vol.16, pp.1-11

¹¹Distortion prediction and compensation in selective laser melting Author links open overlay panelShukriAfazovWillem A.D.DenmarkBorjaLazaro TorallesAdamHollowayAnasYaghi

¹²A multiscale modeling approach for fast prediction of part distortion in selective laser melting Author links open overlay panelC.LiaC.H.FuaY.B.GuoF.Z.Fangb

¹³<https://www-sciencedirect-com.ezproxy.biblio.polito.it/science/article/pii/S0141635917301484>

¹⁴Precision and Energy Usage for Additive Manufacturing, Clemon, LeeSudradjat, AntonJaquez, MaribelKrishna, AdityaRammah, MarwanDornfeld, David

¹⁵<http://www.rm-platform.com/linkdoc/AM%20SRA%20-%20February%202014.pdf>

Chapter 2

Description of molten plastic deposit machines

2.1 Available machine for additive manufacturing

In additive manufacturing everything starts from the CAD design. When the geometry of the file is complete, usually the file is exported in a AMF (additive manufacturing file) compatible extension (usually STL - STereo Lithography interface format that consist in the solid which surface is discretize into triangular). The file is processed by a particular program called "slicer" : the object intended to be printed is cut into 2D planes and converted into g-code set of operation also used by computer numerical control machines.

The different technologies of machines are available in the 3D printing world have been divided by the ASTM F42 committee in 7 different categories ¹:

- Photopolymerization
 - Stereolithography (SLA)
 - Continuous Liquid Interface Production (CLIP)
 - Digital Light Processing (DLP)
- Material jetting
 - multijet modeling (MJM)
- Binder jetting
 - Binder Jetting (BJ)
 - 3D printing (3DP)

¹ASTM, 2009, ASTM International Committee F42 on Additive Manufacturing Technologies, ASTM F279210 Standard Terminology for Additive Manufacturing Technologies, ASTM, West Conshohocken, PA

- Material extrusion
 - Fused deposition Modeling (FDM)
- Powder bed fusion
 - Selective Laser Sintering (SLS)
 - Selective Laser Melting (SLM)
 - Electronic Beam Melting (EBM)
- Sheet lamination
 - Laminated Object Manufacturing (LOM)
- Directed energy deposition
 - Laser metal deposition (LMD)

I will only talk about solutions that allow you to have a finished plastic product and then will enter in detail of FDM process.

2.1.1 SLA

It was one of the first additive manufacturing technologies to be theorized and patented. It's working principle is quite simple: the printing bed is placed on the surface of a liquid sensible to near-UV rays. Layer upon layer, the laser, that can be placed above or under the surface of the liquid, lights up the 2D slice of the object. When the layer is complete, the object is raised just of the layer height (so the object is still in contact with the resin) and the process continue till the end of the piece. It's a good practise to use a post-cure chamber so the printing process finalizes the polymerization process and stabilizes the mechanical properties.

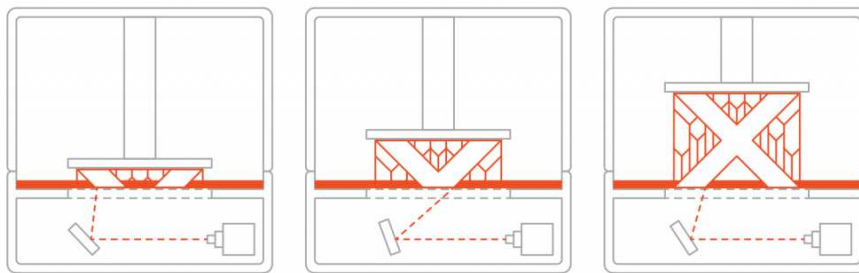


Figure 2.1: SLA schematic working principle ²

²Gentle concession of 3dp.com

Resolution : 25 to 100 microns
Small printing area
SLA is significantly slower than FDM.

2.1.2 CLIP

This type of printer works by projecting a continuous sequence of UV images (usually generated by a digital light projector) through an oxygen-permeable window, that let UV radiation to pass creates a "dead-zone" in order to prevent the resin to chemical attach the window. Unlike SLA, this printing method is continuous and so the final pieces has a better surface finish.

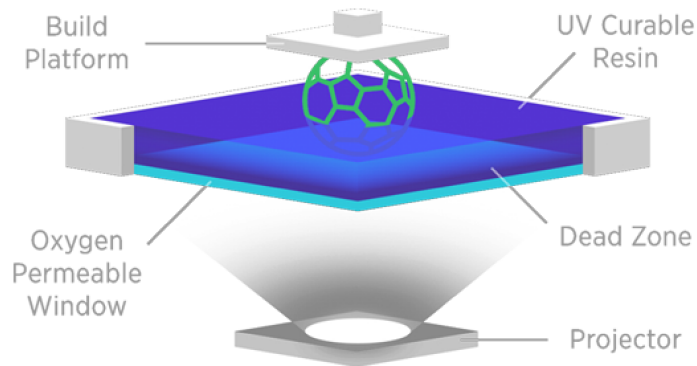


Figure 2.2: Clip schematics

CLIP is "100 times faster" than other printing method ^{3 4}
Resolution of 75 μm
Small printing areas compared to FDM ⁵

2.1.3 DLP

The working principle is similar to SLA but the key difference is that DLP uses a digital light projector to flash the single layer at once.
The surface finish is affected by the use of digital screen to project the image of the lajer thus is possible to see on the final product the presence of square pixels called voxels.

³St. Fleur, Nicholas (17 March 2015). "3-D Printing Just Got 100 Times Faster". The Atlantic.

⁴Saxena, Shalini (19 March 2015). "New nonstop 3D printing process takes only minutes instead of hours". Ars Technica

⁵M2 printer by Carbon has 189mm x 118mm x326mm of building area

Faster than SLA

Same resolution and printing area of SLA

2.1.4 MJM

The print-head of the 3d printer deposit a liquid layer of resin on a support plate. The print head has many very small holes and jet droplets of build and support material simultaneously to create the part one layer at a time. After the deposit, an UV lamp carried by the same print-head solidifies the material and proceed to the upon layer. As FDM, this methods suffer of back draft, so void part are usually filled with support material (wax) that in some case, as closed geometries, is impossible to remove.

It's major application field is lost-wax microfusion or models for silicone molds.

Industrial grade print, tolerances from IT7 to IT11 ⁶

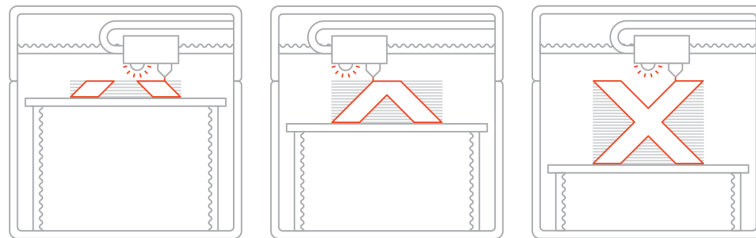


Figure 2.3: mjm

Large printing volume (1000x400x100 mm)

Resolution of 16 microns

2.1.5 BJ

At the begin of each layer, the print-head first spread a layer of sand along the plate and selectively deposit a liquid binding agent into powder particles. Before moving on to the next layer the solvent contained into the powder is evaporated by an incandescent lamp. The powder layer is lowered and a new one is deposited. Parts are supported by the loose powder in the job box, thus eliminating the need for a

⁶”Tolerance Analysis of 3d-MJM parts according to IT grade”, K Kitsakis et al 2016 IOP Conf. Ser.: Mater. Sci. Eng. 161 012024

build plate. At the end of the print, the binder is cured by placing the container in a furnace in case of sand, through a sintering process in case of ceramic and metals, infiltration or high isostatic pressing before being used.

Printer is able to produce metallic, plastic, ceramic and parts made of sand mainly used for mold casting.



Figure 2.4: Binder Jetting

Industrial grade printer

Big print areas

Resolution of 35 micrometers

2.1.6 SLS

A nylon powder is spread in layer and selective sintered the powder with a CO₂ laser. The bed moves down of the height of a layer and the process repeats until the job is complete. The whole bin has to cool before the parts can be removed from the powder.

Usually the laser spot size of SLS system is approximately 0.3 - 0.4 mm in diameter and this affect the minimum dimension for details printable.

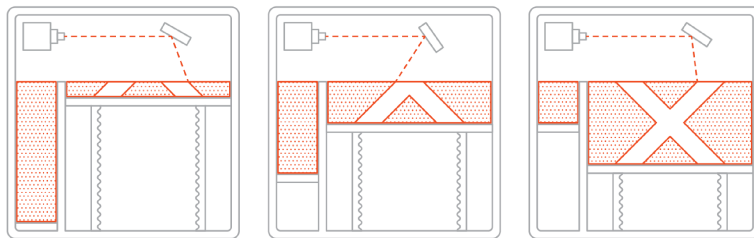


Figure 2.5: sls

No support is needed
Resolution of 100 microns
Small printing volumes (300 x 300 x 300 mm)

2.1.7 LOM

In LOM, adhesive-coated paper, plastic, or metal sheets are unroll from a coil and made adhered to a substrate thanks to the use of an heated roller. A laser carve out the unnecessary part of the sheet and hatches non-part area to facilitate the removal. The parts move down and a new part of the sheet is placed in position and the process continues.

2.2 Machine for fuse plastic deposit- FDM

Fused deposit modeling is an additive manufacturing process that belong to the material extrusion family. Works by extruding a thermoplastic polymer through a heated nozzle and depositing it on a plate, that in many case is also heated to better stick and held the part in place during the process.

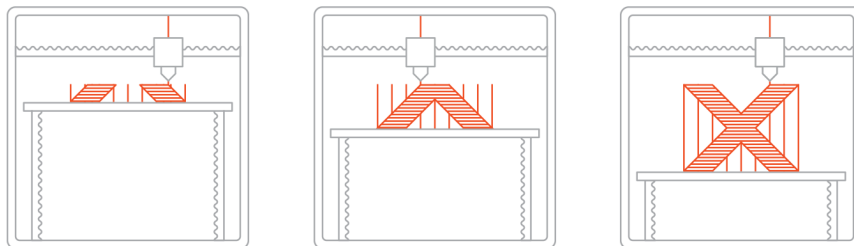


Figure 2.6: fdm

FDM is the most widely used 3D printing technology with a large diffusion in hobbyist for its very low price in both machine and materials thus this process is mainly used for low-cost prototyping and design verification with very fast turn around times.

In FDM machines, the material is stored in spools of filament, with a standardized diameter for filament of 1.75 and 3 mm. At the begin of the print, the material is loaded into the printer after that the nozzle has reached the melting temperature of the filament, parameter that depends by the type of material to be printed.

When the machine receive the code elaborated by the slicer, that represent the first 2D layer of the part that is going to print, first execute an homing procedure to move the carriage in a known position.

This is needed because in low and mid-end systems, the axis are driven by open-loop chain without the use of absolute or relative encoders. At every power-up or in every case that the machine "shut down" the motors to save power, as in idling, homing is needed before printing.

The use of stepper motor, guarantee that in nominal operation the carriages moves of the exacted amount driven by the control circuit. In some case this lead to layer shifting problem: due to excessive acceleration, the motor is not capable to follow the imposed profile and lose steps. The control circuit is not able to detect this position error, so the print continues with the successive layers shifted.

The material is extruded in thin strands with a dimension that is function of the nozzle diameter and is deposited layer-by-layer in predetermined locations, where it cools down and solidifies. Sometimes the cooling of the deposited material is accelerated through the use of cooling fans attached on the extrusion head. This is to prevent that the piece soften and deform under the weight of upon layers.

The layer is usually started from the perimeter, than internal characteristic (as the profile of through holes) are drawn and at last the infill. The progress is repeated until the piece is complete.

Benefits and Limitations		Characteristics	
		Price	\$\$\$\$ Tolerance ± 0.5% (min: ± 0.5 mm)
 Fast turnaround times	 Print layers are likely to be visible	Turnaround time	< 2 days Wall thickness 0.8 mm
		Layer height	50 - 400 µm

Figure 2.7: tab ⁷

Typical build size varies from 200 x 200 x 200 mm in desktop 3D printers to 1000 x 1000 x 1000 mm for industrial ones.

FDM is the most cost-effective technology

⁷<https://www.3dhubs.com/3d-printing/fdm>

Lowest dimensional accuracy between FDM process and visible layer lines.

FDM machines are usually composed by:

- Extruder
The filaments is inserted in a calibrated path and pulled down by the motor. The filament arrives in a hot zone where is melted with a controlled temperature. This temperature is constantly checked with a thermistor or thermocouple cartridge. This zone is usually called hot end: here the filament is fused and pushed through a nozzle with a precise diameter ⁸.

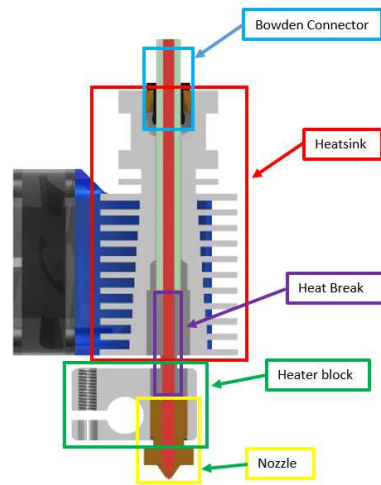


Figure 2.8: extruder

Some extruder comprehend a zone to cool down the fused filament in case of high retraction setting (used to avoid oozing).

- Drive gear and filament pulling motor
The filament must be pulled down the extruder with a velocity that depends from the layer height and print velocity. MK8 like extruder have a L leverage that press the filament between the drive gear and an idle gear. The pression that have to be generated between the drive gear and the filament is set thanks to the use of a spring loaded with a screw.

⁸standard diameters are: 0.2mm - 0.25mm - 0.3mm - 0.4mm - 0.5mm - 0.6mm - 0.8 mm - 1.0mm

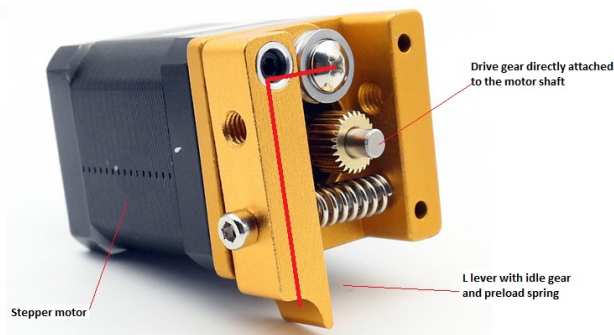


Figure 2.9

Usually two types of configuration exist: direct extruder and bowden.

In direct, the motor and the gears are placed on top of the extruder. This is simplest system to configure because printing parameters are not dependent from installation factors. The torque that the motor that drive extruder axis has to develop and the structure of the printer are bigger with respect to a bowden configuration because the mass that have to be accelerated, so inertia forces, are bigger (450g for MK8 vs 75g for V6 E3D). In bowden, the drive gear are placed somewhere on the structure and the filament is pushed down a PTFE tube down to the extruder. With a bowden configuration, the extruder can be moved faster, reaching the maximum velocity which the material can be printed. Some printer setting, as retraction, varies with installation factors as length of the tube, the curve radii that the tube follows..

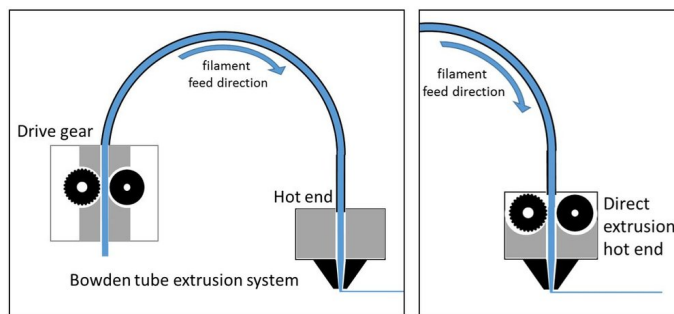


Figure 2.10

- 3 motors to control x,y,z directions
Usually stepper motors, NEMA 17 for small printers while NEMA 23 for industrial ones.

- Control board and motor driver board That implements simple PID controllers and management of few peripheral as small LCD monitor or SD card drive.
- Power supply
- Endstop for homing procedure
Axes need a datum to reference their movements. Before the print, each axis needs to back up until the datum point is reached. The switches also is used to protect the machine, checking if the movement exceed the intended range before damaging itself. Can be electromechanical (a simple switch NO that trigger an interrupt), optical (check the light-level step change) or magnetic (using hall effect sensors).
- Lead screw or belt to transfer the motion from the motors to the carriages.
Usually on cartesian printers Z axis motor is followed by a coupling and a lead screw with trapezoidal profile, while the other motor have standard pulleys and belts (GT format). In delta machine, motors and carriage are all connected with belts.
- Print bed, usually heated for better cohesion of the piece.

Right now for Desktop application there are only two common typologies of printers: Cartesian and Delta printers.

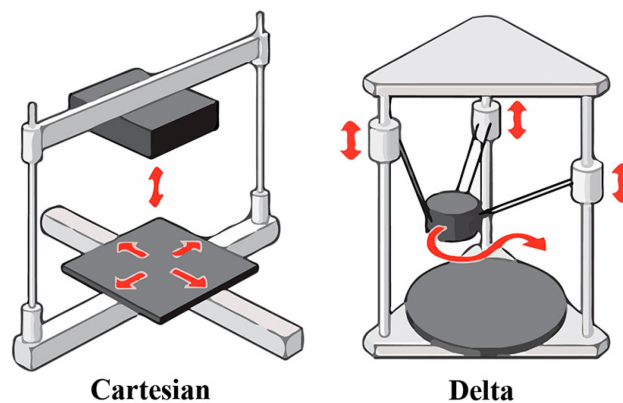


Figure 2.11

The most popular type of 3D printer is the cartesian one, with 80 %⁹ of market share. The working principle is straightforward: every axis is moved by a single motor in xyz position. This lead to a very simple control scheme a no needs for

⁹<http://builda3dprinter.eu/information/why-a-delta/>

inverse kinematics. Various configuration are available: extruder or printing plate can have all three degree of freedom or can be distributed between the two. In term of accuracy for high speed printers is better to have all DOF placed on the extruder because the plate moving with high acceleration can led in flexion on big pieces so lost of precision. In term of cost is better to x placed on plate and yz on extruder. Great disadvantages of this machine are weight and no instant change of direction but it is the cheaper printer available on the market and excels in width prints. Cartesian printer tend to have a better surface finish than Delta because Cartesian printers have more rigid axes, which allow less room for error when the print head moves within the 3D space.

Delta printers also use the Cartesian coordinate system but the extruder is suspended by three arms connected to cylindrical or prismatic linear guide in a triangular configuration (from which came the name DELTA). In this machine the bed is unmovable, usually with circular shape and it is capable of print very tall object with respect to a cartesian one. An important disadvantage is that the accuracy of this machine varies, being more precise in centre than on outer limits. It's very light and designed for speed, so perform a quicker printing process. This printer can only mount bowden extruder configuration that limits the number of filaments that can be used .

There is another emerging configuration: the polar printer that uses, as suggested by the name, polar coordinate system. This printer is available with spinning bed, plus a print head that can move up, down, left and right or two spinning eccentric plates and extruder that moves up and down. The two advantage of this type of printer is that requires a minimum of 2 motors to work and greater build volume within a smaller space thanks to the lacking of space requirement for XYZ framework. This printer represent less that 1 % of market share so will not be analysed.

Chapter 3

Print specifications

3.1 Velocity and precision of the delta printer

For the final aspect of the produced pieces, three characteristics are very important and discriminate the selection of the printer: accuracy, resolution and tolerances. From a total different point of view, namely productivity, takt time and position in the market, is the velocity at which pieces can be produced the key point.

- Accuracy:

It measure the grade of deviation in dimensions between the ideal piece, drawn on CAD software, and the real component.

While some producers specify the accuracy separately in the three directions, some unifies this value with the worst one, as happens for FLUX machine reported in the table.

An important point is that the manufacturers of 3D printers can only promise that the accuracy of the pieces will be equal to the machine one. This because some other factors place an important role during the process as:

- Gravity: usually there is a deviation on the Z axis dimension because gravity pulls down the material, creating a bigger error on the piece with respect to the accuracy of the machine.
- For the quality of the build of printer itself: cheap printers with plastic part suffer of high deviation in the structure with respect to metal machined one.
- Calibration parameters: after some hours of work, machine needs to be re-calibrated. Automatic routines exist but they're not as good as manual procedure.

- Resolution: Is the smallest movement that the machine is able to produce. The smaller the value, the higher will be the details that the printer is able to

produce.

While the resolution for X and Y axis can be generically low, the vertical resolution on the Z axis is limited by the minimum thickness of the layer. This value is chosen during the slicing process and the smaller layer height, the better will be the smoothness of the piece to the detriment of the printing time.

The range in which this parameter can be chosen is imposed by the extruder nozzle. A rule of thumb is that the layer height must be between a maximum of 75 % and minimum of 25 % on the total diameter of the nozzle. During the construction phase, a special attention has to be done in order to have that the layer height must be reached without truncation approximation¹because those errors tend to sum up and screw the print.

Other parameters, like ambient temperature, material shrinkage, direction in which the object is printed change drastically the final result.

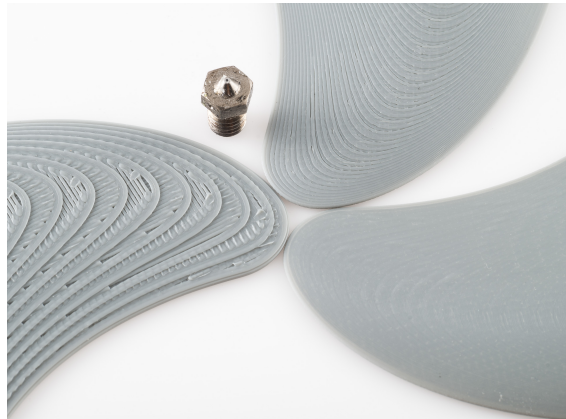


Figure 3.1: Resolution and accuracy change with different layers height

The printers that have been taking into account are the most sold ² for very low range of prices, while for mid and high-end price range have been selected the ones whit the higher specifications found. From the official data-sheet, functional details have been found while for completeness have been reported also the current price of the printers ³, converted in Euro⁴ from the official vendors.

From all the available printers, those that not showed all the necessary product specification have been removed: it was disconcerting discovering that a lot of

¹Given by stepper motor angle,driver micro-stepping capabilities, lead screw or belt pitch,..

²according to Amazon.com

³last check on 30/05/2018

⁴1 Euro = 0.858 Dollars and the total value has been approximated to the nearest integer.

printers manufacturers don't specify important parameters of their machines. Sometimes the characteristics showed in the preface of the data-sheets are referred to the conditions in which the machine does not print. Printing condition usually varies a lot from non-printing ones so they are placed in showcase to boost up the printer on the market.

From this analysis is visible that basically the cost of a Delta printer is proportional to its velocity.

Low cost printers have maximum printing speed declared of $150 \frac{mm}{s}$ while high end one reaches incredible velocities of $500 \frac{mm}{s}$.

Some manufacturers also specifies maximum accelerations and jerks of their products, as WASP machines that can reach up to $15000 \frac{mm}{s^2}$. Low-end printers, usually are flashed with open-source firmwares, configured ad-hoc for the specific machine. One the most popular firmware, MARLIN ⁵, have standard acceleration and jerk parameter set to

```
#define DEFAULT_MAX_ACCELERATION {3000,3000,100,10000}  
#define DEFAULT_ACCELERATION      3000  
#define DEFAULT_XYJERK            20.0  
#define DEFAULT_ZJERK             0.4
```

To explain the just first line of code present in the firmware, the default max acceleration is the limit parameter for the machine acceleration and usually are set to $3000 \frac{mm}{s^2}$ for movements XY plane, $100 \frac{mm}{s^2}$ for Z while $10000 \frac{mm}{s^2}$ for extruder feeder motor. The default acceleration can be overwrite by slicer parameters. Those values can be representative of the low-end class of 3D printers.

Usually big printers have lower accuracy than smaller machine due to geometrical characteristics, as already explained the chapter 2.

The resolution of the printer itself is proportion to the minimal layer-height and usually this parameter varies between 0.05 mm and 0.4 mm, that are the layers height printable with 0.4 mm nozzle, the most common one.

The accuracy however varies a lot with the different manufacturers: from 0.0125 mm to 0.05 mm on planes parallel to the bed, from now on called X-Y, and from 0.0025 mm to 0.05 mm for the Z axis.

As already said, the delta printer is capable to produce very tall objects: while in cartesian machine the printing area has a big bed size and small height, in delta happens the opposite. From this analysis is possible to notice that the printing volume do not influence too much the final cost of the printer.

⁵<http://marlinfw.org/>

Machine name	Manufacturer	Resolution	Accuracy	Printing area [ϕ xh]	Max velocity	Cost [euro]
K280	He3D	0,05 mm to 0,4 mm	0,05 mm	280 mm x 600 mm	150 mm/s	kit
Delta Rockstock	Anycubic	0,1 mm to 0,4 mm	XY 0,0125 mm - Z 0,0025 mm	230 mm x 300 mm	-	kit
Delta Kossel	FLSUN	-	0,012 mm - 0,04 mm	180 mm x 300 mm	20-150 mm/s	210
Mini Delta	Monoprice	0,05 mm	-	110 mm x 120 mm	150 mm/sec	155
Magician Delta	BIQU	0,1 mm	0,01 mm	100 mm x 150 mm	100 mm/s*	197
D1315	CoLiDo	-	0,05	130 mm x 150mm	-	231
Rostock 301	Geetech	0,1mm - 0,05mm*	-	170 mm x 230 mm	80-120mm/s	275
Delta+	FLUX	0,05 mm to 0,3mm	XY 0,02mm	170 mm x 210 mm	200mm/s* - 120	858
K200	He3D	0,05 mm to 0,4 mm	0,0125mm - 0,004mm	200mm x 300 mm	100 - 150 mm/s	189
A4	Anet	-	0,012mm xy - 0,004	200 mm x 210 mm	10-120mm/s	258
QQ	Flsun	0,05 mm to 4 mm	0,01mm - 0,0025 mm	260 mm x 370 mm	100 - 200* - 300 mm/s**	508
ALPHA	HATCHBOX	0,05 mm to 4 mm	XYZ 0,05mm	300 mm x 330 mm	150 mm/s - 300*mm/s	928
The Little Monster	TEVO	0,05 mm to 0,8 mm	0,012 mm - 0,004 mm	340 mm x 500 mm	150 mm/s-300 mm/s*	687
4070	WASP	0,05 mm	XY 0,05 mm - Z 0,01 mm	400 mm x 700 mm	300 mm/s - 400* mm 10,000 mm/s2;	5800
Rostock mini G2s	Geetech	0,05 mm	-	170 mm x 200 mm	60 to 120 mm/sec	258
Rostock MAX v3	SeeMeCNC	0,05 mm to 0,2 mm	-	275 mm 400 mm	100 mm/s-300*	1630
Delta	Spiderbot	0,15 mm to 0,45mm	XY 0,01 mm - Z 0,0056 mm	405 mm x 800 mm	250 mm/sec*-120	-
2040 Turbo2	Wasp	0,05mm	XY 0,05 mm - Z 0,01 mm	200 mm x 400 mm	500 mm/s- 15,000 mm/s2	3080
Mini Delta	MP	0,05 mm	-	110 mm x 120 mm	150 mm/sec	-
Delta	Radik	0,15 mm	-	180 mm x 140 mm	-	2200
Delta	Ares	0,05 mm	0,02mm	160 mm x 160 mm	-	858
Atom 2,5 FX	3dp	0,05 mm	0,02 mm	220 mm x 345 mm	-	2230
Overlord	DreamMaker	0,1 mm	-	170 mm x 260 mm	100 mm/s*	1099
Mirror	BlueFrog	0,05 mm	XYZ 0,01mm	180mm x 255 mm	250 mm/sec	1600
Kossel	Folger Tech	0,05 mm	0,05 mm	210 mm x 310 mm	100 m/s	296
330 PRO	Cybot	0,05 mm	-	330 mm x 330 mm	400 mm/s	-

Table 3.1: Specification comparison between different delta printers available on the market

* Refers to movements when not printing

** Specification's difference between seller and re-seller

3.2 Velocity limit for material deposit

3D printers are not usually able to print all the material available on the market: for example the low-end market only allows to print PLA. This because for other type of filaments, become mandatory to have an heated bed, closed printer with an heater to uniform the internal temperature and an extruder capable to print that material.

Some type of plastics are not well suited to be used at home, as the popular ABS, because they release toxic fumes known as VOCs (Volatile Organic Carbon)⁶. For this type of materials a fume extraction system is needed when 3D printers are placed in closed areas next to people, as offices or apartments.

Maximum velocities limits to deposit different type of filaments are showed in the table below.

Table 3.2: Maximum printing speed for different materials.

Material	Maximum printing velocity
PLA - ABS	10-90 $\frac{mm}{s}$ ⁷
Carbon fiber PLA	10-70 $\frac{mm}{s}$ ⁸
Carbon fiber Nylon (NylonX)	10-80 $\frac{mm}{s}$ ⁹
Nylon	30-60 $\frac{mm}{s}$ ¹⁰
ASA	50-90 $\frac{mm}{s}$ ¹¹
PET	30-80 $\frac{mm}{s}$ ¹²
PVA	<25 $\frac{mm}{s}$ ¹³
HDPE	70-90 $\frac{mm}{s}$ ¹⁴
PETG	40-150 $\frac{mm}{s}$ ¹⁵
HIPS	40-70 $\frac{mm}{s}$ ¹⁶
Flexible PGVA	<25 $\frac{mm}{s}$ ¹⁷
Wood fiber	50-80 $\frac{mm}{s}$ ¹⁸
PolyMax PLA	40-120 $\frac{mm}{s}$ ¹⁹
PolyFlex	30-60 $\frac{mm}{s}$ ²⁰
PP	60-80 $\frac{mm}{s}$ ²¹
TPE	40-50 $\frac{mm}{s}$ ²²
TPU	20-60 $\frac{mm}{s}$ ²³
PC	30-60 $\frac{mm}{s}$ ²⁴

⁶”Emissions of Ultra fine Particles and Volatile Organic Compounds from Commercially Available Desktop Three-Dimensional Printers with Multiple Filaments”, Parham Azimi, Dan Zhao, Claire Pouzet, Neil E. Crain and Brent Stephens

Those data refers the maximum printing speed with the hot-end temperature set at the nominal one at which the filament should be melt according to the producer. The recommended temperature and the maximum printing speed for the filament however varies from seller to seller, so multiple researches have be done in order to find the ones with best product characteristic. Going up with the temperature, the materials tend to burn or carbonize changing drastically their chemical-mechanical proprieties.

The material with the maximum printing speed is PETG with $150 \frac{mm}{s}$. This value is much lower with respect to the velocities that can be reach by a delta printer. Speed constrain are not only related with materials but also with hot ends that starts to have problems keeping up with speeds above $120 \frac{mm}{s}$ with anything but low layer height of 15 microns.

Can be showed that layer heigh is dependent from the printing speed and can be expressed in terms of speed and nozzle flow ²⁵.

The resultant layer height is incompatible also with the minimum nozzle diameter available on the market²⁶.

$$LayerHeight = \frac{Flow}{LineWidth \cdot Speed} = \frac{15 \frac{mm^3}{s}}{0.5mm \cdot 500 \frac{mm}{s}} = 0.025mm$$

⁴www.3dhubs.com

⁵<https://hackaday.com/2016/09/07/3d-printing-xt-cf20-carbon-fiber-filament-review/>

⁶<https://www.matterhackers.com/news/a-closer-look-at-nylon-x>

⁷<https://www.matterhackers.com/articles/printing-with-nylon>

⁸www.slant3d.com/uploads/3/8/.../asa-3d-filament-data-sheet.pdf

⁹<https://www.3ditalyshop.it/prodotto/filamenti/2-85/carbon-pet-2-85/carbon-pet-2-85-mm/>

¹⁰<https://www.hestay.nl/en/3d-print-support/3d-printer.../pva/>

¹¹CIRCO HDPE filament datasheet

¹²<https://www.matterhackers.com/news/how-to-succeed-when-printing-with-petg-filament>

¹³<https://filaments.ca/pages/temperature-guide>

¹⁴<https://www.matterhackers.com/news/how-to-succeed-when-printing-with-flexible-filament>

¹⁵<https://www.hestay.nl/en/3d-print-support/3d-printer-setup-per-material/wood-fiber>

¹⁶<https://filaments.ca/pages/temperature-guide#pc>

¹⁷<https://filaments.ca/pages/temperature-guide#pc>

¹⁸<https://www.filoprint.it/polipropilene-p-lene-o-175-mm/435-polipropilene-p-lene-o-175-mm>

¹⁹www.vepram.com/prodotto/ultraflex-tpe-e/

²⁰https://www.reddit.com/r/3Dprinting/comments/5909rl/tpu_settings

²¹<https://www.filoalfa3d.com/it/filo-175mm/179-policarbonato-neutro-250gr-o-175-mm-8050327034136>

²⁵The optimal line width for 0.4 mm extruder is between 110 % and 150% of the nozzle diameter, so approximately 0.44mm and 0.60mm. The speed is the maximum speed of the wasp printer while the flow is the nominal one for DYZ extruder

²⁶<http://doc.3dmodularsystems.com/what-is-the-best-layer-height-for-your-printer/>

Typical problems related to cranking up with speeds are over-swings and ripples. Those errors are usually amplified by the cantilever setup. This tend to create artifacts on the printed parts such as the infill poking through the perimetral layer. In order to approach high speeds, the set temperature of the hot end has to be very close to the one at which the material perish (250°C for PLA). The flow at this velocities heat-up the filament with an average temperature that is the recommended one.

A great advantage correlated with the increase of temperature in the hot-end is the decrease of the pressure required to push-down the filament, thus lower torque provided by the motor that feeds the extruder.

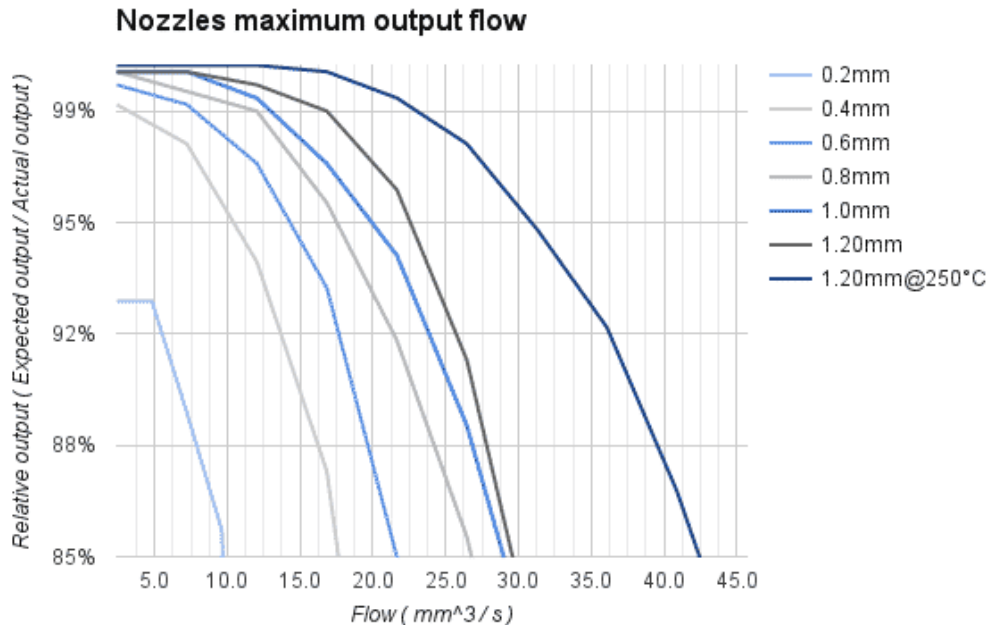


Figure 3.2: Nozzle output flow of PLA at 210° and 250°. The 95% output is 10 $\frac{mm^3}{s}$ for DyzeEnd-X hotend.

Various test from different industries showed that with this technique they are able increase the flow by about 50% reaching an output flow of 15 $\frac{mm^3}{s}$ for 0.4 mm extruder nozzle and 31 $\frac{mm^3}{s}$ for 1.2 mm diameter at 250°C ²⁷. This value is quite impressing compared to the 11 $\frac{mm^3}{s}$ flow reachable for the MK7 feeder.

However even with this kind of adjustments, the extruder manufacturer tells that there is the possibility to work with velocity of about 300 $\frac{mm^3}{s}$ and not the 500 $\frac{mm^3}{s}$ of the WASP delta.

²⁷dyzedesign.com/2016/10/printing-300-mm-s-part-1-basics-hardware/

Chapter 4

Parallel machines

A parallel robot is a closed-loop kinematic chain mechanism which rigid body, called end-effector, is linked to the base by several kinematic chains. This means that every link (with exclusion of the base) has a connection degree bigger or equal to three. Currently the large part of robots available on the market are serial: they are composed by a succession of rigid bodies, each one linked to the following with joint of one degree of freedom.

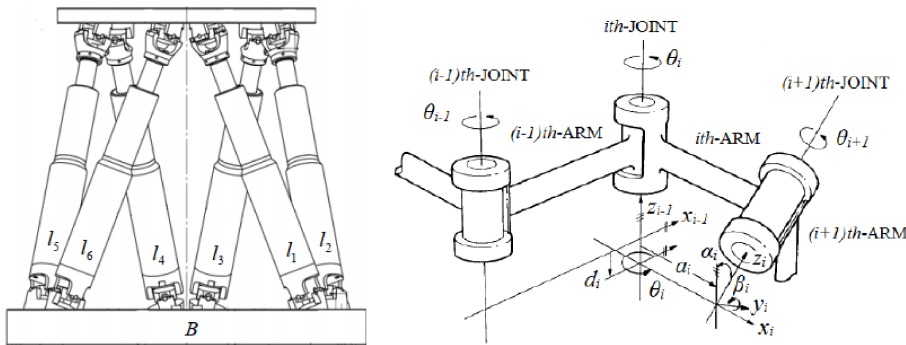


Figure 4.1: Example of parallel robot on the left and a serial robot on the right

With respect to serial robots, parallel can show:

- Higher structural rigidity

The stiffness-to-mass ratio is far bigger than serial robots: their specific kinematic structure allows to place the actuators very close to the manipulator base. Besides, the links act in parallel against the external forces or torques, suppressing the cantilever type of loading and increasing the manipulator stiffness¹.

¹"Stiffness Analysis of over-constrained Parallel Manipulators" by Anatol Pashkevich, Damien Chablat, Philippe Wenger

-
- Higher service life
 - Higher motion precision
Parallel robots have better accuracy and repeatability. For serial machines, each joint have to support the masses and inertia forces of all the joints that comes after in addition to the load. This lead in a large flexural torque that, to be reduced, makes the robot very heavy.
Accuracy is dependent from the internal stresses of the robot because lead to deformations that are not easily measurable by the internal sensors installed. Errors on early links lead to large errors in the final pose of the end-effector.
 - Big improvement in the load/mass ratio
Scara robot have generally the higher load/mass coefficient of the serial robots family, with 0.25. This mean that those type of machines are usually 4 time heavier than the load that they have to carry.
In parallel robots the load can be shared by the actuators: load/mass property is generally higher thanks to lightweight rigid bodies and the high mechanical stiffness.

PKM (Parallel kinematic machines) find a place where accuracy in positioning is crucial and the workspace dimension is less so. These types of robots can execute tasks with very high speeds (like pick-and-place operations) which need a machine with a very light moving part.

Another key-point is related to the compliance of the machine itself: when the end-effector is subjected to forces or torques, elastic deformations in the links or the backlash inside the driving gears will create errors that are difficult to correct or compensate (due to the open-loop structure). In parallel robots, deformations are more easily measurable and in some case, like assembly building jobs, the lack of elasticity of the machine can be modified voluntarily to be stiff along some directions and soft along others².

With those characteristics it's clear why PKM are employed in 3D printing, flight simulators, stress-bench for pneumatics, astronomy or material sorting in assembly lines.

²"Parallel Robots" J.P. Merlet, p.8-12, Second Edition

<i>Feature</i>	<i>Serial robot</i>	<i>Parallel robot</i>
<i>Workspace</i>	<i>Large</i>	<i>Small and complex</i>
<i>Solving forward kinematics</i>	<i>Easy</i>	<i>Very difficult</i>
<i>Solving inverse kinematics</i>	<i>Difficult</i>	<i>Easy</i>
<i>Position error</i>	<i>Accumulates</i>	<i>Averages</i>
<i>Force error</i>	<i>Averages</i>	<i>Accumulates</i>
<i>Maximum force</i>	<i>Limited by minimum actuator force</i>	<i>Summation of all actuator forces</i>
<i>Stiffness</i>	<i>Low</i>	<i>High</i>
<i>Dynamics characteristics</i>	<i>Poor, especially with increasing the size</i>	<i>Very high</i>
<i>Modelling and solving dynamics</i>	<i>Relatively simple</i>	<i>Very complex</i>
<i>Inertia</i>	<i>Large</i>	<i>Small</i>
<i>Areas of application</i>	<i>A great number in different areas, especially in industry</i>	<i>Currently limited, especially in industry</i>
<i>Payload/weight ratio</i>	<i>Low</i>	<i>High</i>
<i>Speed and acceleration</i>	<i>Low</i>	<i>High</i>
<i>Accuracy</i>	<i>Low</i>	<i>High</i>
<i>Uniformity of components</i>	<i>Low</i>	<i>High</i>
<i>Calibration</i>	<i>Relatively simple</i>	<i>Complicated</i>
<i>Workspace/robot size ratio</i>	<i>High</i>	<i>Low</i>

Figure 4.2: Comparison table between parallel and serial machines

4.1 Classification of PKM

There is not an uniform notation in literature to describe the mechanical architecture of a parallel robot.

In order to find the perfect robot for a certain job, the first element to be analyzed is the number of DOF (Degree of freedom) required to accomplish that task.

A PKM has at least two linkage to support the end-effector and the number of actuators matches the parallel manipulator. Hence the minimum number of degree of freedom for a parallel robot is 2 while the maximum in a three dimensional environment is 6.

Note that the choice of a PKM with DOM (Degree of motion) bigger than the required DOF, condition called redundancy, can give the possibility to overcome to obstacle but may lead to parasitic motion that will lead to poor performance or accuracy.

After the identification of the DOM, the right topology for a given job is a complex choice and only recently was possible to synthesize and develop the theory behind the selection of right architecture. Furthermore, while the possible architectures for serial robot are very limited, for PKM there are a very large number of possible choices of the close-loop mechanisms. The topology will greatly affect the overall performance of the robot, so it have to be chosen wisely.

The three main strategies to evaluate the machines architectures are: graph theory, the group theory and the screw theory approach.

In the page that follows will proposed a classification scheme based on the most common architecture for i -th degree of freedom.

An important remark is about the type of joints that characterize PKM and the notation behind the schematisation of those robots. While for serial robots only one degree of freedom kinematic pair are used, as prismatic (denoted with the letter P) and revolute joints (R), in parallel machine are also common spherical joints (S) that hold three rotational degrees of freedom at a single pivot point. Different combination of these joints create the universal joint (U) composed by two revolute joint that therefore allows rotation on two axis (2 DOF). Another item that have to be itemize is the parallelogram (P_a) that are the bars that maintain the output link at fixed orientation with respect to the input link.

To outline join types and connection of the various legs from the base to the end-effector is commonly used a graphical layout.

4.2 Two degree of freedom PKM

Planar manipulators use only revolute and prismatic joints. These configurations are well taken in analysis by McCloy³. In his research were exploited more than 20 different combinations of planar robots that were grouped in six different families with the assumption of a fixed base.

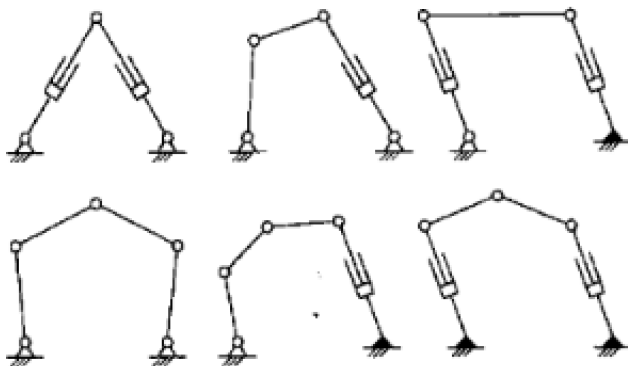


Figure 4.3: The six different families of 2 DOF parallel manipulator

4.3 Three degree of freedom PKM

They represent the 40% of the market. The most common are the one with all the 3 degree of freedom in translation, used mainly for pick and place operations as the delta robot, developed by Clavel at EPFL.

The delta developed by Clavel is composed by 3 revolute joint in RRP_aR configuration. This structure can be modified substituting the revolute joints with linear actuators⁴: this model is usually called linear delta or linapod and will be discussed into this thesis work.

Another famous robot that belong to this category is the orthoglide that present homogeneous kinematic performance in all the workspace⁵. The configuration of the PRP_aR joints moreover permits to eliminate any constraint singularity.

³“Some comparisons of serial-driven and parallel-driven manipulators”, D. McCloy, Cambridge University Press 1990

⁴Zobel P.B., Di Stefano P., and Raparelli T. The design of a 3 dof parallel robot with pneumatic drives. In 27th ISIR, pages 707710, Milan, October, 6-8, 1996.

⁵ashkevich, A., Chablat, D., & Wenger, P. (2006). Kinematics and workspace analysis of a three-axis parallel manipulator: The Orthoglide. *Robotica*, 24(1), 39-49.

Tricept, patented by Neumann⁶ is powered by prismatic joints, using a RRPS configuration. This robot has passive constrain for the end-effector.

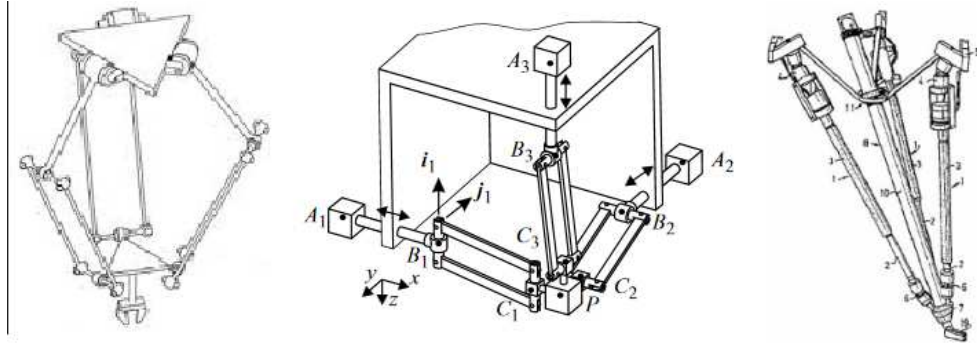


Figure 4.4: From left to right: Clavel delta robot, orthoglide and tricept robot.

4.4 Four and five degree of freedom PKM

This two categories have been mixed together cause those designs will be composed with at least one passive constrain and have the disadvantage that is not possible to design 4 and 5 DOF parallel robot with identical legs.

One of the oldest 4 DOF robot is the koevermans, used for flight simulators: this robot is capable of performing RPY rotation and Z traslation.

The use of passive mast in those machines creates both advantage and disadvantage: on one side it increase the total stiffness of the robot that became comparable to a 6 DOF one, on the other side decrease the total workspace area.

Some complex mechanical design can be made in order use one of the active leg as a constrains for the platform.

4.5 Six defree of freedom PKM

Are the most common and have the widest treatment in the literature. The first realization of this type of parallel manipulator can be attributed to McCallion. Today there are so many different structure of this category of robot that is impossible to adequately discuss or summarize in few lines all the work done.

Six degree of freedom PKM can be found with all type of chains (RUS, PUS and UPS). These parallel manipulators have the highest stiffness due to the high number of arm, a low inertia for the moving parts, and the larger payload capacity thanks

⁶Hosseini, M., & Mohammadi Daniali, H.-R. (2012). Kinematic Analysis Of Tricept Parallel Manipulator. IIUM Engineering Journal, 12(5).

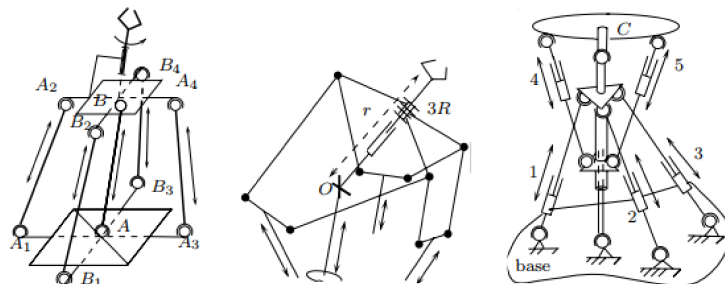


Figure 4.5: Example of 5 DOF robot design: at right Zamanov, at center Zoppi and at right Austad design.

the possibility to share the payload on six actuators.

Unfortunately they suffer of very small workspace and complex kinematics.

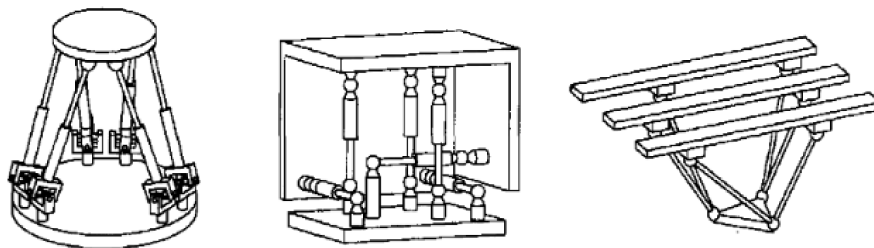


Figure 4.6: Stewart platform on the left, 3-2-1 arrangement in the middle and slide manipulator on the right.

4.6 Other classification scheme

Some other classification scheme ⁷ divide those machine for their motion capacities

- Mechanism for translation
 - Speed-R-Man, Orthogloide robot
- Mechanism for rotation
 - Agile Eye
- Mechanism for translation and rotation
 - Quadro, Gough-stewart, Delta, 3RRR, T3R1 robot

⁷Erol zgr. From lines to dynamics of parallel robots. Other. Universit Blaise Pascal - ClermontFerrand II, 2012.

or the type of joints that compose the structure

- Prismatic joint between the two bodies of each cinematic leg
-Gough-Stewart robot
- Prismatic joint between the base and each cinematic leg
-Orthoglide robot
- Lack of prismatic joints
-Quadro robot

Usually classifications are done by comparing one or more characteristics critical to the job that have to be carried out, as isotropy, manipulability, dexterity, workspace and singularity of the machine, or criteria based on the dynamic behaviour as dexterity or natural frequency.

Depending on the application of these manipulators, more criteria can be found on the broad literature available ⁸.

In AM machines that work with plastic deposition, only 3 DOF are required. Those and are essentially the three traslation along x y z axis because the orientation of the extruder with respect to the plane is fixed and constant.

Not always the extruder is placed perpendicular to the bed and exist printer with tilted bed ⁹ or tilted extruder.

Using more degree of freedom is quite useless because slicers plans motion without the needs to overcome to obstacle and the rotation of the extruder is not needed. Anyway configuration with more DOF exist ¹⁰ but they are used only for research purposes.

⁸MIRSHEKARI, Erfan; GHANBARZADEH, Afshin and SHIRAZIA, Kourosh Heidari. Structure Comparison and Optimal Design of 6-RUS Parallel Manipulator Based on Kinematic and Dynamic Performances. *Lat. Am. j. solids struct.* [online]. 2016, vol.13, n.13

⁹<https://hackaday.com/2017/01/19/3d-printer-with-tilted-bed/>

¹⁰Ismayuzri Ishak, Joseph Fisher, Pierre Larochelle. Robot Arm Platform for Additive Manufacturing: Multi-Plane Printing, Robotics & Spatial Systems Laboratory at Florida Institute of Technology, Melbourne, Florida.

Chapter 5

Delta Robot

5.1 Description

Starting from the DELTA robot invented by Clavel where the active joint are revolute joint directly attached to the motors, the linear delta is powered by linear actuators. The main advantage of this modification is the robustness against external forces. The first machines to implement this kinematics were the Rostock¹ and the Kossel² and still today most of the machine sold are modifications of those prototypes. The actuators moves linear guides (from which the name linear delta) that transfer the motion to the moving platform by mean of six links. The arms connect the actuators to the base platform with universal joints that allow higher repeatability. Accordingly, the robot architecture is the 3-PUU.

¹<https://reprap.org/wiki/Rostock>

²<https://reprap.org/wiki/Kossel>

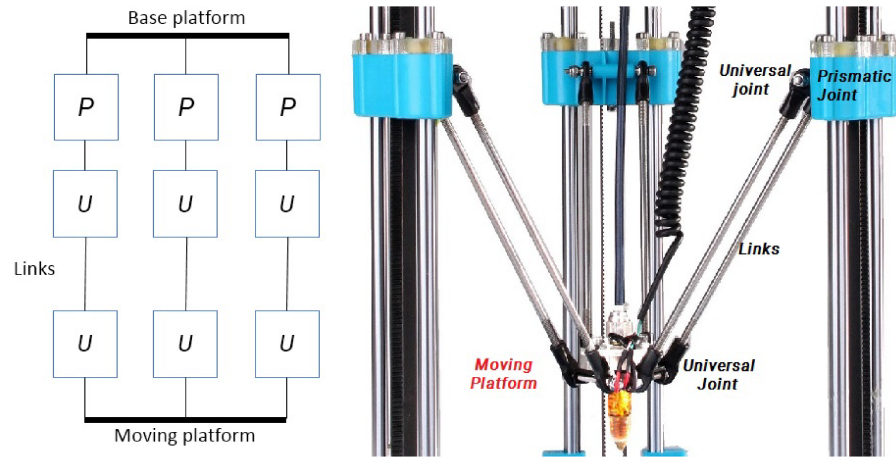


Figure 5.1: Architectural scheme of a delta linear 3D printer

Each carriage has two parallel arms with the same length and the line passing through the two universal joint (that lie on the same carriage) is perfectly parallel to the printing bed. Thus the connection points on each carriage and the effector platform are at same distance for each leg. This condition forces the moving platform to be parallel to the bed.

To obtain a prismatic joints usually two cylindrical rod and linear bearings are used, with a single carriage intercepting them.



Figure 5.2

Two other implementation are also common: the linear slider with ball recirculation carriage (MGN12H like) or a dolly bonded in standard aluminium slot profiles. The best option is the linear slide that provide the maximum stiffness and flexural rigidity with minimum backlash.

For this type of printer, to transform the motion from rotary to linear, belts are used while lead screws are not employed due to the low rotation speed of a stepper motor that combined with screws led to excessively slow movement of the carriages.

The actuators are in general the heaviest parts of a manipulator, and in this printer are fixed at the base, so their weight do not influence the dynamic behaviour.

5.2 Geometry and assumptions

There are few assumption that will be used to develop dynamic models and reachable workspace.

- Columns form an equilateral triangle
The three prismatic joint are along what will be defined the z axis and are disposed equally spaced at 120° among the x-y plane. They have the same distance that will be called S. When not specified, the origin of the coordinate system will be placed with origin on the prismatic rail of interest.
- All three pairs of arms are the same length
- End-effector is placed exactly at the center of the moving platform.

For the models the system will be simplified choosing the line that pass from the pivot point of the carriage through the end effector. The line that connect the carriage from its offset to the mean of the connection point of the moving platform, with a distance equally to the end-effector offset, is called in litterature "line of action".

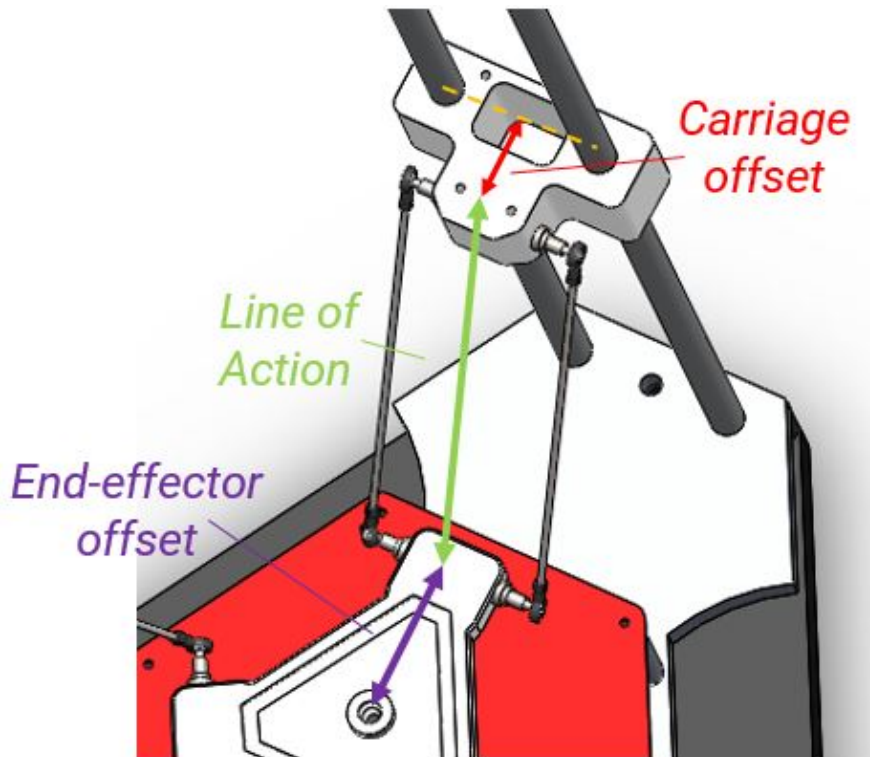


Figure 5.3

There are some implicit limitation in delta printer. One of them is the maximum arm angle reachable. While the this angle reduces the coefficient that combine the velocity of the carriage to the velocity of the moving increases rapidly.

Low angle decrease effector stability. Usually, in common printer the minimum angle is considered to be 20° and induces a speed coefficient of 2.75 times. Some printers with theoretical minimum angle of 15° may experience lost steps at their maximum diameter.

A value of the effector horizontal speed higher than 2.5 times the carriage speed was highlighted in orange in the graph below. For this value a minum angle of 21.8° was found. The maximum value is usually constrained by cables, fans or tubes. Some printer are able to reach this geometric configuration as the delta rockstock max ³.

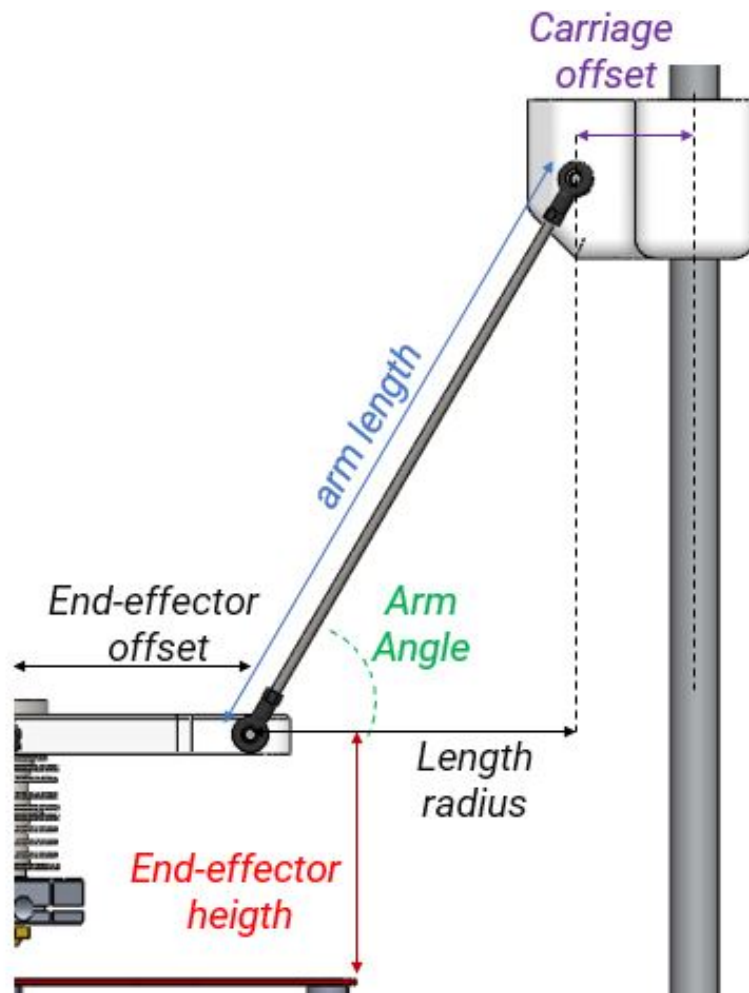


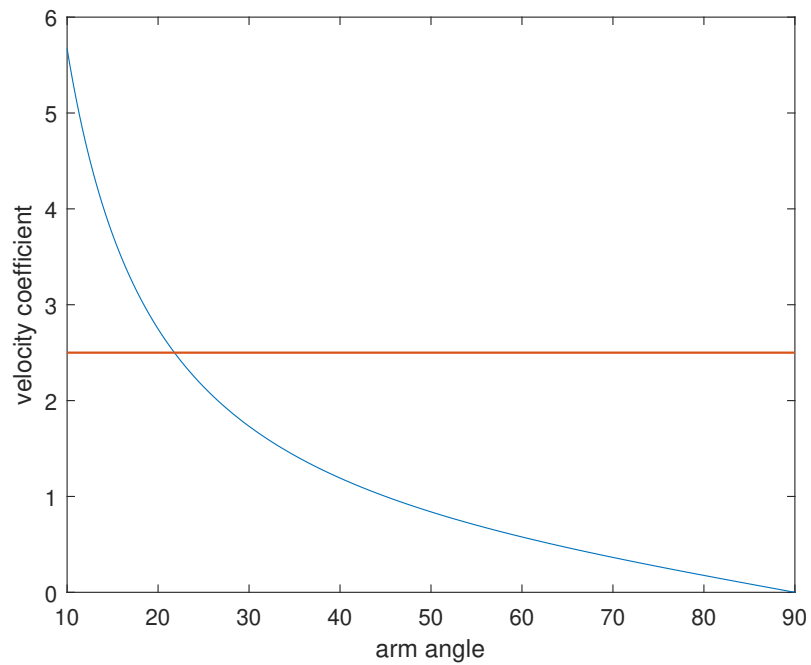
Figure 5.4

³https://reprap.org/wiki/Rostock_MAX

```
inital_angle=10;
final_angle=90;

arm_angle=deg2rad(inital_angle):0.0001:deg2rad(final_angle);

for i=1:1:length(arm_angle)
speed(i) = cos( arm_angle(i) )/sqrt(1-( cos(arm_angle(i)) )^2);
end
arm_angle_deg=linspace(inital_angle,final_angle,length(arm_angle));
plot(arm_angle_deg,speed)
xlabel('arm angle');
ylabel('velocity coefficient');
hold on;
plot(arm_angle_deg,2.5*ones(size(arm_angle)), 'LineWidth', 1);
```



5.3 Degree of freedom

Are the number of independent parameters that define completely the configuration of the robot.

A generally criteria is very difficult to be defined as Hunt ⁴ denoted in his work. In literature it's common to use Chebychev - Grübler - Kutzbach criterion to determines the degree of freedom of a linkage, but in some cases, as over-constrained mechanisms, some degree of freedom can be neglected.

This is what happens in the non simplified version of the delta robot.

$$M = p \cdot n - \sum_{i=1}^j (6 - f_i) = p \cdot (N - 1 - j) + \sum_{i=1}^j (f_i)$$

where

M is the degree-of-freedom of this system

p is the screw system order and is three for planar and spherical movement while is 6 for spatial movements.

n is the number of moving bodies

N is the number of moving bodies including the fixed frame

i, j are respectively the first and the last joint

f_i are the degree of freedom associated with the i-th joint.

Considering

- 4 spherical joints (3DOF) for each leg $J_3 = 12$
- 2 cylindrical joints for each carriage (2DOF) $J_2 = 6$
- 2 links per leg, 2 vertical rail per carriage, the ground and the moving platform
 $N = 18$

$$M = 6 \cdot (17 - 1) - 5 \cdot 0 - 4 \cdot 6 - 3 \cdot 12 = 36$$

This result is clearly incorrect.

Simplifying the structure, substituting the two parallel rail on which the carriage moves with a single rail and a prismatic joint, and the two links with a single one with universal joints(2dof),the Kutzbach criterion return the right DOF of the end-effector.

$$M = 6 \cdot (8 - 1) - 5 \cdot 3 - 4 \cdot 6 - 3 \cdot 0 = 3$$

⁴Duffy J (1991) Kinematic geometry of mechanisms (k. h. hunt). SIAM Rev 33(4):678679

5.4 Workspace

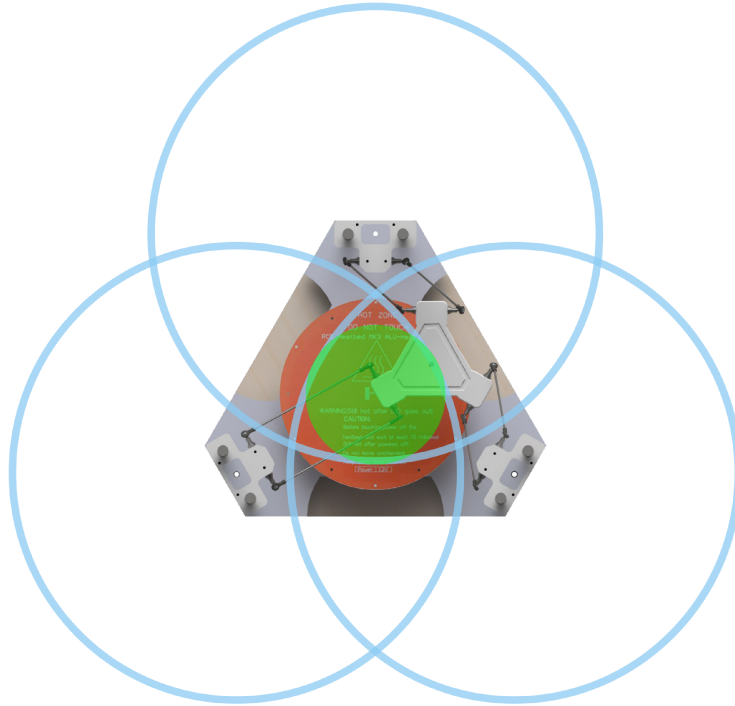


Figure 5.5: Workspace geometrical analysis, in blue area virtually reachable by a single chain, in green area reachable.

The end effector movement can space in a circumference centred where the line of action intersect the carriage. The radius of this circle, drawn in light blue in figure 5.5 is not the arm length L but is limited by the minimum arm angle.

$$R = L \cdot \cos(Arm_{Angle_{min}}) = L \cdot \cos(0.11 \cdot \pi)$$

This area is also limited by the presence of the two linear rod that sustain the carriage, and the maximum range of motion for the ball joints, that can be restricted to $\pm 20^\circ$.

The available workspace is given by the interception of the three circumference. Not all of this area is utilized, because it's limited by the slicer settings that consider only the inscribed circumference, highlighted in green in the image 5.5.

Chapter 6

Kinematic of the Delta robot

6.1 Direct Kinematic

The forward problem, so the transformation from joint space to task space coordinate systems can be solved in different ways as

- Writing the closure formulas for the linear delta printer and imposing that the lengths of the links are constant

$$\begin{cases} \{B_i^B\} + \{q_i^B\} + \{l_i^B\} = \{P_p^P\} + [R_R^B] \cdot \{P_i^B\} = \{P_i^P\} + \{P_p^B\} \\ l_i = \|\{l_i^B\}\| = \|\{P_p^B\} + \{P_i^P\} - \{B_i^B\} - \{q_i^B\}\| \end{cases}$$

Where

- B exponent refers to the base reference system, represented in black
- P exponent refers to the moving platform reference system, represented in yellow
- l is the link length, misused between the pivot point of the two universal joints, in pink
- L is the prismatic joint variable
- i is the index of the i-th chain so i=1,2,3

The P_p^B is pose vector.

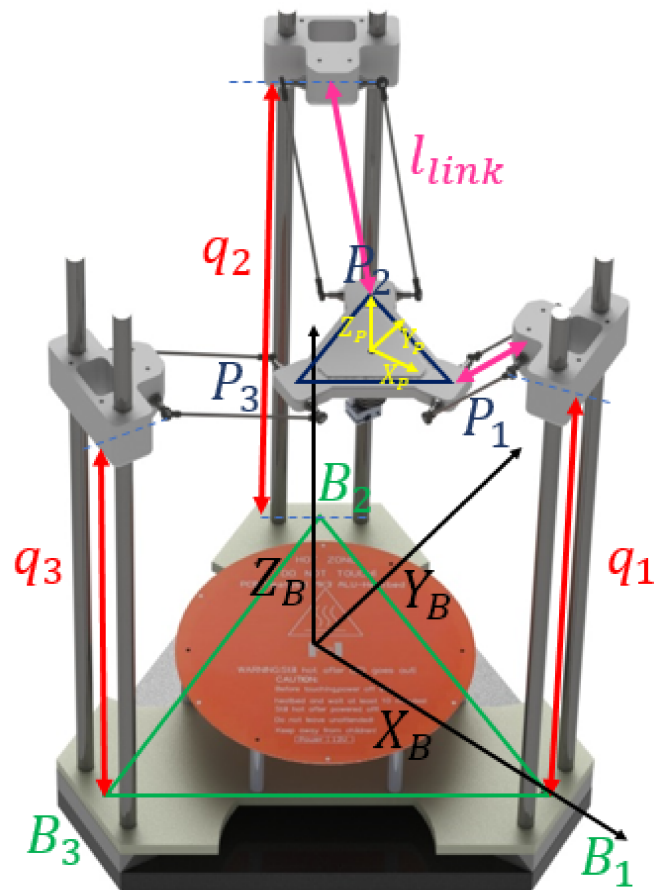


Figure 6.1: Schematic of the printer with reference system name convention

B_1, B_2, B_3 are located in between each tower columns, starting from the one pointed by the X_B, X axis of the base reference frame.

P_1, P_2, P_3 in the same way are located in the between of the two pivot point of the spherical joints that lay on the same carriage.

- Using the three sphere intersection algorithm.

Can be noticed that the system can be simplified into the intersection of three spheres: each one lies on the relative carriage, and where the spheres intersect, there is the center of the moving platform.

Will be assumed that the three sphere are $C_1 = \{c_1, r_1\}$, $C_2 = \{c_2, r_2\}$, $C_3 = \{c_3, r_3\}$, with the spheres radii constant ed equal for all of them $r_1 = r_2 = r_3$.

The centers of the spheres are located at $c_1 = \{x_1, y_1, z_1\}$, $c_2 = \{x_2, y_2, z_2\}$ and $c_3 = \{x_3, y_3, z_3\}$.

The system of spheres equations is coupled non-linear with the three unknowns x , y , and z , that are the coordinate of the intersection point $P = \{x, y, z\}$. This point is located in the center of the moving platform, so an offset on the z coordinate has to be applied to consider the presence of the extruder $z_{extruder}$.

$$\begin{cases} (x - x_1)^2 + (y - y_1)^2 + (z - z_1)^2 = r_1^2 \\ (x - x_2)^2 + (y - y_2)^2 + (z - z_2)^2 = r_2^2 \\ (x - x_3)^2 + (y - y_3)^2 + (z - z_3)^2 = r_3^2 \end{cases}$$

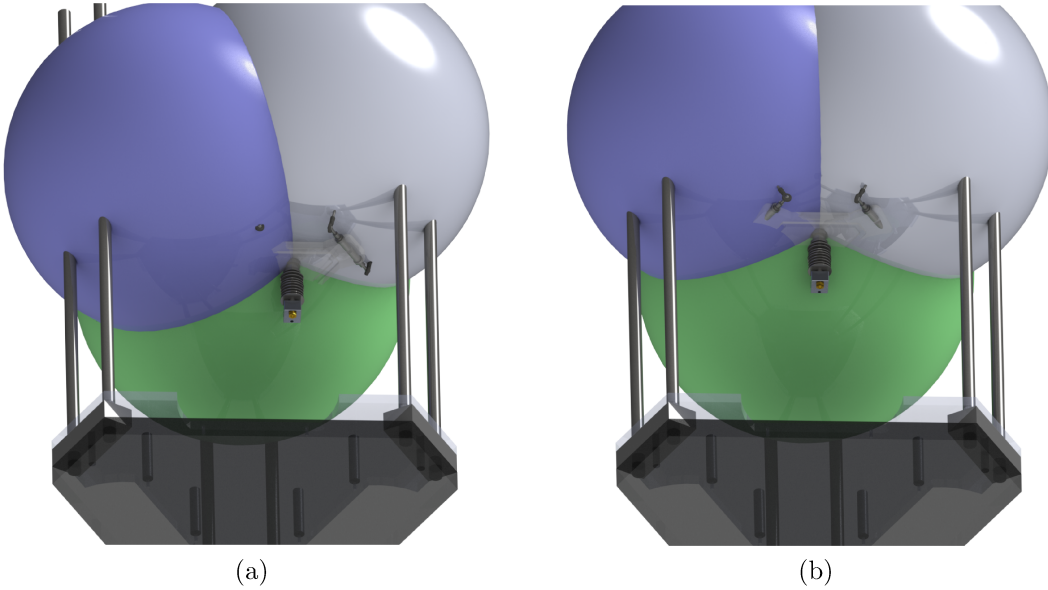


Figure 6.2: Two different visual example of the intersection algorithm

The centers of the spheres, however, are placed on the line of action, with an offset from the center of the rail that is the sum of the distances between this point and the pivot point of the spherical joint on the carriage and the distance between the center of the moving platform and the the pivot point of the spherical joint that lies on the moving platform.

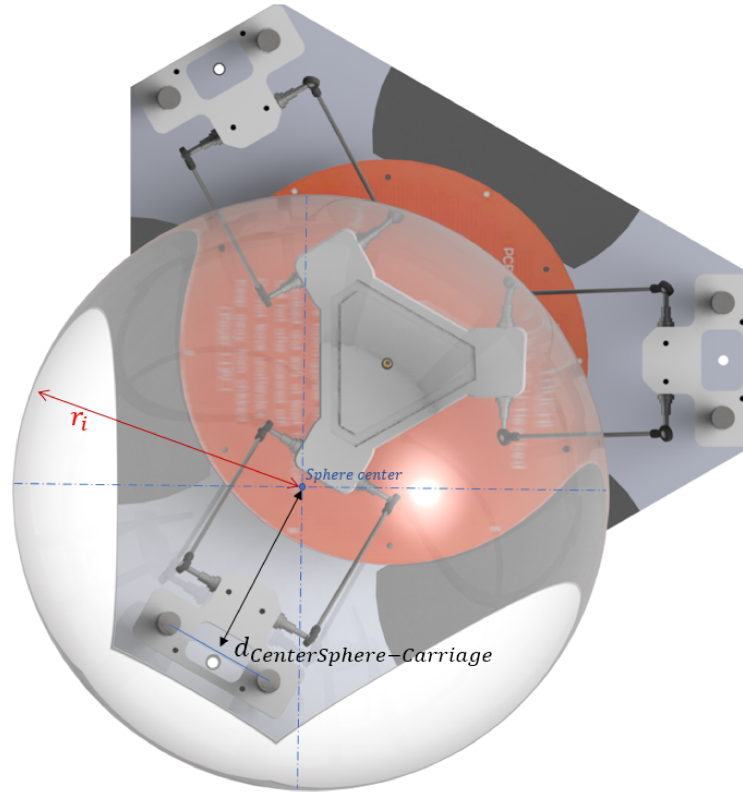


Figure 6.3: Sphere center location on one of the carriages

The name convention refers to the figure 5.4 .

$$d_{CenterSphere-Carriage} = d_{End-effectorOffset} + d_{CarriageOffset} = 95.72mm$$

The inertial reference system is placed in the center of the bed, at the same level of it.

The spheres centers are placed on a circumference with a radii of

$$r = 155.95mm$$

from the inertial reference system.

Because the three pair of rods are placed at exactly 120° , the center location can be written as

$$\begin{aligned} c_1 &= \{0, -R, L1\} = \{0, -79.80, L_1\} \\ c_2 &= \{-R \cdot \frac{\sqrt{3}}{2}, \frac{R}{2}, L2\} = \{-69.11, 39, 39.90, L_2\} \end{aligned}$$

$$c_3 = \left\{ R \cdot \frac{\sqrt{3}}{2}, \frac{R}{2}, L_3 \right\} = \{69.11, 39.90, L_3\}$$

L_1, L_2, L_3 are the joints variables that are equal to 133mm when the extruder is centred and touching the heating bed and when are zero, it means that are at the same level of the bed. As before, the extruder offset have to be considered and summed on all the three joints variables.

The system of equation can be resolved simply squaring all the terms and expanding the equations. The third and second equations are subtracted from the first

$$2(x_3 - x_1) \cdot x + 2(y_3 - y_1) \cdot y + 2(z_3 - z_1) \cdot z = r_1^2 - r_3^2 - x_1^2 - y_1^2 - z_1^2 + x_3^2 + y_3^2 + z_3^2$$

$$2(x_3 - x_2) \cdot x + 2(y_3 - y_2) \cdot y + 2(z_3 - z_2) \cdot z = r_2^2 - r_3^2 - x_2^2 - y_2^2 - z_2^2 + x_3^2 + y_3^2 + z_3^2$$

we can solve the two equation for the z variable

$$z = \frac{r_1^2 - r_3^2 - x_1^2 - y_1^2 - z_1^2 + x_3^2 + y_3^2 + z_3^2}{2(z_3 - z_1)} - \frac{(x_3 - x_1)}{(z_3 - z_1)} - \frac{(y_3 - y_1)}{(z_3 - z_1)}$$

$$z = \frac{r_2^2 - r_3^2 - x_2^2 - y_2^2 - z_2^2 + x_3^2 + y_3^2 + z_3^2}{2(z_3 - z_2)} - \frac{(x_3 - x_2)}{(z_3 - z_2)} - \frac{(y_3 - y_2)}{(z_3 - z_2)}$$

The subtraction between the last set of equation give the possibility to eliminate z and leave x as function of y.

$$z = f(y) = \frac{-\left(\frac{(x_3 - x_2)}{(z_3 - z_2)} - \frac{x_3 - x_2}{z_3 - z_2} - \frac{y_3 - y_2}{z_3 - z_2}\right)}{\frac{(x_3 - x_1)}{(z_3 - z_1)} - \frac{x_3 - x_1}{z_3 - z_1} - \frac{y_3 - y_2}{z_3 - z_2}} - \frac{r_2^2 - r_3^2 - x_2^2 - y_2^2 - z_2^2 + x_3^2 + y_3^2 + z_3^2}{z_3 - z_2} + \frac{r_1^2 - r_3^2 - x_1^2 - y_1^2 - z_1^2 + x_3^2 + y_3^2 + z_3^2}{z_3 - z_1} \cdot \frac{1}{\frac{(x_3 - x_1)}{z_3 - z_1} - \frac{x_3 - x_2}{z_3 - z_2}}$$

Also x can be re-written to became only a function of y, $x = f(y)$, and the same apply for $z = f(y)$; substituting them into the main equations it is possible to obtain quadratics in which only one of the x,y and z variable is present.

Those equations can be simplified substituting the z_1, z_2, z_3 variables with joint variable L_1, L_2, L_3 and exploiting the spheres centers location $x_{1,2,3}, y_{1,2,3}, z_{1,2,3}$ using the relation with R. For the sake of brevity only y solutions will be showed.

$$\begin{aligned}
 y^+ = \sqrt{3} &(- (108R^6 - 108R^4r^2 + 72R^4L_1^2 - 72R^4L_1L_2 - 72R^4L_1L_3 + 72R^4L_2^2 - \\
 &72R^4L_2L_3 + 72R^4L_3^2 - 48R^2r^2L_1^2 + 48R^2r^2L_1L_2 + 48R^2r^2L_1L_3 - 48R^2r^2L_2^2 + \\
 &48R^2r^2L_2L_3 - 48R^2r^2L_3^2 + 12R^2L_1^4 - 24R^2L_1^3L_2 - 24R^2L_1^3L_3 + 36R^2L_1^2L_2^2 + \\
 &36R^2L_1^2L_3^2 - 24R^2L_1L_2^3 - 24R^2L_1L_3^3 + 12R^2L_2^4 - 24R^2L_2^3L_3 + 36R^2L_2^2L_3^2 - \\
 &24R^2L_2L_3^3 + 12R^2L_3^4 + 4L_1^4L_2^2 - 8L_1^4L_2L_3 + 4L_1^4L_3^2 - 8L_1^3L_2^3 + 8L_1^3L_2^2L_3 + 8L_1^3L_2L_3^2 - \\
 &8L_1^3L_3^3 + 4L_1^2L_2^4 + 8L_1^2L_2^3L_3 - 24L_1^2L_2^2L_3^2 + 8L_1^2L_2L_3^3 + 4L_1^2L_3^4 - 8L_1L_2^4L_3 + 8L_1L_2^3L_3^2 + \\
 &8L_1L_2^2L_3^3 - 8L_1L_2L_3^4 + 4L_2^4L_3^2 - 8L_2^3L_3^3 + 4L_2^2L_3^4)/(R^2(L_2 - 2L_1 + L_3)^2))^{1/2}
 \end{aligned}$$

$$\begin{aligned}
 y^- = - &((L_2 - 2L_1 + L_3)^2(2R + (23^{1/2}))(- (27R^6 - 27R^4r^2 + 18R^4L_1^2 - 18R^4L_1L_2 - \\
 &18R^4L_1L_3 + 18R^4L_2^2 - 18R^4L_2L_3 + 18R^4L_3^2 - 12R^2r^2L_1^2 + 12R^2r^2L_1L_2 + \\
 &12R^2r^2L_1L_3 - 12R^2r^2L_2^2 + 12R^2r^2L_2L_3 - 12R^2r^2L_3^2 + 3R^2L_1^4 - 6R^2L_1^3L_2 - \\
 &6R^2L_1^3L_3 + 9R^2L_1^2L_2^2 + 9R^2L_1^2L_3^2 - 6R^2L_1L_2^3 - 6R^2L_1L_3^3 + 3R^2L_2^4 - 6R^2L_2^3L_3 + \\
 &9R^2L_2^2L_3^2 - 6R^2L_2L_3^3 + 3R^2L_3^4 + L_1^4L_2^2 - 2L_1^4L_2L_3 + L_1^4L_3^2 - 2L_1^3L_2^3 + 2L_1^3L_2^2L_3 + \\
 &2L_1^3L_2L_3^2 - 2L_1^3L_3^3 + L_1^2L_2^4 + 2L_1^2L_2^3L_3 - 6L_1^2L_2^2L_3^2 + 2L_1^2L_2L_3^3 + L_1^2L_3^4 - 2L_1L_2^4L_3 + \\
 &2L_1L_2^3L_3^2 + 2L_1L_2^2L_3^3 - 2L_1L_2L_3^4 + L_2^4L_3^2 - 2L_2^3L_3^3 + L_2^2L_3^4)/(R^2(L_2 - 2L_1 + \\
 &L_3)^2))^{1/2})/3 - (3R(2L_1^2 - 2L_1L_2 - 2L_1L_3 + L_2^2 + L_3^2))/(L_2 - 2L_1 + L_3)^2 + \\
 &(4(L_1/2 - L_2/2)(L_1 - L_3)(L_2 - L_3)^2)/(R(L_2 - 2L_1 + L_3)^2)))/(2(9R^2 + 4L_1^2 - \\
 &4L_1L_2 - 4L_1L_3 + 4L_2^2 - 4L_2L_3 + 4L_3^2))
 \end{aligned}$$

The sphere intersection algorithm yield to 2 different solutions in which the spheres intersect: those two equations cannot be switched because symbolize the "link up" and "link down" solutions, so the condition with the links of the printers pointing towards the top or towards the bottom. Only the second solution will be chosen.

This algorithm have some backwards as the presence of singularities due mathematical conditions as the division by zero. In reality also in those situations no problem occurs (as lost in degree of freedom or gain). To overcome to this situation different set of equation can be derived with others singularity condition.

The four mathematical singularities that can happen are:

$$z_3 - z_1 = 0;$$

$$z_3 - z_2 = 0;$$

$$\frac{(x_1 - x_3)}{(z_1 - z_3)} - \frac{(x_2 - x_3)}{(z_2 - z_3)} = 0$$

$$\frac{(x_1y_2 - x_2y_1 - x_1y_3 + x_3y_1 + x_2y_3 - x_3y_2)^2}{(x_1z_2 - x_2z_1 - x_1z_3 + x_3z_1 + x_2z_3 - x_3z_2)^2} + \frac{(y_1z_2 - y_2z_1 - y_1z_3 + y_3z_1 + y_2z_3 - y_3z_2)^2}{(x_1z_2 - x_2z_1 - x_1z_3 + x_3z_1 + x_2z_3 - x_3z_2)^2} = -1$$

6.2 Inverse Kinematic

The inverse kinematic transform task space pose into the joint space variables. In particular from the pose vector

$$pose = [x \quad y \quad z]^T$$

that establish the position of the extruder, we want to derive the vector containing the lengths of linear actuators that move the carriages, so the joint space variables.

For this problem the same formulation as before applies, but this time MATLAB solver have been used to find the solution of the IKP.

Those equations are specific for the model used and so are valid only for this type of printer ¹.

$$L1 = z + 0.5\sqrt{-4.0x^2 - 4.0y^2 - 638.0y + 7.18e4}$$

$$L2 = z + 0.5\sqrt{-4.0x^2 - 553.0x - 4.0y^2 + 319.0y + 7.18e4}$$

$$L3 = z + 0.5\sqrt{-4.0x^2 + 553.0x - 4.0y^2 + 319.0y + 7.18e4}$$

Can be noticed that z coordinates apply just an offset on all the three carriages.

¹all the variable are expressed in mm

6.3 Jacobian

Jacobian matrix can be found using the derivative of the three positions constraint equations.

$$\begin{cases} (x - x_1)^2 + (y - y_1)^2 + (z - L_1)^2 = r^2 \\ (x - x_2)^2 + (y - y_2)^2 + (z - L_2)^2 = r^2 \\ (x - x_3)^2 + (y - y_3)^2 + (z - L_3)^2 = r^2 \end{cases}$$

$$\begin{cases} (x - 0)^2 + (y - R)^2 + (z - L_1)^2 = r^2 \\ (x + R\frac{\sqrt{3}}{2})^2 + (y - \frac{R}{2})^2 + (z - L_2)^2 = r^2 \\ (x - R\frac{\sqrt{3}}{2})^2 + (y - \frac{R}{2})^2 + (z - L_3)^2 = r^2 \end{cases}$$

expanding all the terms

$$\begin{cases} x^2 + y^2 + R^2 + 2Ry + z^2 + L_1^2 - 2L_1z = r^2 \\ x^2 + R^2\frac{3}{4} + xR\sqrt{3} + y^2 + R^2\frac{1}{4} - Ry + z^2 + L_2^2 - 2L_2z = r^2 \\ x^2 + R^2\frac{3}{4} - xR\sqrt{3} + y^2 + R^2\frac{1}{4} - Ry + z^2 + L_3^2 - 2L_3z = r^2 \end{cases}$$

and deriving with respect to time

$$\begin{cases} 2\dot{x}x + 2\dot{y}y + 2R\dot{y} + 2z\dot{z} + L_1\dot{L}_1 - 2\dot{L}_1z - \dot{z}L_1 = 0 \\ 2\dot{x}x + \dot{x}R\sqrt{3} + 2\dot{y}y - R\dot{y} + 2\dot{z}z + 2L_2\dot{L}_2 - 2\dot{L}_2z - 2\dot{z}L_2 = 0 \\ 2\dot{x}x - \dot{x}R\sqrt{3} + 2\dot{y}y - R\dot{y} + 2\dot{z}z + 2L_3\dot{L}_3 - 2\dot{L}_3z - 2\dot{z}L_3 = 0 \end{cases}$$

rewriting the equations into matrices

$$\begin{bmatrix} x & y + R & z - L_1 \\ x + R\frac{\sqrt{3}}{2} & y - R & z - L_2 \\ x - R\frac{\sqrt{3}}{2} & y - R & z - L_3 \end{bmatrix} \cdot \begin{bmatrix} \dot{x} \\ \dot{y} \\ \dot{z} \end{bmatrix} = - \begin{bmatrix} L_1 - z & 0 & 0 \\ 0 & L_2 - z & 0 \\ 0 & 0 & L_3 - z \end{bmatrix} \cdot \begin{bmatrix} \dot{L}_1 \\ \dot{L}_2 \\ \dot{L}_3 \end{bmatrix}$$

$$J_x \cdot \begin{bmatrix} \dot{x} \\ \dot{y} \\ \dot{z} \end{bmatrix} = J_q \cdot \begin{bmatrix} \dot{L}_1 \\ \dot{L}_2 \\ \dot{L}_3 \end{bmatrix}$$

The Jacobian can be found as

$$J^{-1} = J_q^{-1} \cdot J_x$$

to find singularities points, the determinant of the Jacobian matrix is imposed equal to zero

$$\det(J) = 0 \implies (z - L_1)(z - L_2)(z - L_3) = 0$$

$$(z = L_1) \vee (z = L_2) \vee (z = L_3)$$

Singularities can be found when one or more link become perpendicular to the direction of one of the prismatic joints.

To avoid those singularities conditions, the workspace have to be smaller of the maximum area reachable by the extruder when it is full extended.

6.4 Resolution variation along X Y plane

As already mentioned, the resolution trend along the XY plane is very different with respect to a cartesian printer. The end-effector motion varies greatly, with the same relative motion of the carriage, depending where the moving platform is located in the workspace.

First of all, was important to know the trend of change of the resolution on an arbitrary XY plane. To have a visual representation, three concatenated loops, that moved the carriage along all the workspace, were used. The discretize value of L_1, L_2, L_3 generated were feed into the direct kinematics and all the point that fell inside a z boundary were saved.

From this slice of the total workspace, the distances between points was calculated and was used to generate a map of the resolution drift.

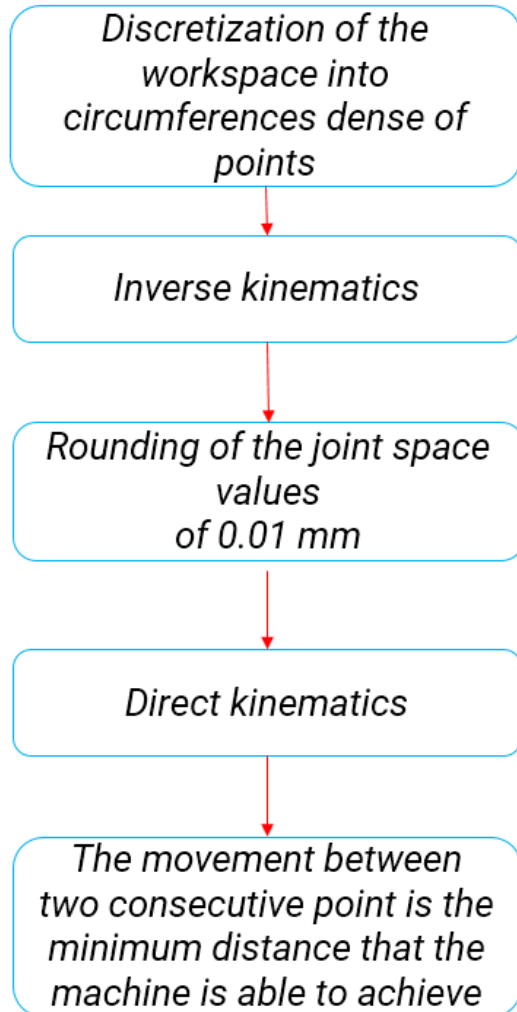
This method works very well using 0.1 mm of steps for the carriages.

Using the following hypothesis

- Radius of the circumference on which the median point of the two rails of each tower have been placed equal to 175.5 mm
- GT2 2 mm pitch gear with 16 teeth
- Motor with 1.8° of rotation angle for step
- 1/16 micro-stepping driver

A minimum tower resolution of 10microns (0.010mm) can be found.

Trying to change the minimum displacement of the carriage to this value was a total insuccess due to the very long time needed for the calculations with the method just mentioned (about 16 days).



The problem was re-formulated as: the total workspace area along the X Y plane was discretized into circumferences with different radii. Those circumferences were created with a high quantity of points such as, the distance between two consecutive points was much lower than the minimum displacement that the printer is able to achieve.

Those paths were fed into the inverse kinematics block that transformed $\{x,y,z\}$ values into $\{L_1,L_2,L_3\}$ displacement for the carriages. Those floating point values with 32-bit of precision were rounded to the second decimal digit to reproduce the resolution of the carriage. The rounded $\{L_1,L_2,L_3\}$ values were converted back to task space quantity and the distances between two consecutive points, that is the resolution in that area, was measured. The maximum value (higher resolution that is the worst case) was calculated of each circumference and plotted in function of the circumference radii.

To use this technique along the reachable area, that hopefully is bigger than the heated bed and is not circular but triangular-like shaped, the imaginary solutions of the inverse kinematics problem were excluded.

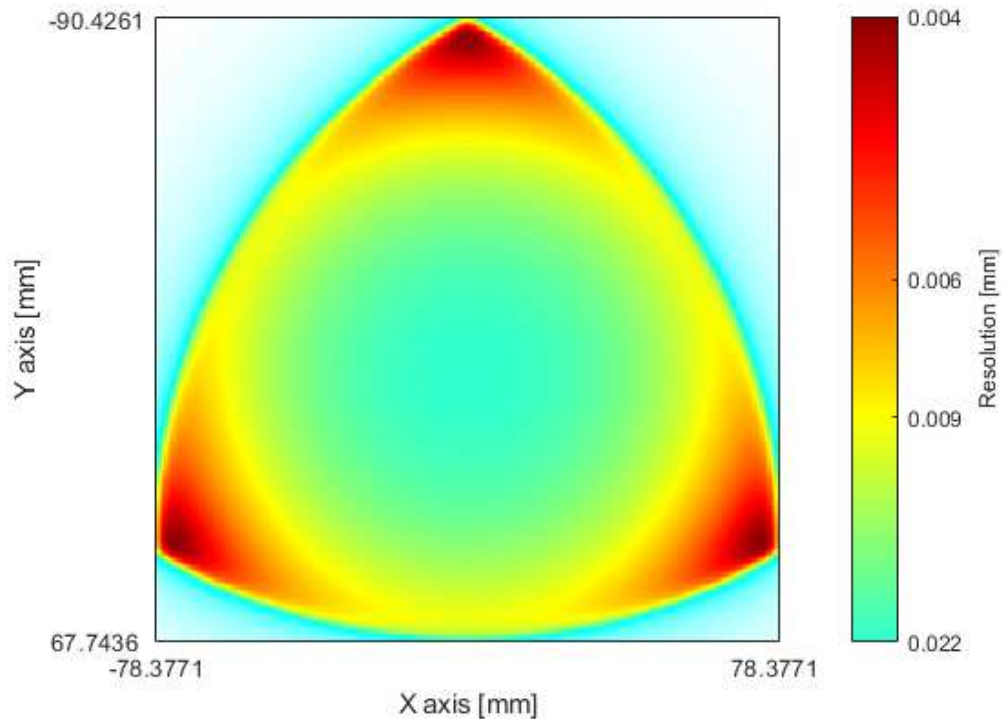


Figure 6.4: Maximum resolution along circumference centred in $(0,0)$ with 0.01mm of step for the carriages.

Can be well seen that the areas with lowest resolution are the ones near the towers, while it tends to be lower in the center. The resolution of the printer under analysis is similar to the typical one for the desktop class of printers.

The turquoise colour outside the yellow triangular-like shaped figure has no meaning and is produced by the interpolation algorithm at the boundary.

The values showed in the 3.1 relate each circular section with the lowest resolution encountered while following that path. For this reason it is not possible to see along the yellow or the green-light blue regions which of those points are affected by the worst or the better resolution.

A further analysis was done to understand where those points fall in, relating the research of a maximum and a minimum value of resolution with a specific X-Y coordinate.

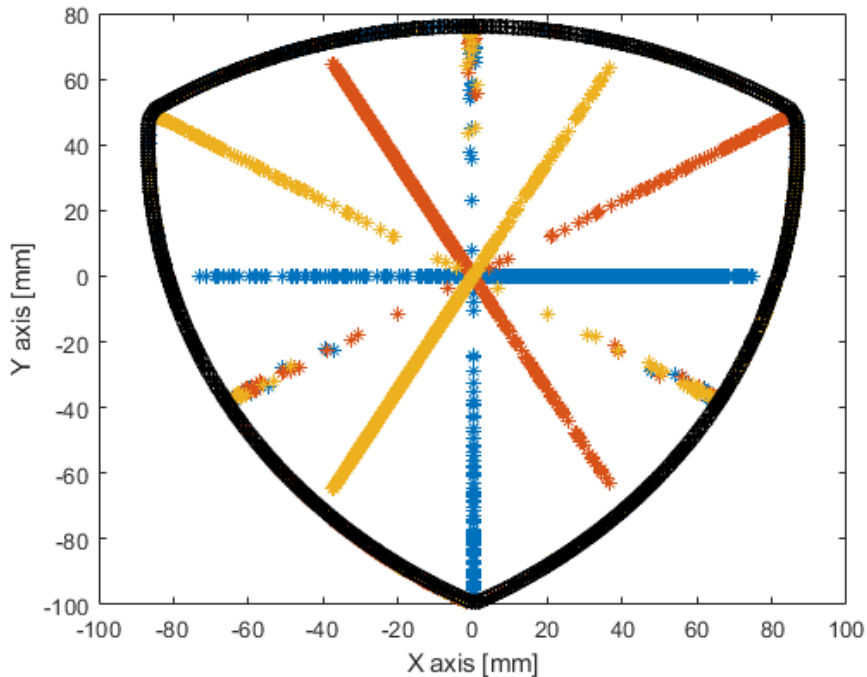


Figure 6.5: Points affected by the highest resolution

For the symmetry condition along this plane, the analysis was done only on a section of the workspace.

The results have been rotated of 120° around the center ($x=0, y=0$). For that reason the points appear to be coloured differently in blue, red and yellow. The black colour was used to highlight the boundary of the reachability workspace.

Only one point for the maximum and for the minimum were saved along a single circumference, but may exist more points with the same values that are not showed in the figure 8.8.

From the begin it was clear that the points with best resolutions were the one in front on the towers.

Was for me unexpected to also find the point perpendicular to it passing through the center.

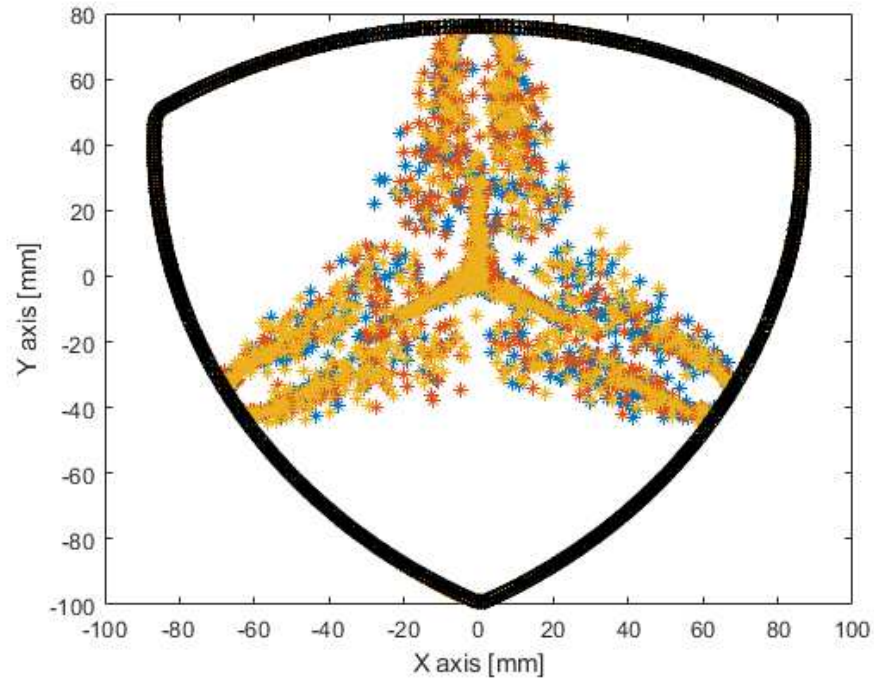


Figure 6.6: Points affected by the lowest resolution

The areas with the worst resolution are the one in between of the two towers, points that are very far from the tower ahead. This because while the arm angle become smaller, the resolution on the carriage is multiplied by the already discussed coefficient used to show in cap 5.0.2 the relation between the velocity of the carriage and the the moving platform.

6.5 Workspace

From the reachability workspace, a circular subspace have been selected with circumference radii that, in this printer, is smaller than 76 mm.

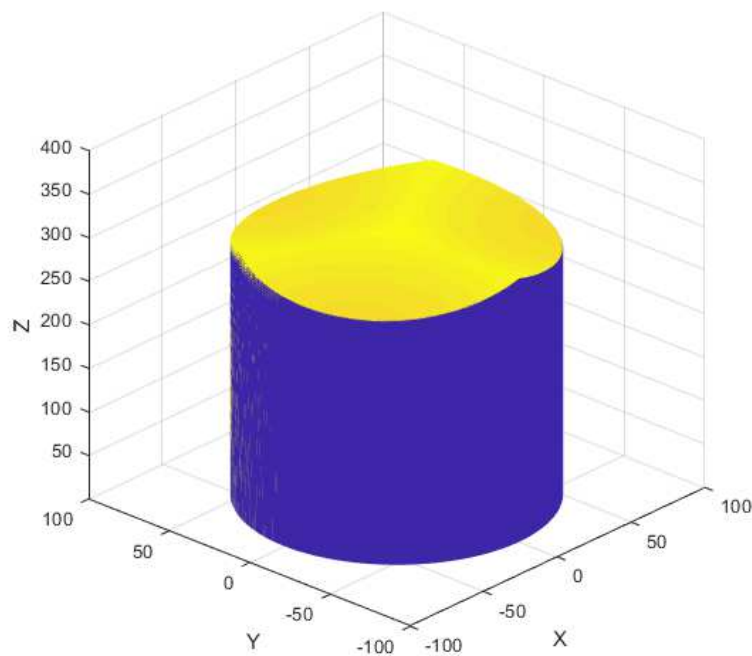


Figure 6.7: workspace of the delta printer

The arm length selection affects the amount of unusable z height that cannot be used to print a part. Using as hypothesis that we want to be able full print in XY plane at any height, the top part of the reachable volume cannot be used and thus has to be eliminated.

Using the hypothesis of circular bed plates, and minimum arm angle (as already discussed in chapter 5.0.2 and 5.0.4) the volume assumes the shape of a cylinder.

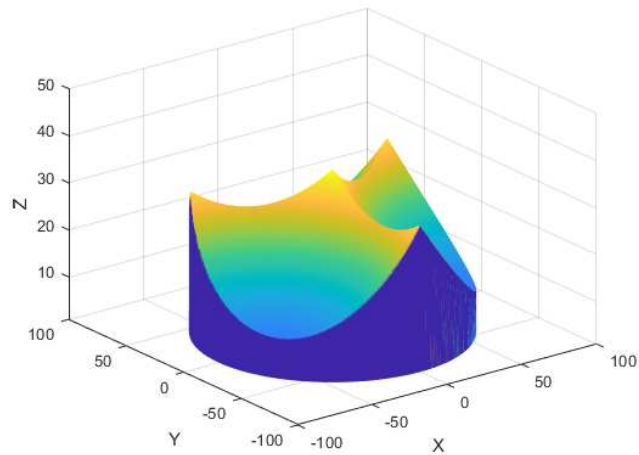


Figure 6.8: Detail of the top part of the volume

Starting from a total height ,from the bed plate to the end of the rail of 439.5 mm, only 279.5 mm were usable².

Another part of the total reachable volume is removed due the fact that lies beneath the heated bed. This volume generates from the fact that when the extruder is in contact with the bed, the three carriages are not about the same height of the moving platform at the same time. This volume tend to shrink and became a point when the three carriage are placed at bed level.

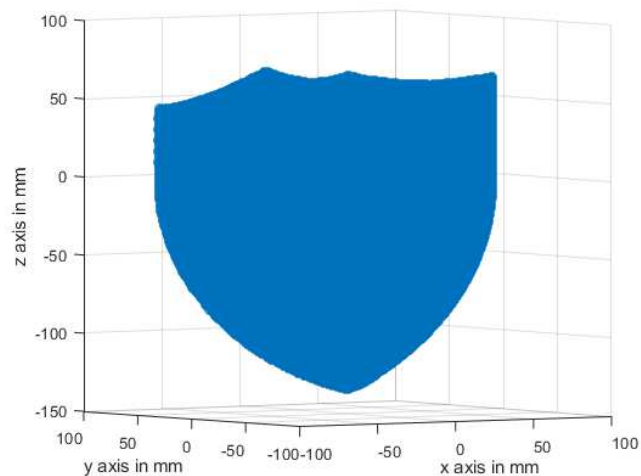


Figure 6.9: Workspace lost beneath the bed, placed conventionally at 0 mm.

²refers to the printer with 160.4 mm of link lengths

Chapter 7

Model

To chose and size the best motor to fit this application, forces and angular velocities at which the motor should work must be to known.

To evaluate the those values during the working operations of the Delta printer, a MATLAB Simmechanics model and a simplified dynamic have been created.

The procedure that follows was adopted:

- A path was be choose.
This path was generated only on the XY plane, so without a change of the z height, hypothesis that is true if the spiral contour feature is disabled, so z height do not continuously increases to create a seamless surface ¹
- The path was discretize and velocity constrain were added in order to create the required trajectory
- Inverse kinematics was used to extrapolate the desired joints space values
- The displacement of the prismatic joints in time was fed to both dynamic model and Matlab model and forces acting on the carriages was acquired
- Data was compared to show where the approximations adopted to simplify the dynamic model had a greater impact.

¹usually used for pots

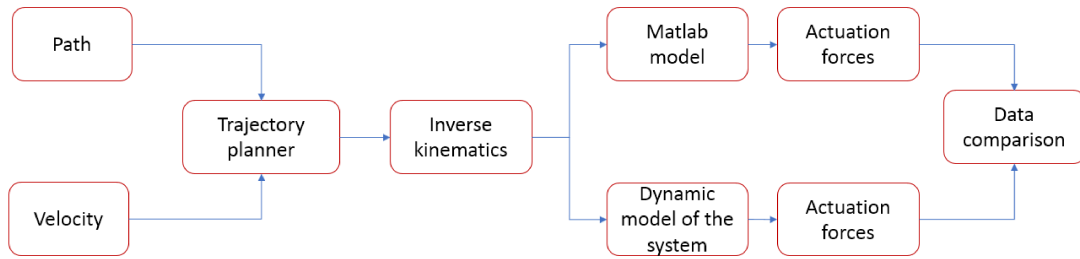


Figure 7.1: General scheme of the procedure used

7.1 Numerical data used for simulation

All the inertia matrix are related to the center of mass and aligned with the coordinate system showed on the relative parts in light pink colour.

Carriage



Materials = plastic for the body and steel for the spherical joints.

Mass = 104.21g

Distance between the pivot point of the spherical joints = 76.59mm

The mass of the linear bearings was not included because of their low weight ^a.

^aBearings reference <https://www.euro-bearings.com/eurocatonline.pdf>

<https://www.euro-bearings.com/eurocatonline.pdf>

Link



Materials = rubber for the spherical joint head and steel for the link's body .

Mass = 5.96g

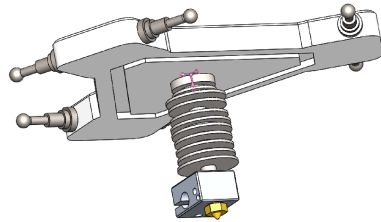
Lenght^a = 157.79mm

$$I_{link} = \begin{bmatrix} 13387.48 & 0 & 0 \\ 0 & 6.58 & 0 \\ 0 & 0 & 13385.78 \end{bmatrix} [g \cdot mm^2]$$

For the symmetry and homogeneity of the object, the center of mass is in the middle of the link's body.

^abetween the two pivot point of the spherical joints

Moving platform



Materials = plastic for the body, steel for the spherical joints and aluminium for the extruder.

Mass = 84.31g

$$I_{MovingPlatform} = \begin{bmatrix} 77767.24 & 0 & 0 \\ 0 & 77912.40 & 0 \\ 0 & 0 & 137437.58 \end{bmatrix} [g \cdot mm^2]$$

The origin of the reference system lie in the center of the cylindrical body of the extruder (heatsink) regarding X Y axis ², while there is an offset of 7.95 mm on Z axis from the top surface.

The minimum distance between the axis passing in the middle of the two pivot points of spherical joint (connected to the same moving platform) and the center of the moving platform on XY plane is h=59.67 mm.

²non-centred assembly of the heating block with respect of the heatsink makes the center of mass translate of 0.4 mm on the Y axis. For this reason this offset has been neglected in the dynamic model.

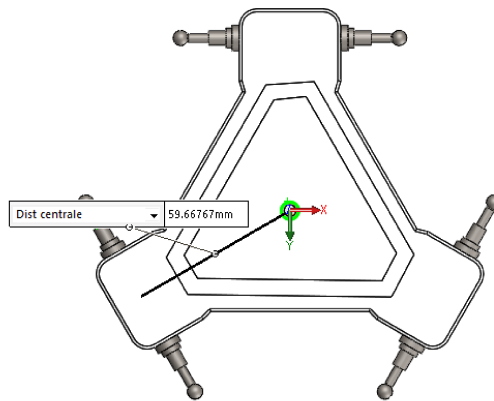


Figure 7.2: Offset between spherical joints and the center of the moving platform.

7.2 Simmechanics model

The CAD files from Solidworks were saved into .step format and imported in a simulink simmechanics project.

In order to make system more readable, input ports were placed on the left part of the model while output ports can be found on the left. Masks with a image of the what the subsystem represent was added to make it more understandable.

The three blocks on the the right are simmechanics-specific and are needed to: specify the axis on which the gravity acts, the inertial reference system and the solver parameters. A variable step solver with relative tolerance and filtering constant of 10^{-3} was chosen.

The 3D-Printer subsystem accept as input the displacements of the prismatic joints L_1, L_2, L_3 . Those discrete-time values are then linearly interpolated in order to use a continuous time solver. This was done using the repeating sequence interpolated block configured with a lookup method of "use end values".

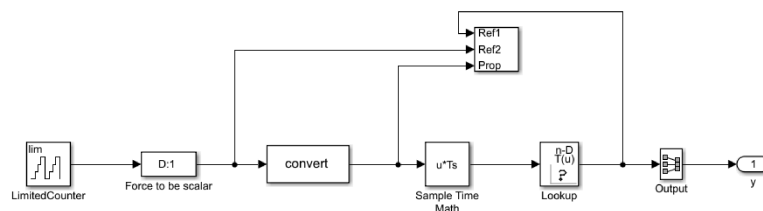


Figure 7.3: Repeating sequence interpolated under the mask

Those values are converted to simulink to simmechanics world using a $S - PS$ block. Those blocks were set using a second order filtering with an input filtering time of 10^{-3} s. This block also calculates the derivatives of the input signal and provide it to the following block.

The forces values that came as an output of the subsystem are then re-converted using $PS - S$ blocks and then save a "timeseries" format in the workspace using a "To Workspace" block.

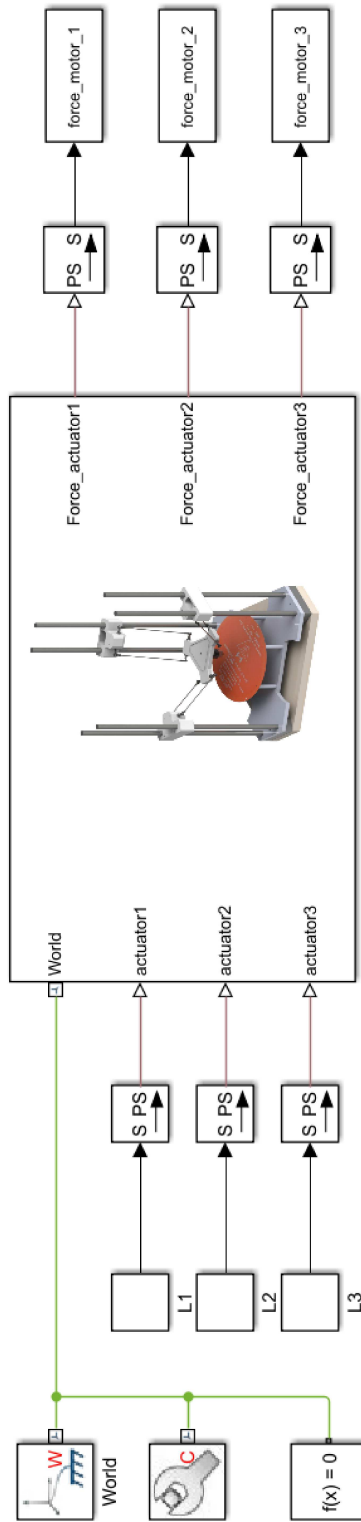


Figure 7.4: Simulink simmechanics model

The model of the printer was modified until the maximum simplicity was reached. The "world" inertial reference frame is directly connected to the structure of the machine. This was considered without any mass or inertia property because it is not a moving part and is used only for visual purpose.

Connected to it there are the prismatic joints, modified to accept as input the position and to sense the force. Those joints are directly conjoined to the moving carriage, with mass and inertia property discussed before.

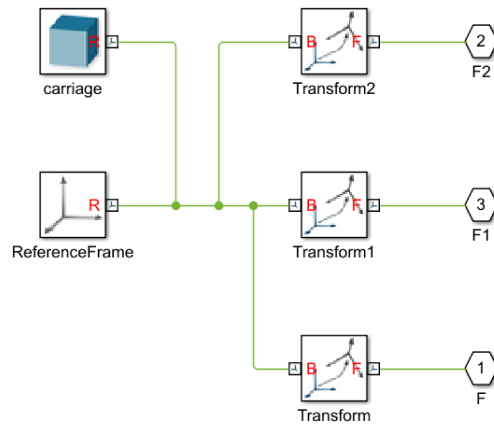


Figure 7.5: Inside the carriage block

The joint is connected at F input blocks, while the two spherical joints are connected to F1 and F2. The three transformations are used to geometrically place the solid bodies, symbolized with the blue cubic icon. To help the debug, during the assembly construction the "ReferenceFrame" block was used because it can be highlighted in the explorer window.

The Matlab model of the printer was build to be mechanically equal to the real one and so every carriage is connected by two spherical joints blocks to the links, and all the links are connected to the moving platform.

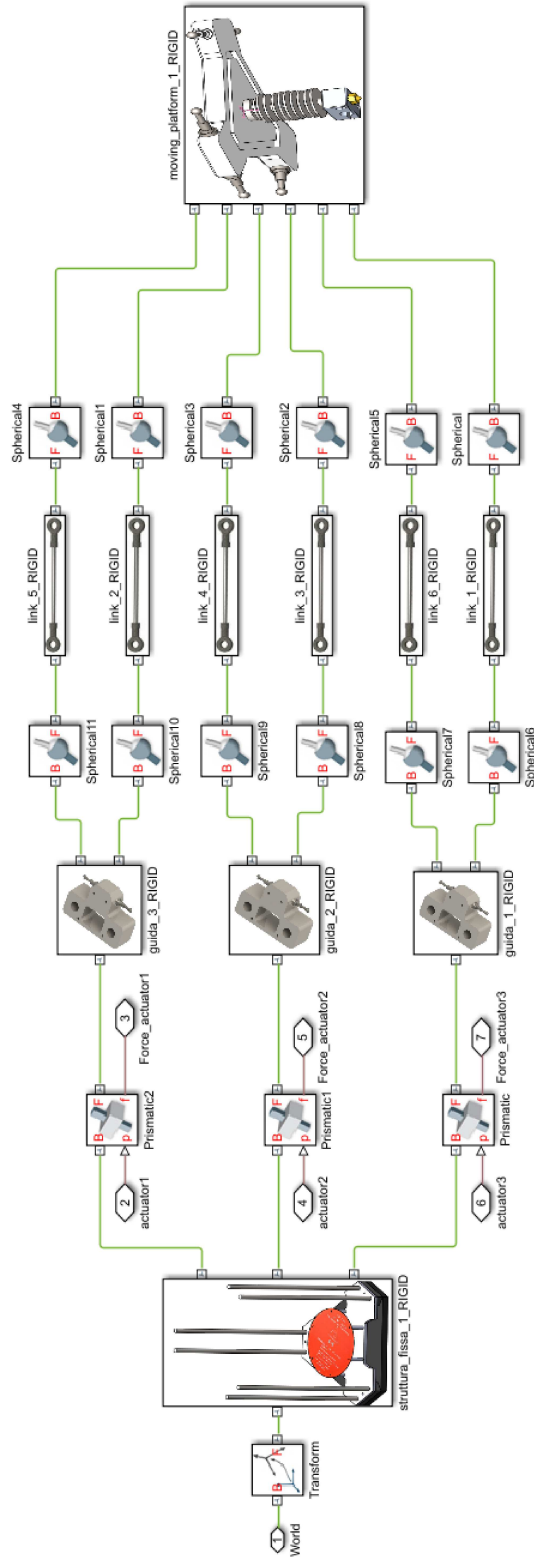


Figure 7.6: Simulink simmechanics model of the printer

7.2.1 Reference frame and translation

Under each single mask various subsystem that compose a single part have been compacted.

Each assembly that forms a single part (ex.the rigid structure, in which can be found towers,plate and enclosure) was compressed in a single Solidworks part with extension .slprt .

All this files were imported into Matlab using Simscape Multibody Link³ utility that automatically fills the various fields of the solid object including mass property, inertia, translation from a reference frame R, automatically placed by Matlab during file import, to the COG.

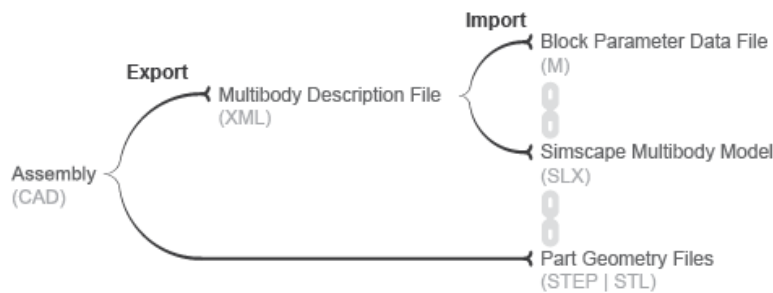


Figure 7.7: Importing procedure for CAD files

Printer structure

Starting from the left of the image 7.6 is possible to see an arbitrary translation from the simulink world reference frame to Ref.frame F3 that is where the reference frame of STEP file containing all the fixed printer structure was automatically placed by MATLAB.

As can be noted by the image, in the inertial RF is the Y axis pointing toward the top part of the printer and in fact the gravitation acceleration was selected along this axis in the configuration blocks.

³<https://it.mathworks.com/help/physmod/smlink/index.html>

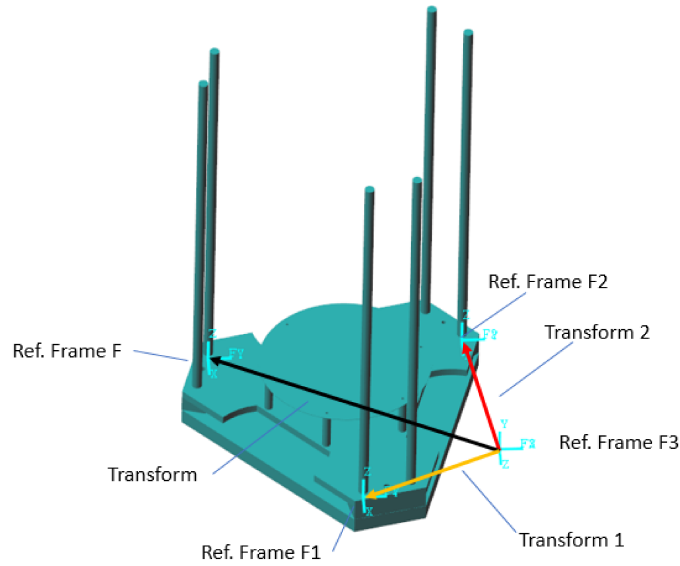


Figure 7.8: Printer structure on simulink with traslation and reference frame.

The reference frame F3 was used to visualize the local reference frame created by MATLAB when a external CAD file is imported. This reference frame, called R, is usually randomly placed, usually around the corners or on some feature but not in this case. New reference frame however can be expressed in "solid option" > "frames" > "New frame" but its definition on an imported file is quite difficult and time consuming. As already explained Simscape Multibody Link was used to automatically create the translation from R to the joints location.

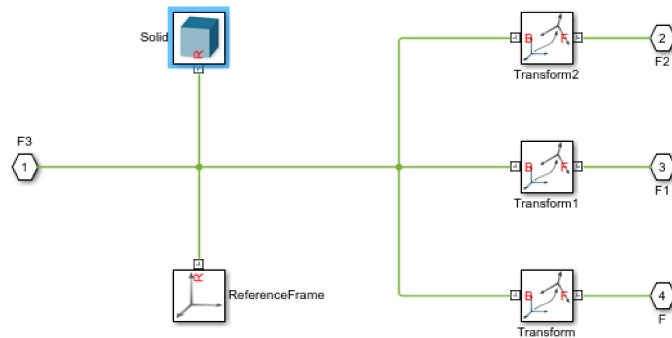


Figure 7.9: Simulink block scheme of the inertial structure

This block is essentially composed by the solid object of the printer (block object) and three translation. The reference frames F, F_1, F_2, F_3 are placed to shows the orientation on the ports namesake.

From Ref. frame F3, three transformation take place:

- Transform 1
Roto-traslation from reference frame F3 to reference frame F1
- Transform 2
Roto-traslation from reference frame F3 to reference frame F2
- Transform 3
Roto-traslation from reference frame F3 to reference frame F

Transformation name in the sub-block	Trasformation name in configuration file
Transformation 1	RigidTransform(19)
Transformation 2	RigidTransform(25)
Transformation 3	RigidTransform(15)

These roto-translation moves from the reference frame F3 to one of the columns of the printer from which will be attached a prismatic joint.

The rotation was needed because, on Simulink, 1 degree of freedom joints can move only along the Z axis.

Each property of a "Solid" block is defined in a separate file. Here will be report a general configuration of this type of block.

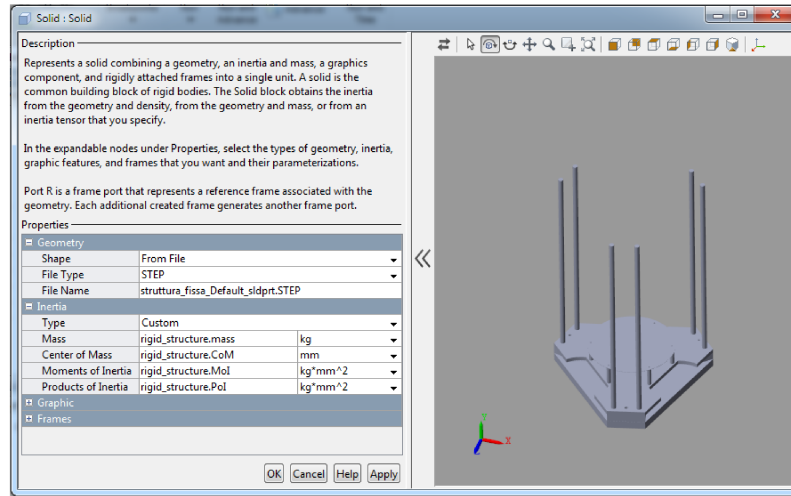


Figure 7.10: Solid configuration parameters, generally adopted

The inertia property are equal to the mass option of the part on SolidWorks. Step file format does not take any information of material, density, position of the center of mass,...., so it is necessary to specify them.

Matlab could also calculate inertial properties from geometry, but this is valid only if the part is composed by only one material type.

The base of the printer, as already said, does not need any of this information, because it has no motion and is considered rigid, so it was imported only for a graphical purpose.

carriages

At the ports F_2, F_1 and F of the inertial subsystem, three different prismatic joints were connected. The joints are defined to be commanded in position and to sense the force that is automatically computed.

To also have an idea of the effect of friction, a parameter called `beta_linear` was specified in the main script that launch both simulink and Lagrangian models.

Inside the mask of the carriage can be found "input" F , connected to the other end of the prismatic joint. A translation from this point, that lay along one of the towers, to R was defined .

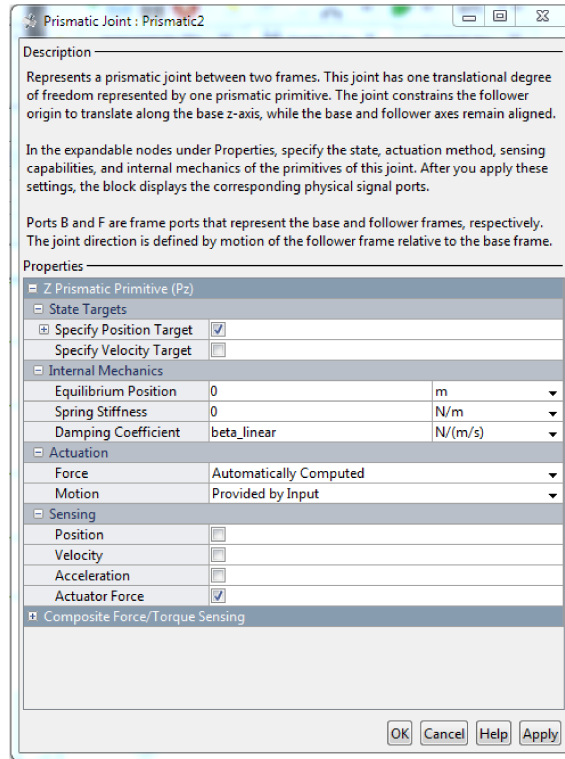


Figure 7.11: Configuration of the actuated joints

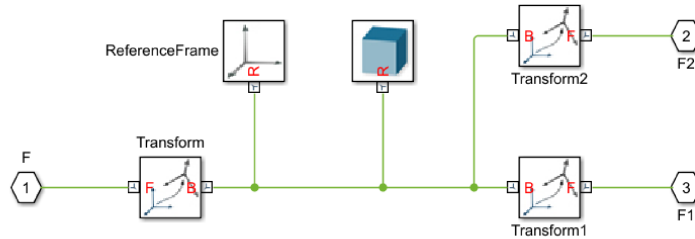


Figure 7.12: Carriage simulink block

From R two transformation to the pivot point of each spherical joint is placed to be connected to the "spherical joint" block.
 From R also a traslation to the COG is defined inside the "Solid" block and is called carriage.CoM.

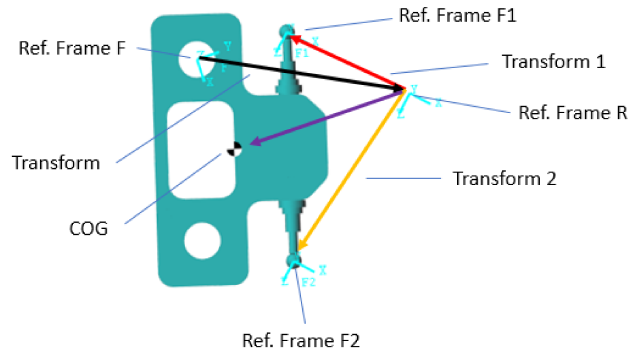


Figure 7.13: Transformation of carriage sub-block

	Transformation name in the sub-block	Transformation name in configuration file
Carriage 1	Transformation	RigidTransform(14)
	Transformation 1	RigidTransform(15)
	Transformation 2	RigidTransform(17)
Carriage 2	Transformation	RigidTransform(20)
	Transformation 1	RigidTransform(21)
	Transformation 2	RigidTransform(23)
Carriage 3	Transformation	RigidTransform(26)
	Transformation 1	RigidTransform(27)
	Transformation 2	RigidTransform(29)

link

The same discussion applies for the link.

At the reference frame F1 and F2 of each carriage two spherical joint were connected. Those joint have 3 DOF so is not important to manage the Z axis. Each spherical joint is connected to a link sub-system.

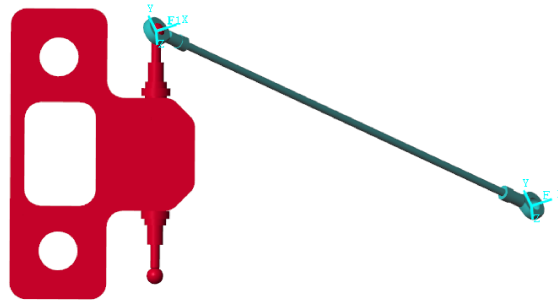


Figure 7.14: Connection of the carriage to the link

The sub-system of each link is very simple and follow the same rules of the carriages: At the left there is the port F connected to the carriage, and at the right there is the port F1 connected to the moving platform. In between there are the two transformation to connect those point with R. From R to the center of mass a translation called link.CoM was created by Simscape Multibody Link.

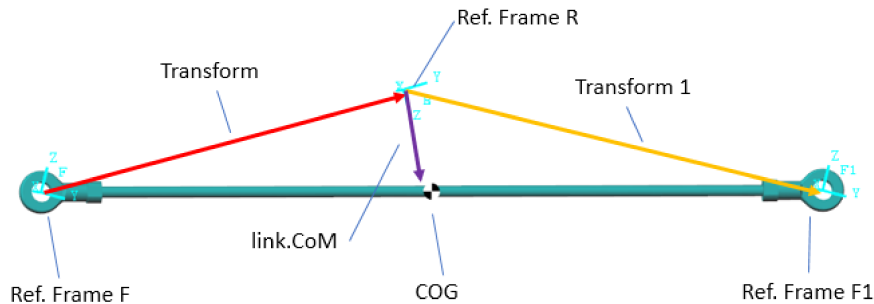


Figure 7.15: Reference system and transformation on each link

In all the spherical joints blocks was specified the viscous friction coefficient called $\beta_{spherical}$ discussed in chapter 8.1.1 .

For each of those joints, initial condition were set, so at the beginning of the simulation the extruder is centred in the platform as it normally happens after the calibration procedure.

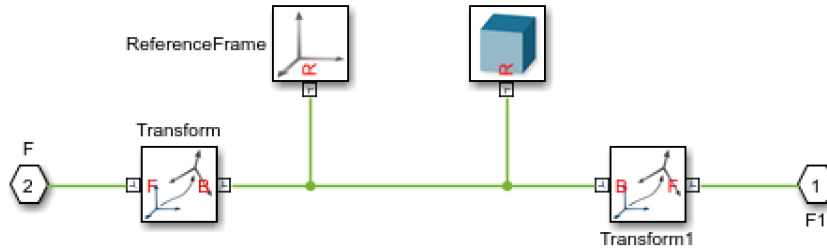


Figure 7.16: Simulink block

	Transformation name in the sub-block	Trasformation name in configuration file
Link 1	Transformation Transformation 1	RigidTransform(2) RigidTransform(16)
Link 2	Transformation Transformation 1	RigidTransform(4) RigidTransform(28)
Link 3	Transformation Transformation 1	RigidTransform(6) RigidTransform(22)
Link 4	Transformation Transformation 1	RigidTransform(8) RigidTransform(24)
Link 5	Transformation Transformation 1	RigidTransform(10) RigidTransform(30)
Link 6	Transformation Transformation 1	RigidTransform(12) RigidTransform(18)

Moving platform

The moving platform block is connected to each link, so it has 6 input ports. After each spherical joint block a traslation from the pivot point to R is present.

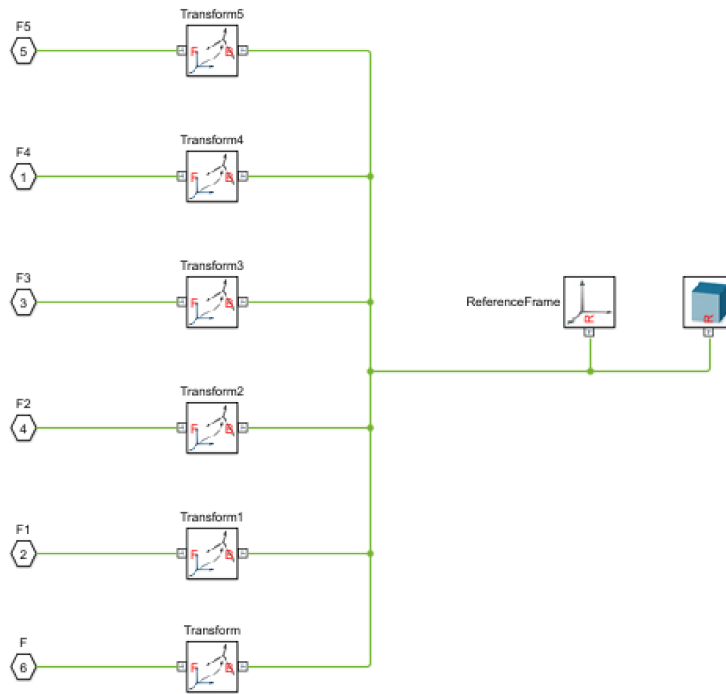


Figure 7.17: Simulink scheme

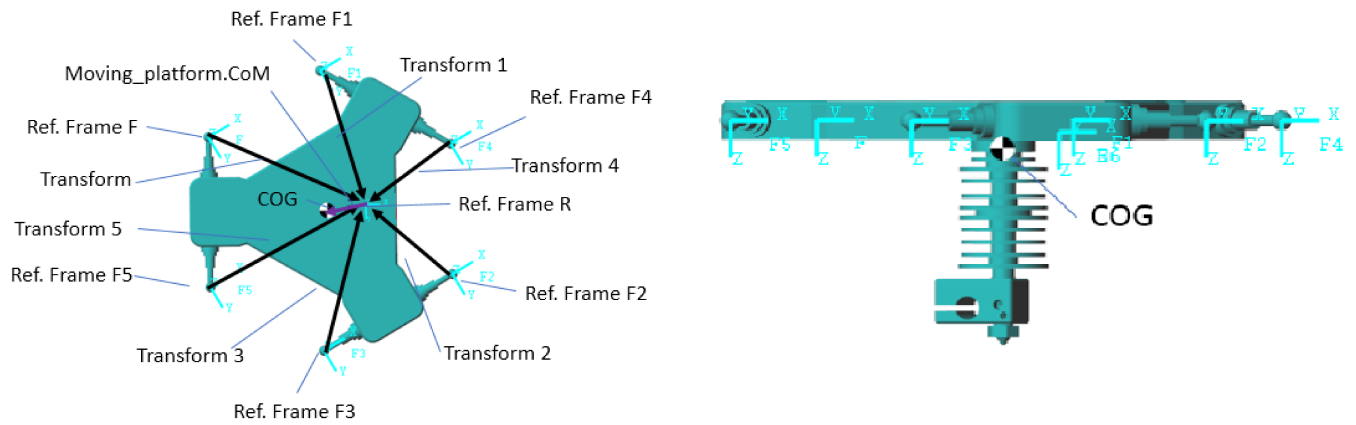


Figure 7.18: Transformation and reference frame for the moving platform

The transformation parameters can be found in the configuration file and are called:

Transformation name in the sub-block	Transformation name in configuration file
Transformation	RigidTransform(1)
Transformation 1	RigidTransform(3)
Transformation 2	RigidTransform(5)
Transformation 3	RigidTransform(7)
Transformation 4	RigidTransform(9)
Transformation 5	RigidTransform(11)

7.2.2 Path checking

The simulink model take as input the linear displacement on the carriages. To check if the path in the task space match with the desired one, a "Translation sensor" was used.

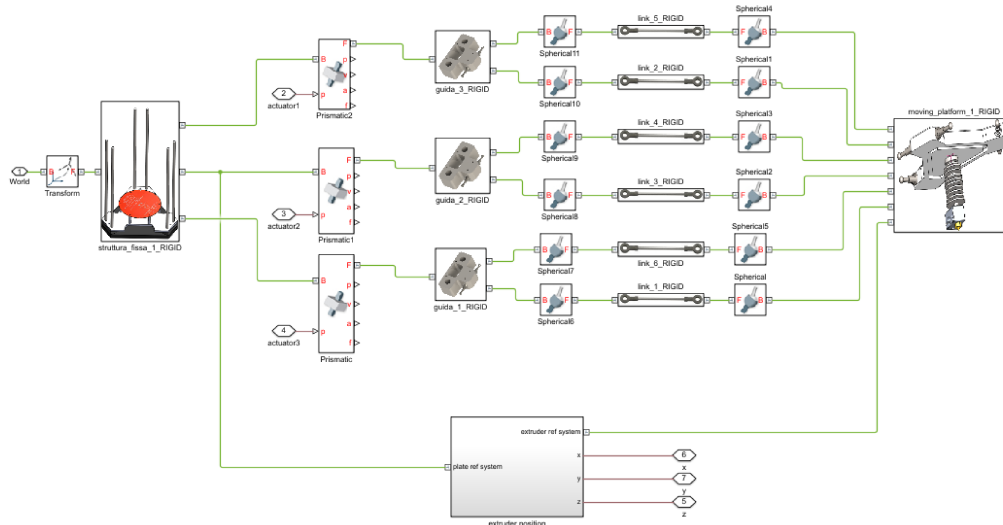


Figure 7.19: Location of the sensing subgroup

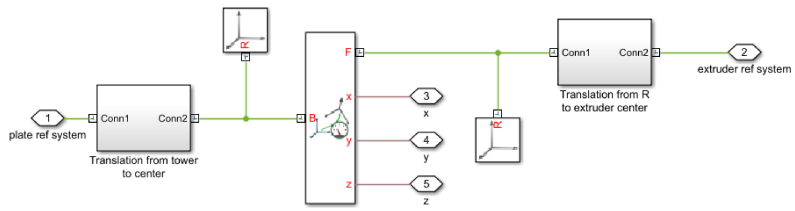


Figure 7.20: Sensor sub-system

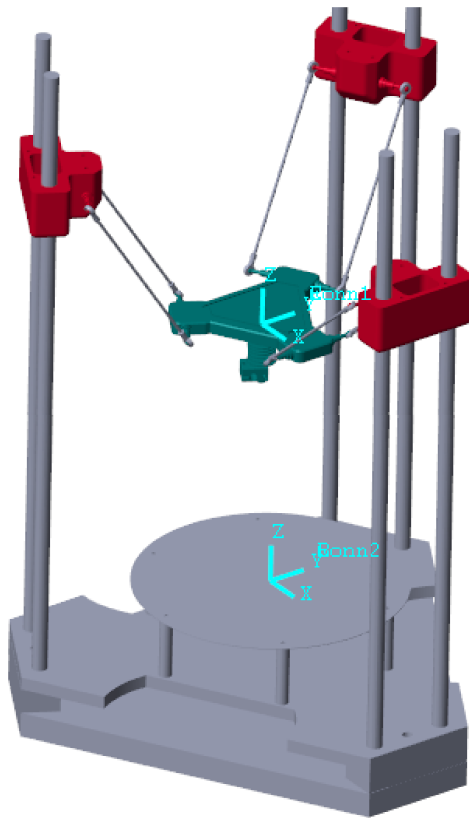


Figure 7.21: Two reference system whom the sensor is connected

7.3 Lagrangian model

The most common analytical approaches for dynamic modelling are:

- the Principle of Virtual Work
- the Newton-Euler Formulation
- the Lagrangian Formulation

An overview about those approaches can be found at ⁴ and ⁵.

The three approaches are theoretically equivalent, but the computational cost generated by solving those dynamical equations may varies significantly as showed by Lin and Song ⁶

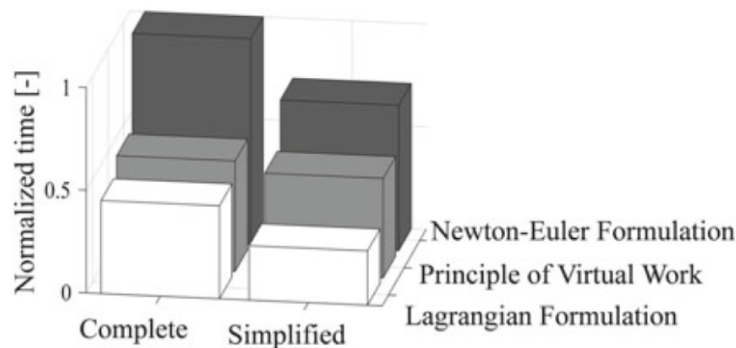


Figure 7.22: Comparison of the computation times for complete and simplified approaches

”It can be seen that independent of the underlying model shortest processing times are achieved applying the Lagrangian approach. The relative saving of time between complete and simplified models is 42, 10, and 29% for the NewtonEuler Formulation, the Principle of Virtual Work, and the Lagrangian Formulation, respectively. Referring to the simplified NewtonEuler Formulation, the application of the Principle of Virtual Work reduces the computation time by 32%. Applying the simplified Lagrangian approach, relative saving of time is 63% compared to the NewtonEuler Formulation. To sum up, the minimum computation time is 74% less

⁴”Robot analysis:the mechanics of serial and parallel manipulators”, John Wiley and sons, Tsai L.W.

⁵”Parallel robots”,Merlet J.-P. ,Springer Dordrecht, 2006

⁶Lin Y.-J. and Song S.-M. A Comparative Study of Inverse Dynamics of Manipulators with Closed-Chain Geometry. In Journal of Robotic Systems, 7(4):507-534, 1990.

than the reference time and obtained using the simplified Lagrangian approach”⁷.

The Lagrangian formulation describes the equation of motion of a generic mechanical system as a direct function of the Lagrangian variable, composed by both contribution of kinetic and potential energy.

Differently from the Newton-Euler Formulation, the Lagrangian one does not involve the all reaction forces and moments between each body that compose the system and for that is more computational efficient.

To simplify the model, the rotational inertias of the of the light-weight links (6g) has been neglected. The mass of the link however was distributed between the carriage and the moving platform, condition often used while modelling parallel machine with low-weight arm.

⁷Merlet,Lenarc in ”Advanced in robot kinematics”, p.123

7.3.1 Generalized coordinates

For closed loop robots, such parallel manipulators, the expression of the kinetic co-energy and potential energy are very difficult to obtain only as a function of the active joint variables, in this case the three prismatic joints. Therefore it was used a vector of generalized coordinates that also included additional variables as the platform cartesian coordinates.

$$\mathbf{q} = [q_1, q_2, q_3, p_x, p_y, p_z]^T$$

This redundant set of coordinate was chosen. Obviously the variables p_x, p_y, p_z are not independent and will be linked to q_1, q_2, q_3 thanks to the use of a constraint equation.

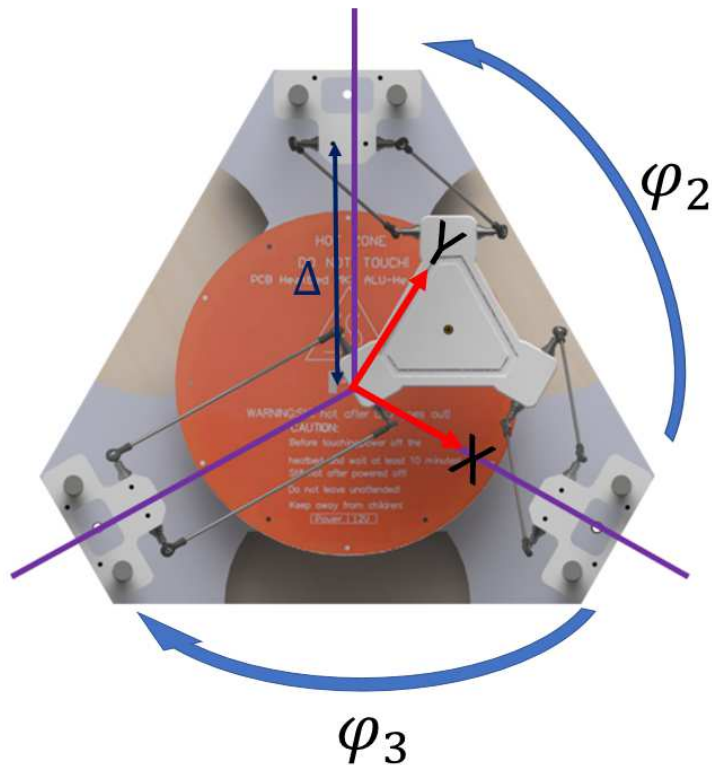


Figure 7.23: Reference system used to develop the dynamic set of equations.

7.3.2 Kinetic Co-energy

The total kinetic co-energy K is a non-negative scalar function of the joint coordinates $q(t)$ and velocities $\dot{q}(t)$. It is an additive function and is calculated for every component of the manipulator.

$$K = K_{MovingPlatform} + \sum_{j=1}^6 K_{link_j} + \sum_{i=1}^3 K_{carriage_i}$$

where

$$K_{MovingPlatform} = \frac{1}{2} \cdot m_{MovingPlatform} \cdot (\dot{p}_x^2 + \dot{p}_y^2 + \dot{p}_z^2)$$

$$K_{carriage_i} = \frac{1}{2} \cdot m_{carriage} \cdot \dot{q}_i^2$$

The links connected to the parallelogram are the main reason for complexity. For simplicity, the mass of each link was considered equally distributed and concentrated at the two connections points on the carriages and on the moving platform. Other treatments also use different masses distribution as showed by Codourey⁸ that distributes the mass of the links 2/3 at the top-link and 1/3 at the platform.

$$K_{link} = \frac{1}{2} \cdot 3m_{link} \cdot \dot{q}_i^2 + \frac{1}{2} \cdot 3m_{link} \cdot (\dot{p}_x^2 + \dot{p}_y^2 + \dot{p}_z^2)$$

For each chain there are two different links for a total of six in a 3D printer.

$$K = \frac{1}{2} \cdot (m_{MovingPlatform} + 3m_{link}) \cdot (\dot{p}_x^2 + \dot{p}_y^2 + \dot{p}_z^2) + \frac{1}{2} \cdot (m_{carriage} + m_{link}) \cdot \dot{q}_1^2$$

$$+ \frac{1}{2} \cdot (m_{carriage} + m_{link}) \cdot \dot{q}_2^2 + \frac{1}{2} \cdot (m_{carriage} + m_{link}) \cdot \dot{q}_3^2$$

7.3.3 Potential energy

Position energy, due to gravitational effects, is considered a potential energy term included into the total potential energy. As assumption the potential energy is zero when the center of mass is at the same level of the plane. It is only function of the

⁸Codourey, A.: Dynamic modeling of parallel robots for computed-torque control implementation. Int. J. Robot. Res. 17(12), 13251336 (1998)

joint coordinate $q(t)$ alone and is, as the kinetic energy, additive. The potential energy was derived

$$U = U_{MovingPlatform} + \sum_{j=1}^6 U_{link_j} + \sum_{i=1}^3 U_{carriage_i}$$

$$U_{link_j} = m_{link} \cdot g \cdot (p_z + q_i)$$

$$U_{MovingPlatform} = m_{MovingPlatform} \cdot g \cdot p_z$$

$$U_{carriage_i} = m \cdot g \cdot q_i$$

$$U = m_{MovingPlatform} \cdot g \cdot p_z + m_{link} \cdot g \cdot (p_z + q_1) + m_{link} \cdot g \cdot (p_z + q_2) + m_{link} \cdot g \cdot (p_z + q_3) \\ + m_{carriage} \cdot g \cdot q_1 + m_{carriage} \cdot g \cdot q_2 + m_{carriage} \cdot g \cdot q_3$$

7.3.4 Lagrangian

The Lagrangian function is a state-function defined as

$$L = K - U$$

The value of this function deepens only on the state of the system at time t . Once the Lagrangian is known, all the system dynamic can be described using n scalar differential equations, where n is the number of state function of the system, in this case equal to 6.

and the Lagrange equations of the first type can be written as

$$\frac{d}{dt} \left(\frac{\partial L}{\partial \dot{\mathbf{q}}_i} \right) - \frac{\partial L}{\partial \mathbf{q}_i} = \sum_{i=1}^k \lambda_i \cdot \frac{\partial \Gamma_i}{\partial \mathbf{q}_j} + F_i$$

with j from 1 to 3. λ_i is the i -th multiplier while Γ_i is the i -th constraint equation.

7.3.5 Generalized Forces

To compute generalized forces, the effect of the weight forces, whose causes have been already included in the potential energy.

All the generalized forces are due to the action of actuators moving the joints and to the generalized interaction forces exchanged with the environment. They are the sum of all the effects associated with the virtual work of the i -th coordinate q_i . In the actuated prismatic joints, the total virtual work is the sum of the virtual works done by all linear forces

$$\delta W = \sum_{k=1}^{Nf} \mathbf{f}_k \cdot \delta \mathbf{r}_k$$

Where Nf is the number of point masses, each one located in space by a position vector r_i , on which act Nf forces f_i . δW is virtual displacement associated with the force f_i .

The system is in equilibrium state if $\delta W = 0$.

$\delta \mathbf{r}_k$ can be rewritten highlighting the contribution of the single generalized coordinates q_i on the total virtual displacement.

$$\delta W = \sum_{k=1}^{Nf} \mathbf{f}_k \cdot \left[\sum_n \frac{\partial \mathbf{r}_k}{\partial q_i} \cdot \delta q_i \right] = \sum_{k=1}^{Nf} \left[\sum_n \mathbf{f}_k \cdot \frac{\partial \mathbf{r}_k}{\partial q_i} \right] \cdot \delta q_i$$

Can be seen that the virtual work is now function on the variation of the single generalized coordinates.

That contribution along the single gen.coordinate is the force F_{li} or the linear generalized force that is the force that actuate the i -th joint.

$$F_{li} = \sum_n \mathbf{f}_k \cdot \frac{\partial \mathbf{r}_k}{\partial q_i}$$

The variation of the work can be rewritten

$$\delta W = \sum_{k=1}^{Nf} F_{li} \cdot \delta q_i$$

The external forces are produced by the three stepper only on the prismatic joints. For this reason only the generalized forces for the first three state variables are present.

$$F_i = \tau_i + \mathbf{J}_i^T \cdot \mathbf{F}_{TCP_{external}}$$

Where $\boldsymbol{\tau}$ is vector containing the force acting on each joint.

$$\boldsymbol{\tau} = \{F_{stepper1}, F_{stepper2}, F_{stepper3}, 0, 0, 0\}$$

Excluding the interaction of the TCP with the environment, no external generalized interaction force was considered. However, during the filament deposition, a force is surely exchanged between the tip of the extruder and the piece. Due to the unknown relation with the material and no idea on a possible value of that force, this force was not taken into account.

$$F_{TCP_{external}} = 0$$

7.3.6 Constraint equations

Thanks to the fact that our system has 3 DOF, it can be fully described by 3 generalized coordinates. The set of \mathbf{q}_i chosen is therefore formed by three dependent variable connected via some constraint equation to the independent ones.

$$\boldsymbol{\Gamma}(q_1, q_2, q_3, p_x, p_y, p_z, t) = 0$$

To sintetize the tractation

$$\boldsymbol{\Gamma}(\mathbf{q}_{independent}, \mathbf{q}_{dependent}, t) = 0$$

where Γ is the constrain function of those seven variables. According to the Hamilton's principle

$$\begin{aligned} \delta \int_{t_1}^{t_2} L dt &= \int_{t_2}^{t_1} \left\{ \sum_{i=1}^6 \left[\frac{d}{dt} \left(\frac{\partial L}{\partial \dot{\mathbf{q}}_i} \right) - \frac{\partial L}{\partial \mathbf{q}_i} \right] \cdot \delta \mathbf{q}_i \right\} \\ &= \int_{t_2}^{t_1} \left\{ \left[\frac{d}{dt} \left(\frac{\partial L}{\partial \dot{\mathbf{q}}_{ind}} \right) - \frac{\partial L}{\partial \mathbf{q}_{ind}} \right] \cdot \delta \mathbf{q}_{ind} \right\} + \left[\frac{d}{dt} \left(\frac{\partial L}{\partial \dot{\mathbf{q}}_{dep}} \right) - \frac{\partial L}{\partial \mathbf{q}_{dep}} \right] \cdot \delta \mathbf{q}_{dep} = 0 \end{aligned}$$

In any given instant there is a relation between the prismatic joints and the platform position and this relation is geometrically fixed. Varying one of the dependent or independent variables, the others will vary consequently.

$$\delta \boldsymbol{\Gamma} = \frac{\partial \boldsymbol{\Gamma}}{\partial \mathbf{q}_{dep}} \cdot \delta \mathbf{q}_{dep} + \frac{\partial \boldsymbol{\Gamma}}{\partial \mathbf{q}_{ind}} \cdot \delta \mathbf{q}_{ind} = 0$$

It possible then to substitute inside the dynamical equation of the first three independent generalized coordinates the contribution of the other three over the constrain function.

$$\int_{t_2}^{t_1} \left\{ \left[\frac{d}{dt} \left(\frac{\partial L}{\partial \dot{\mathbf{q}}_{ind}} \right) - \frac{\partial L}{\partial \mathbf{q}_{ind}} \right] \cdot \frac{\partial q_{ind}}{\partial f} - \left[\frac{d}{dt} \left(\frac{\partial L}{\partial \dot{\mathbf{q}}_{dep}} \right) - \frac{\partial L}{\partial \mathbf{q}_{dep}} \right] \cdot \frac{\partial q_{dep}}{\partial f} \right\} \cdot \delta q_{ind} \cdot dt = 0$$

This equation can be solved separating both sides that are the same function of time

$$\left[\frac{d}{dt} \left(\frac{\partial L}{\partial \dot{\mathbf{q}}_{ind}} \right) - \frac{\partial L}{\partial \mathbf{q}_{ind}} \right] \cdot \frac{\partial q_{ind}}{\partial f} = \left[\frac{d}{dt} \left(\frac{\partial L}{\partial \dot{\mathbf{q}}_{dep}} \right) - \frac{\partial L}{\partial \mathbf{q}_{dep}} \right] \cdot \frac{\partial q_{dep}}{\partial f}$$

$$\left[\frac{d}{dt} \left(\frac{\partial L}{\partial \dot{\mathbf{q}}_{ind}} \right) - \frac{\partial L}{\partial \mathbf{q}_{ind}} \right] = \frac{\partial f}{\partial q_{ind}} \left\{ \left[\frac{d}{dt} \left(\frac{\partial L}{\partial \dot{\mathbf{q}}_{dep}} \right) - \frac{\partial L}{\partial \mathbf{q}_{dep}} \right] \cdot \frac{\partial q_{dep}}{\partial f} \right\}$$

The second part of the equation, function of the dependent variable can be substitute with λ that is the Lagrangian multiplier

$$\left[\frac{d}{dt} \left(\frac{\partial L}{\partial \dot{\mathbf{q}}_{ind}} \right) - \frac{\partial L}{\partial \mathbf{q}_{ind}} \right] = \frac{\partial f}{\partial q_{ind}} \lambda$$

To link the carriage to the moving platform, the constraint equation chosen was the one along all the three chains that compose the printer. With the simple condition that the distance between two spherical joints that connect the carriage to the moving platform is equal to the link length it is possible to write

$$\Gamma_i = \overline{AB}^2 - link^2 = (q_i - pz)^2 + (p_x + h \cdot \cos(\phi_i) - \Delta \cdot \cos(\phi_i))^2 +$$

$$(p_y + h \cdot \sin(\phi_i) - \Delta \cdot \sin(\phi_i))^2 - link^2 = 0$$

for $i=1,2,3$.

$l_Z = (q_i - pz)$ is the projection of the link along the Z axis

$l_X = p_x + h \cdot \cos(\phi_i) - \Delta \cdot \cos(\phi_i)$ is the projection of the link along the X axis

$l_Y = p_y + h \cdot \sin(\phi_i) - \Delta \cdot \sin(\phi_i)$ is the projection of the link along the Y axis

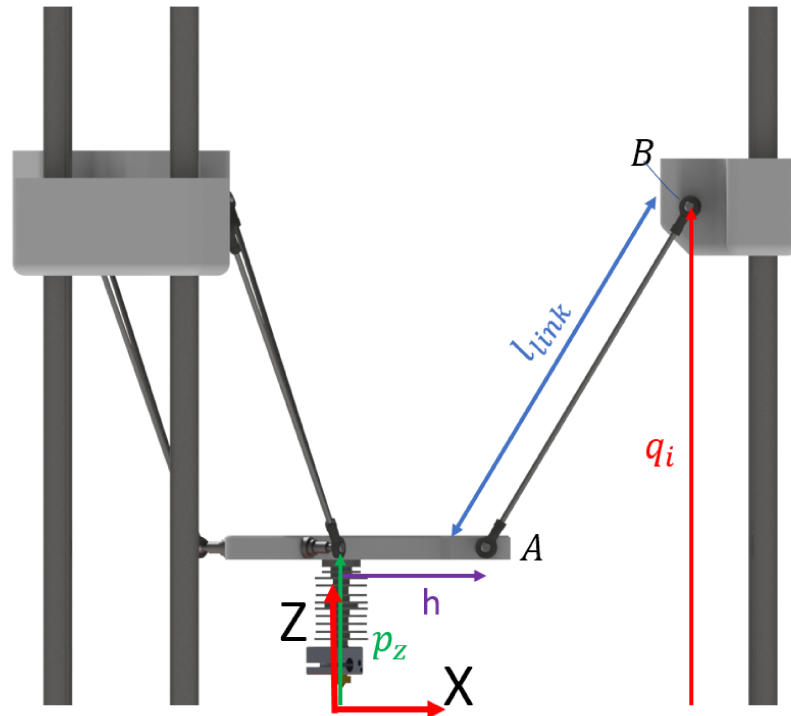


Figure 7.24

- Δ is the distance between the center of the printing plate (origin of the RF) and the circle that contains the three tower's centers.
- p_x, p_y, p_z are the position with respect to the origin of the inertial RF, placed in the center of the plate, of the moving platform center along X, Y and Z axis.
- l_{link} is the length of the link⁹.
- h is the offset between the center of the platform (where the extruder is located) and the minimum distance between the axis passing in the middle of the two pivot points of spherical joint, as already showed in fig 7.2
- ϕ is the angle between the tower pointed by X axis (named 1), and the other two, named anticlockwise 2 and 3 as showed in fig 7.23

The ϕ was used to generalize the three links equations. The three towers are placed along a circumference at 120° on XY plane. Because X points one of those (tower 1),

⁹the three links have the same length

$$\phi_1 = 0^\circ$$

While the other two tower are placed at

$$\phi_2 = 120^\circ$$

$$\phi_3 = 240^\circ$$

with respect to tower 1.

The Γ constrain equation links together all the six generalized coordinates.

The Lagrangian of the fist type was calculated for the last three generalized coordinates.

Lagrangian for the generalized coordinate p_x

$$\begin{aligned} \frac{d}{dt} \left(\frac{\partial L}{\partial \dot{p}_x} \right) - \frac{\partial L}{\partial p_x} &= \sum_{i=1}^3 \lambda_i \cdot \frac{\partial \Gamma_i}{\partial p_x} \\ \frac{d}{dt} \left(\frac{\partial L}{\partial \dot{p}_x} \right) &= m_{MovingPlatform} \cdot \ddot{p}_x + 3m_{link} \cdot \ddot{p}_x \\ \frac{\partial L}{\partial p_x} &= 0 \\ \frac{\partial \Gamma_i}{\partial p_x} &= 2p_x + 2h \cdot \cos(\phi_i) - 2\Delta \cdot \cos(\phi_i) \end{aligned}$$

Summing up all the contributes

$$\begin{aligned} (3m_{link} + m_{MovingPlatform}) \cdot \ddot{p}_x &= 2\lambda_1 \cdot (p_x + h \cdot \cos(\phi_1) - \Delta \cdot \cos(\phi_1)) \\ &+ 2\lambda_2 \cdot (p_x + h \cdot \cos(\phi_2) - \Delta \cdot \cos(\phi_2)) + 2\lambda_3 \cdot (p_x + h \cdot \cos(\phi_3) - \Delta \cdot \cos(\phi_3)) \end{aligned}$$

Lagrangian for the generalized coordinate p_y

$$\begin{aligned} \frac{d}{dt} \left(\frac{\partial L}{\partial \dot{p}_y} \right) - \frac{\partial L}{\partial p_y} &= \sum_{i=1}^3 \lambda_i \cdot \frac{\partial \Gamma_i}{\partial p_y} \\ \frac{d}{dt} \left(\frac{\partial L}{\partial \dot{p}_y} \right) &= m_{MovingPlatform} \cdot \ddot{p}_y + 3m_{link} \cdot \ddot{p}_y \end{aligned}$$

$$\frac{\partial L}{\partial p_y} = 0$$

$$\frac{\partial \Gamma_i}{\partial p_y} = 2p_y + 2h \cdot \sin(\phi_i) - 2\Delta \cdot \sin(\phi_i)$$

Summing up all the contributes

$$\begin{aligned} (3m_{link} + m_{MovingPlatform}) \cdot \ddot{p}_y &= 2\lambda_1 \cdot (p_y + h \cdot \sin(\phi_1) - \Delta \cdot \sin(\phi_1)) \\ &+ 2\lambda_2 \cdot (p_y + h \cdot \sin(\phi_2) - \Delta \cdot \sin(\phi_2)) + 2\lambda_3 \cdot (p_y + h \cdot \sin(\phi_3) - \Delta \cdot \sin(\phi_3)) \end{aligned}$$

Lagrangian for the generalized coordinate p_z

$$\frac{d}{dt} \left(\frac{\partial L}{\partial \dot{p}_z} \right) - \frac{\partial L}{\partial p_z} = \sum_{i=1}^3 \lambda_i \cdot \frac{\partial \Gamma_i}{\partial p_z}$$

$$\frac{d}{dt} \left(\frac{\partial L}{\partial \dot{p}_z} \right) = m_{MovingPlatform} \cdot \ddot{p}_z + 3m_{link} \cdot \ddot{p}_z$$

$$\frac{\partial L}{\partial p_z} = g \cdot (m_{MovingPlatform} + 3m_{link})$$

$$\frac{\partial \Gamma_i}{\partial p_z} = 2p_z - 2q_i$$

Summing up all the contributes

$$\begin{aligned} (3m_{link} + m_{MovingPlatform}) \cdot \ddot{p}_z + (3m_{link} + m_{MovingPlatform}) \cdot g &= 2\lambda_1 \cdot (p_z - q_1) \\ &+ 2\lambda_2 \cdot (p_z - q_2) + 2\lambda_3 \cdot (p_z - q_3) \end{aligned}$$

Those equations were solved as function of $\lambda_1, \lambda_2, \lambda_3$ to be substitute inside the main dynamical equations in variables q_1, q_2, q_3 .

7.3.7 Dynamic equations of the 3D printer

The three dynamic equations are then computed for q_1, q_2, q_3 and the partial derivative of the constrain function with respect to the i -th variable was calculated.

$$F_1 = \ddot{q}_1 \cdot (m_{link} + m_{carriage}) + g \cdot (m_{link} + m_{carriage}) - 2\lambda_1 \cdot (q_1 - p_z)$$

$$F_2 = \ddot{q}_2 \cdot (m_{link} + m_{carriage}) + g \cdot (m_{link} + m_{carriage}) - 2\lambda_2 \cdot (q_2 - p_z)$$

$$F_3 = \ddot{q}_3 \cdot (m_{link} + m_{carriage}) + g \cdot (m_{link} + m_{carriage}) - 2\lambda_3 \cdot (q_3 - p_z)$$

7.4 Comparison between Matlab and dynamic equations

To understand where the two models differs, different paths, with different combinations of velocities and accelerations, were used as input of the trajectory planner block.

The maximum velocity was constrained to $200 \frac{mm}{s}$, while acceleration up to $15 \frac{m}{s^2}$ were considered for the moving platform.

Even if the a constant velocity was set, it is possible to see on the force plot the effect of the acceleration from steady-state condition.

Here are reported some examples

7.4.1 straight line on X-Y plane

velocity= $60 \frac{mm}{s}$

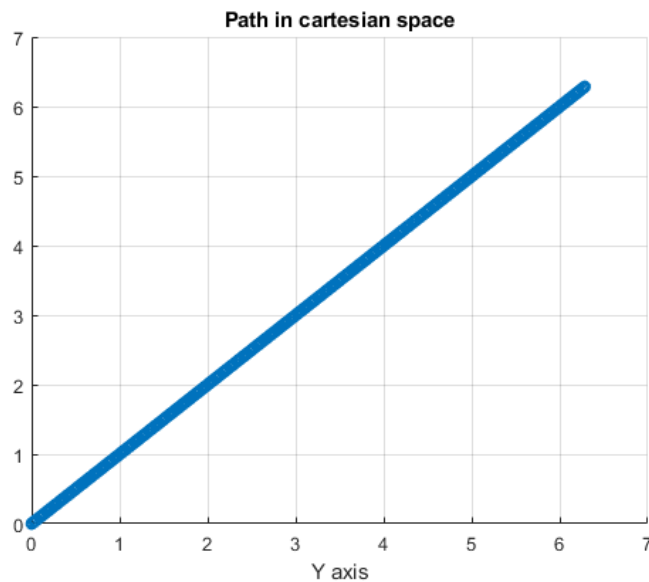


Figure 7.25: Path on X-Y plane

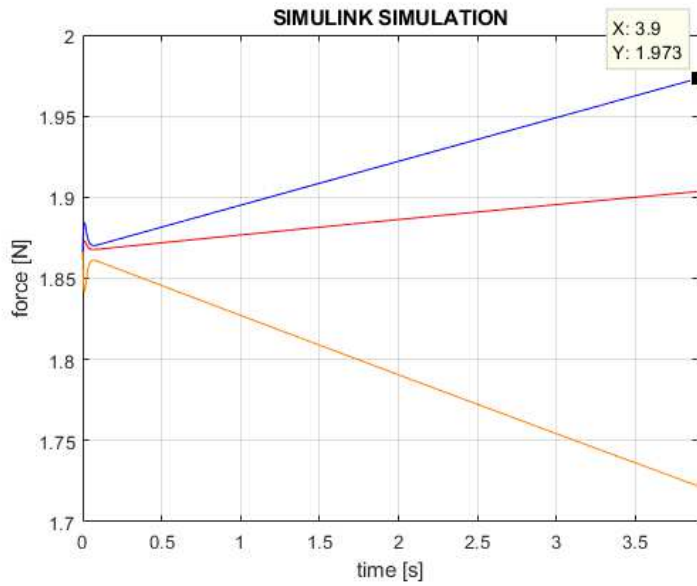


Figure 7.26: Simulink model, force evaluation

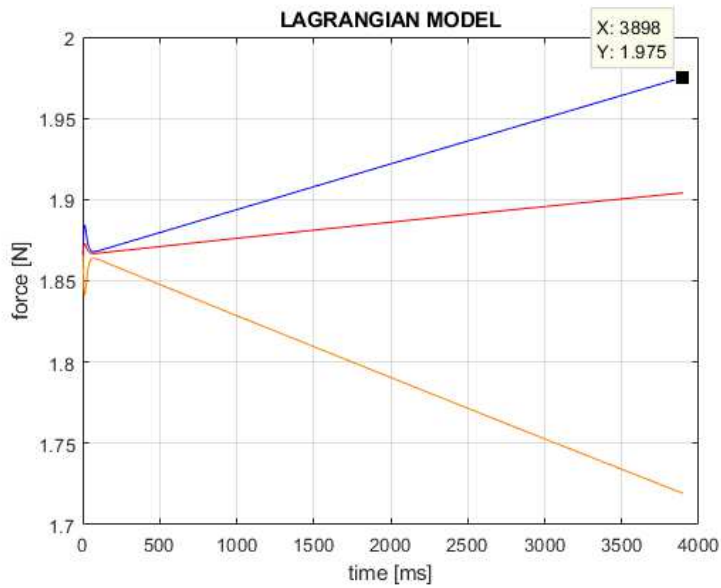


Figure 7.27: Lagrange model, force evaluation

7.4.2 Circular path X-Y plane

velocity= $40 \frac{mm}{s}$

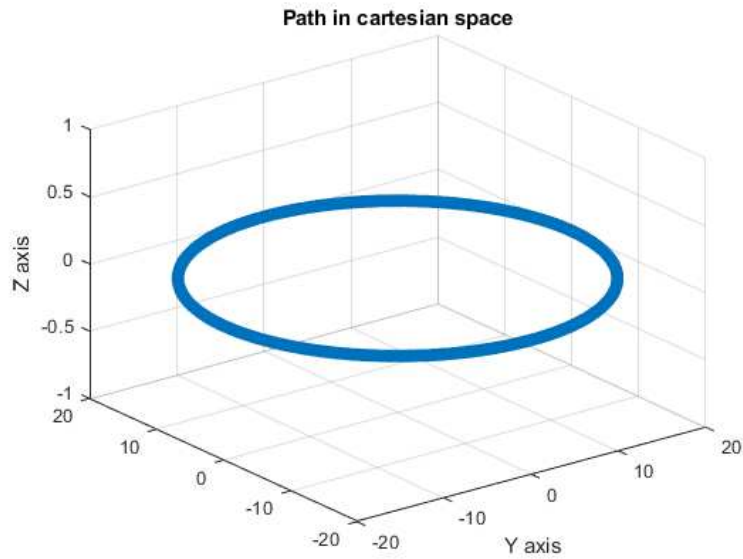


Figure 7.28: Path on X-Y plane

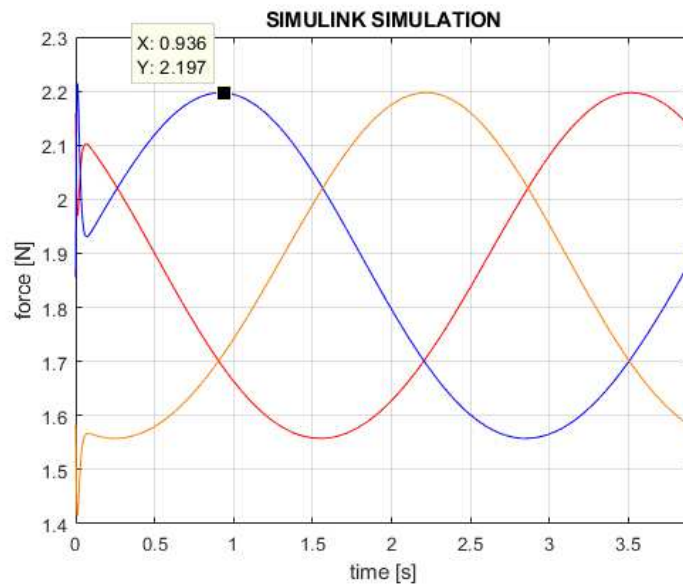


Figure 7.29: Simulink model, force evaluation

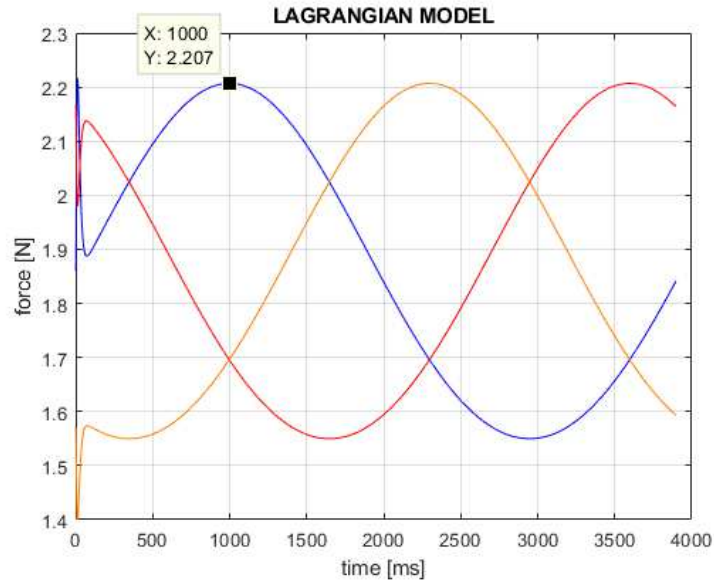


Figure 7.30: Lagrange model, force evaluation

7.4.3 Acceleration on Z axis

$$\text{acceleration} = 2.4 \frac{m}{s^2}$$

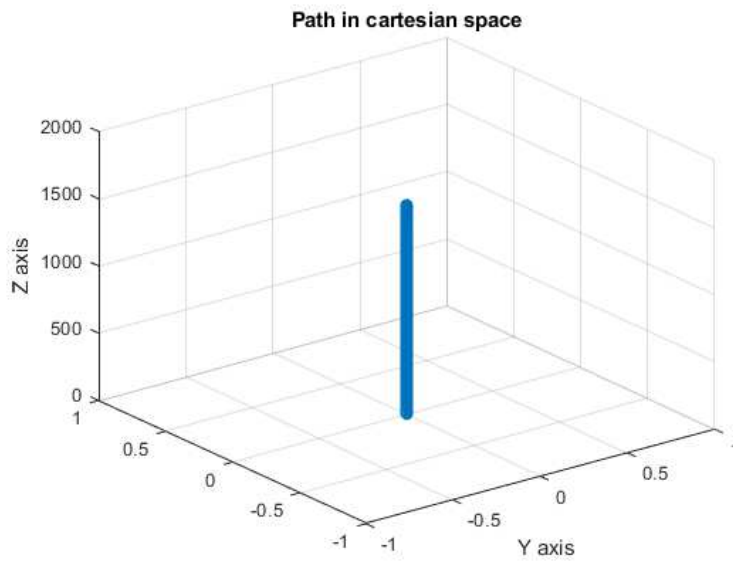


Figure 7.31: Path on X-Y plane

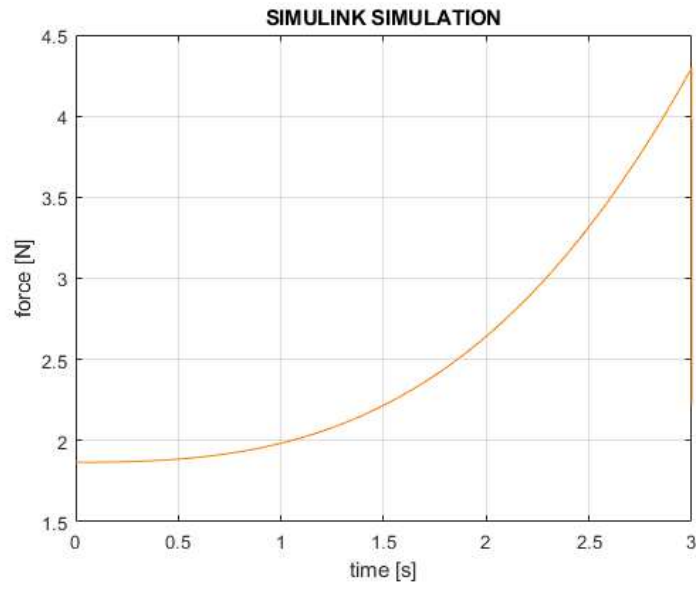


Figure 7.32: Simulink model, force evaluation

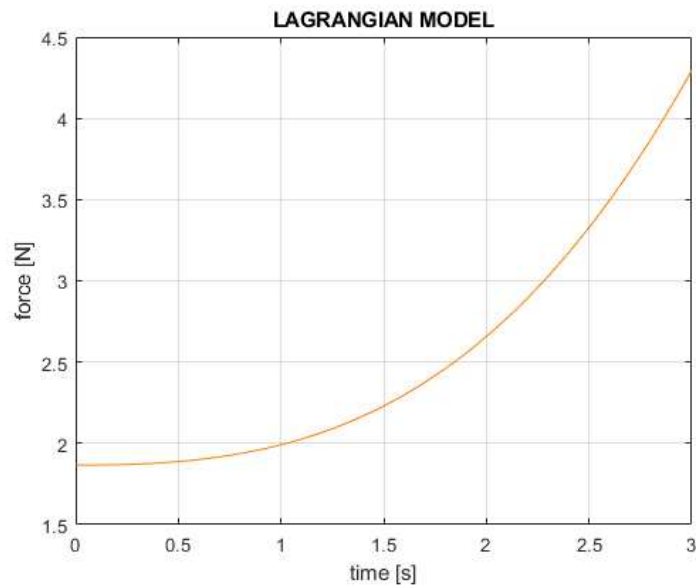


Figure 7.33: Lagrange model, force evaluation

7.4.4 Lissajous curve on X-Y plane

velocity = $200 \frac{mm}{s}$

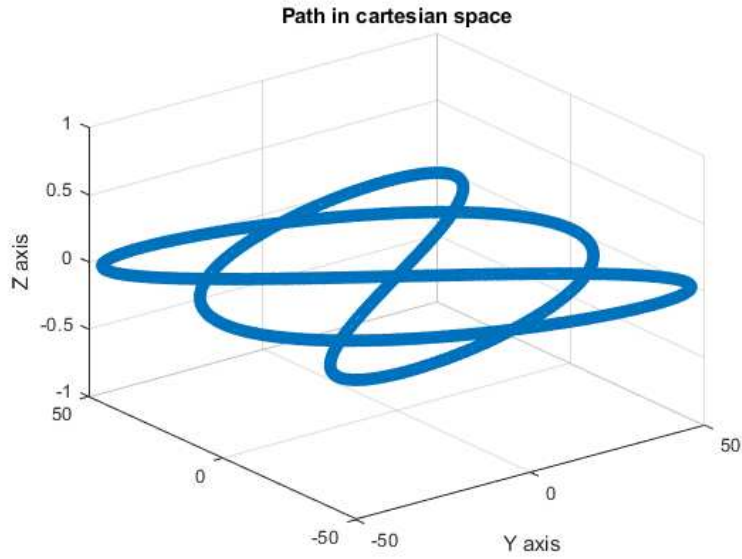


Figure 7.34: Path on X-Y plane

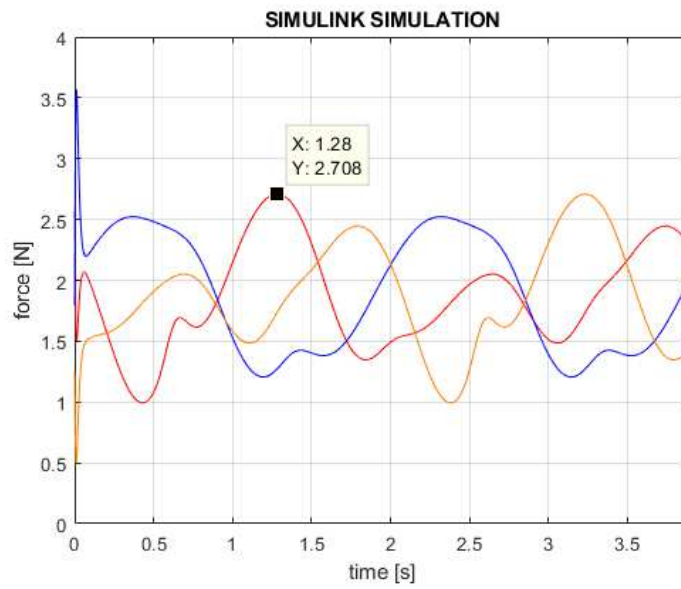


Figure 7.35: Simulink model, force evaluation

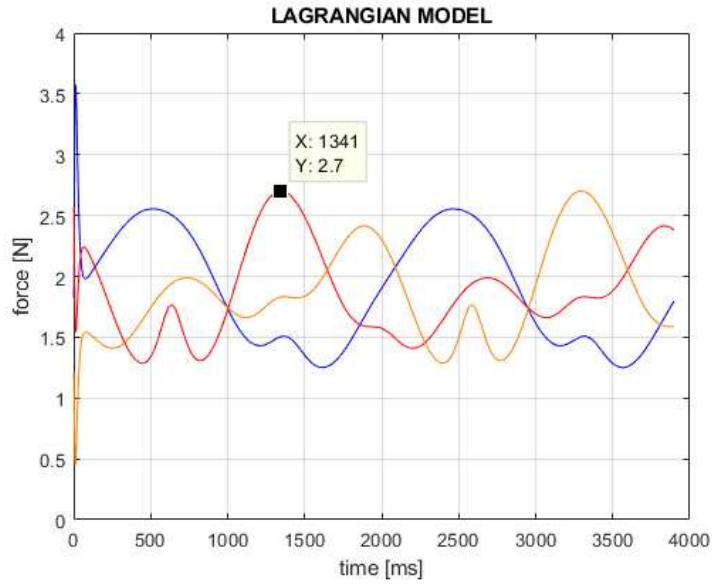


Figure 7.36: Lagrange model, force evaluation

7.4.5 Random curve on X-Y plane

velocity = $33 \frac{mm}{s}$

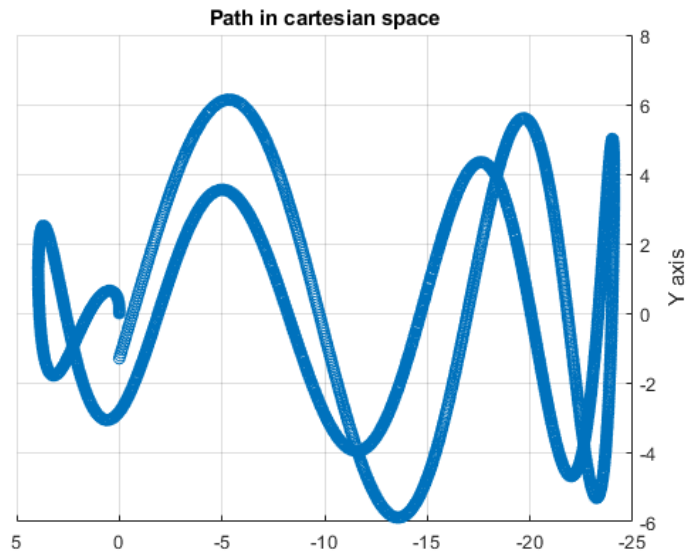


Figure 7.37: Path on X-Y plane

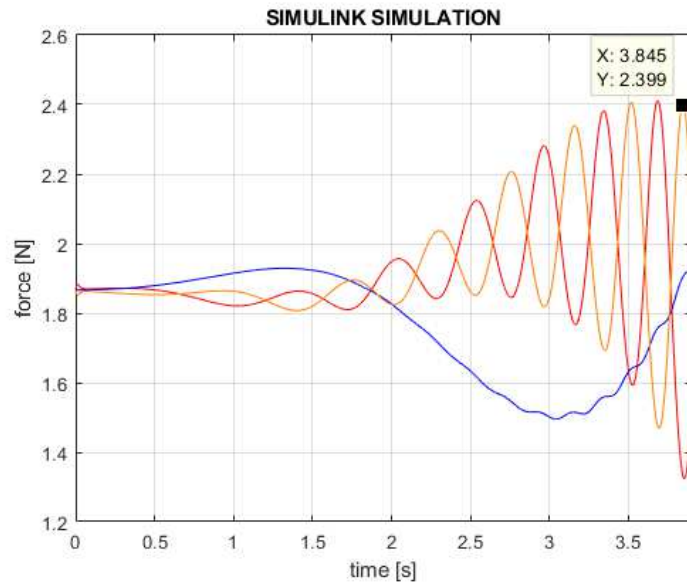


Figure 7.38: Simulink model, force evaluation

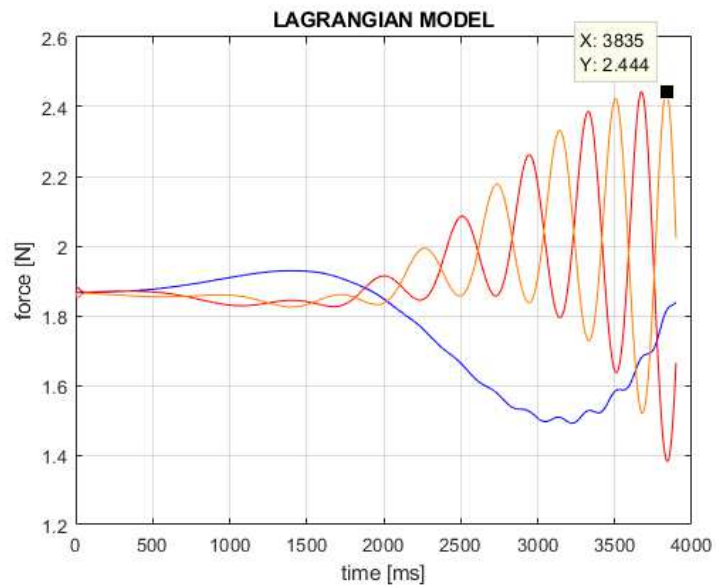


Figure 7.39: Lagrange model, force evaluation

7.4.6 Circular curve on the edge of workspace

velocity=113 $\frac{mm}{s}$

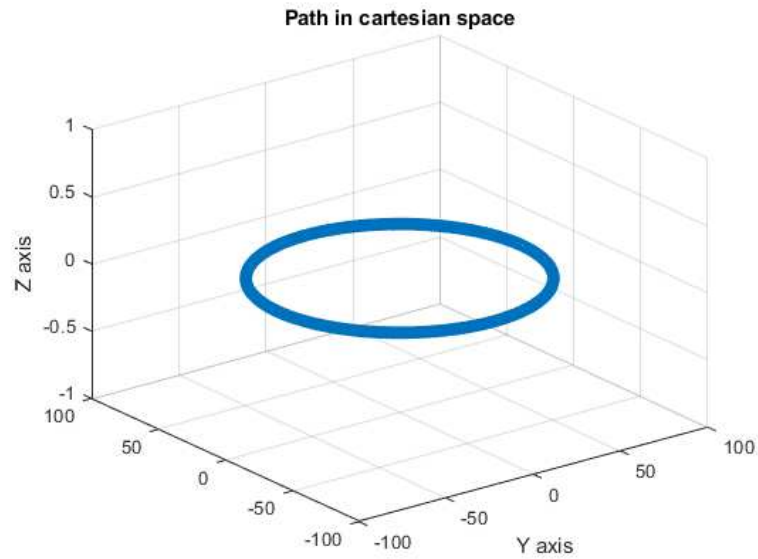


Figure 7.40: Path on X-Y plane

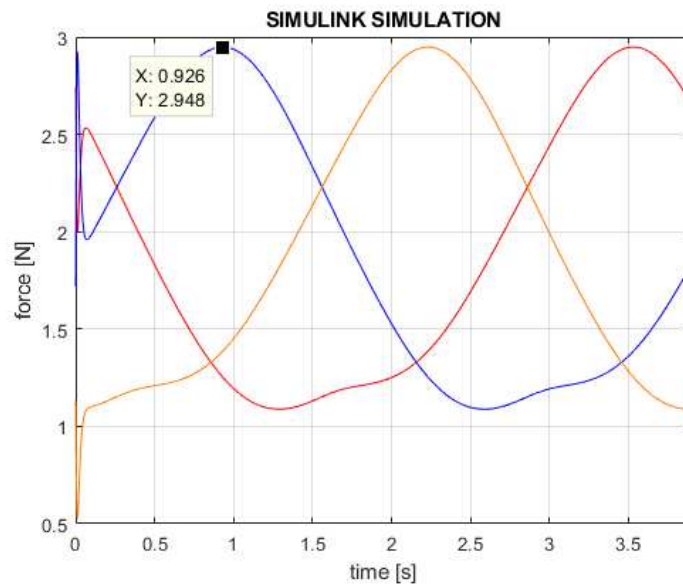


Figure 7.41: Simulink model, force evaluation

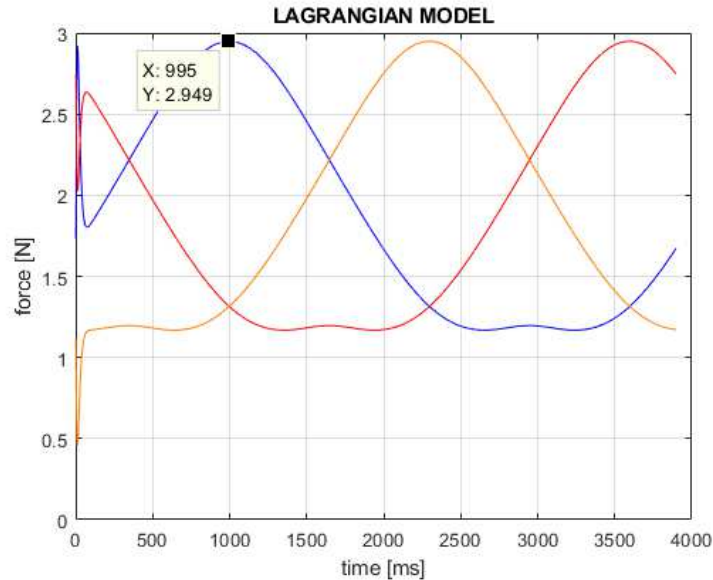


Figure 7.42: Lagrange model, force evaluation

7.4.7 Evaluation of the data obtained

The bigger difference that was found is when the carriage reach an height similar to the one of the moving platform. This difference is prevalently in the trend of the forces. That seems to have a displacement needle of some degrees. This effect can be clearly seen in the lower trend force of chapt. 7.4.6

Some difference in the total force values are due to decimal approximation of weights, lengths and gravity force, errors that tend to be higher increasing the accelerations on the moving platform.

The approximation done by not considering the inertia of the links doesn't have a big impact due to low rotation velocities of the links when printing on the same plane, things that usually happens during normal operational conditions.

As can be seen in a comparison between the two models outputs that Lagrangian one is shifted by 10 ms. This happens because the first point was not considered and the time step between two consecutive points is of 10ms. This because the first point has no velocity or acceleration correlated with it.

Chapter 8

Motor

The class of motor that best suit an application as a 3D printer are the stepper motors.

This because they can move of small controlled angles (down to 0.9°) in open-loop, so without any feedback circuit making the motor simpler and less costly to control. The accuracy of 3 – 5% of a step and this error is non cumulative from one step to the one that follows. Due to the required high accuracy in position, gearboxes are excluded due to backlash errors, that are for multi-stage gearbox order of magnitude bigger than the required accuracy. For this reason those motors are usually direct connected to the load or belts are used.

Nowadays the most used type of stepper motors are the hybrid synchronous: they combines the features of the variable reluctance and permanent magnet motors with the highest linearity.

MOTOR	COST	STEP ANGLE	LINEARITY	DETENTION TORQUE	NOTES
Variable reluctance	Intermediate	Any	Very Low	0	-Noisy -Good torque/inertia ratio
Permanent magnet	Low	$\geq 7.5^\circ$	Low	Very High	-Only for low power applications
Hybrid	Intermediate	Typ. 1.8°	High	In between	-High efficiency -Accurate
Can-Stack	Very Low	$\geq 7.5^\circ$	Low	High	-Best solution for general purpose applications

Figure 8.1: Stepper motor comparison

Torque is a critical consideration when choosing a stepping motor. Steppers have different types of rated torque:

- Holding torque
The maximum static torque that can be applied to the shaft of an excited motor without causing a continuous motion
- Detent torque
The maximum static torque that can be applied to the shaft of an unexcited motor without causing a continuous motion. The detent torque appears only in motor having a permanent magnet.
- Pull-in torque
The maximum torque at which an energized step motor will start and run in synchronism, without losing steps, at constant speed. The pull-in torque depends on the driving circuit and the measuring methods.
- Pull-out torque
It is the maximum total available torque when the motor runs at constant speed at a given frequency and that not cause it to lose step. In data-sheets, the pull-in and pull-out torque are given, as functions of stepping rate, for different types of motor and driver combinations.

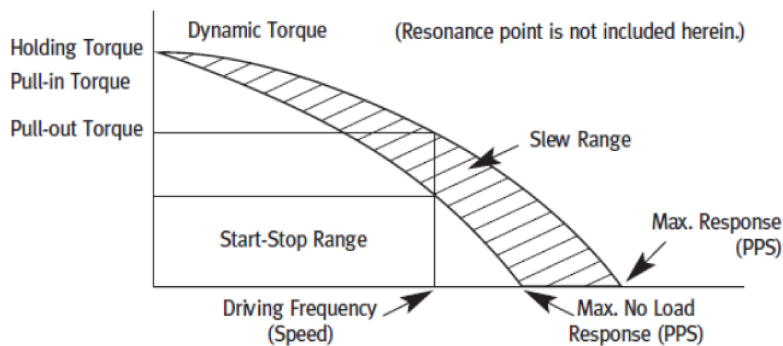


Figure 8.2: Torque-speed characteristic of a stepper motor

The slewing range is the area in between the pull-in and the pull-out torque curves, where the motor can run without losing steps. ¹

Start-stop range is the where the stepper motor can start, stop and reverse the motion without losing steps.

¹Motor must be brought up to the slew range with acceleration and deceleration technique known as ramping

As can be seen, also for this type of motor, the torque falls rapidly as the stepping rate is raised.

8.1 Force and acceleration required

To size the motor for an acceleration of the extruder up to $15000 \frac{mm}{s^2}$, it was important to understand where this acceleration weighed more on the motors.

It is natural to think that the less the number of motors that have to generate that force to the higher will be the stress on a single motor. For this reason the best case is when this acceleration is purely on the Z axis because it is shared between all the three motor, and this force is maximum when the motion that cause the extruder to move is generate by a single motor. On a delta printer, while moving on a single XY plane it is impossible to have the extruder motion purely produced by a single motor but on the plane there are some area where only one of the carriages greatly contribute to the end-effector movements.

It was also considered the effect of the link, that as a gearbox, multiplies the speed of the carriage at the cost of the force used.

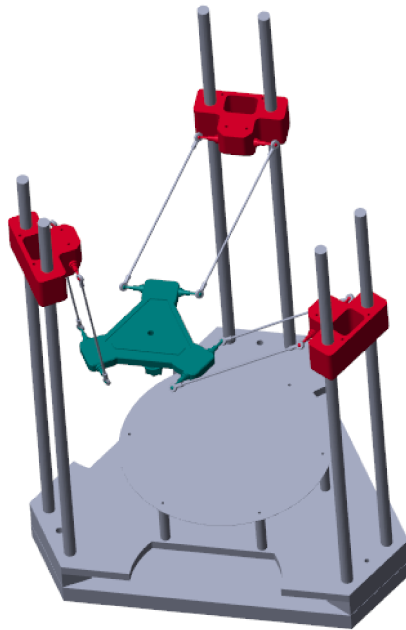


Figure 8.3: Matlab explorer viewer of the model implemented in the case 1

The maximum "gear" ratio between the carriage and the end effector is when the

latter is placed under the carriage. In this condition, however, the carriages facing, will mostly share the load coming from this high acceleration.

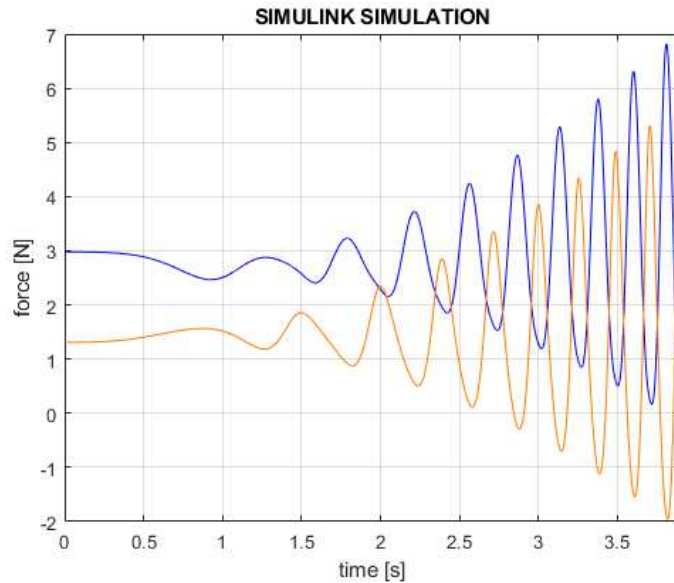


Figure 8.4: Force share when the acceleration is reached near a tower

Can be seen that the load on the carriage on top and at the bottom right is the same (showed in orange in fig 9.2 and 9.4) when the acceleration is performed on the X axis², perpendicular to the tower on the left (marked in blue in fig 9.2 and 9.4). This graph was done while the acceleration increase and the motion is reversed.

The case when the force acting on a single carriage is the maximum is when the end effector is near to the facing towers.

²Refers to the figure 7.8

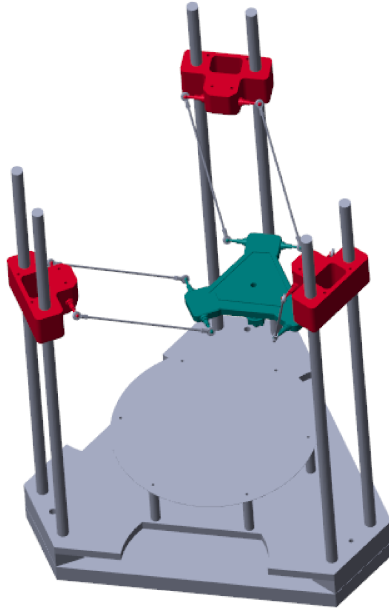


Figure 8.5: Matlab explorer viewer of the model implemented in the case 2

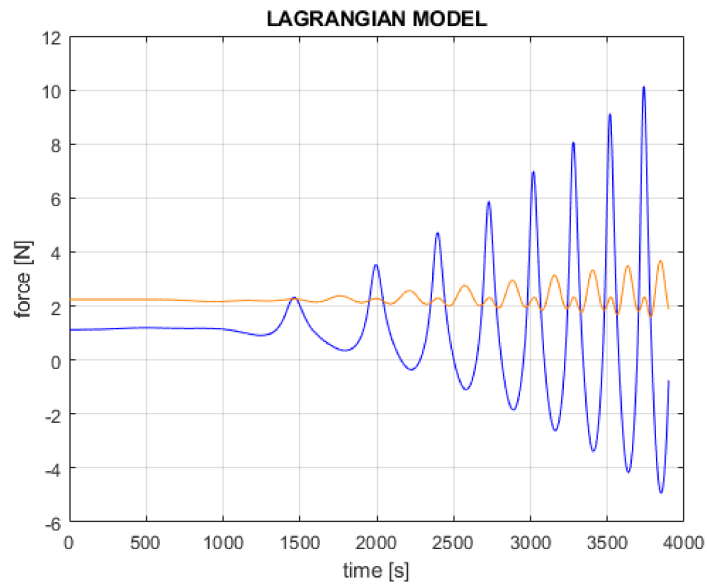


Figure 8.6: Force share when the acceleration is reached far from a tower

With a required acceleration of $15000 \frac{mm}{s^2}$, the maximum force required is 10.1 N and a carriage acceleration of $11020 \frac{mm}{s^2}$.

As a confirm, if the motion is on the Y axis³, the total force is shared between the carriages.

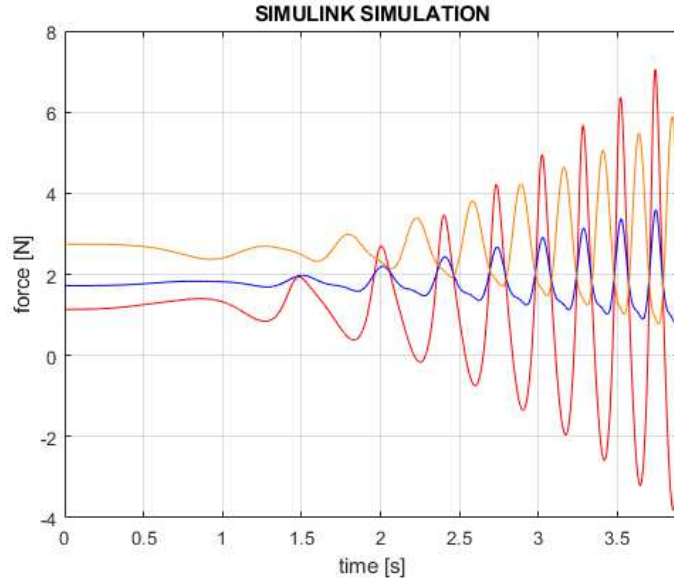


Figure 8.7: Motion on axis Y

In the maximum force instant, there is simultaneously one of the highest carriage acceleration⁴ because the moving platform is far away from the tower.

Motor torque estimation using belt and timing pulley

$$T = I_{motor} \cdot \alpha + F_{pulley} \cdot r$$

$$\alpha \cdot r = \ddot{q}_i$$

$$r = N_{TeethNumber} \cdot Pitch \cdot \frac{1}{2\pi}$$

Another specification is the printer speed. Taking into account the velocity coefficient⁵, in the worst case the carriage has to move 2.5 times faster than the end-effector.

³Refers to the figure 7.8

⁴At a given acceleration of the moving platform

⁵Chapter 5.0.2

$$w_{max} = \frac{v_{coefficient} \cdot v_{max}}{N_{TeethNumber} \cdot Pitch \cdot \frac{1}{2\pi}}$$

$$T_{max} = I_{motor} \cdot \ddot{q}_i + F_{pulley} \cdot r$$

From the specifications

$$\begin{aligned}v_{max} &= 120 \frac{mm}{s} \\v_{coefficient} &= 2.5 \\F_{pulley} &= 10.1N \\\ddot{q}_i &= 11 \frac{m}{s^2}\end{aligned}$$

8.1.1 Friction consideration

The matlab model was used to have a clearer idea about the effects of the friction on the bearings. Using a viscous friction coefficient ⁶ of

$$\beta_{linearBearing} = 0.02$$

$$\beta_{SphericalBearing} = 0.02$$

and using a maximum speed of $120 \frac{mm}{s}$, a circular path of the biggest diameter was chosen in order to have the maximum joints velocities.

The results showed that the model with friction and the one without differs by no more than 0.5 N.

⁶web.mit.edu/2.75/fundamentals/FUNdaMENTALs%20Book%20pdf/FUNdaMENTALs%20Topic%2010.PDF

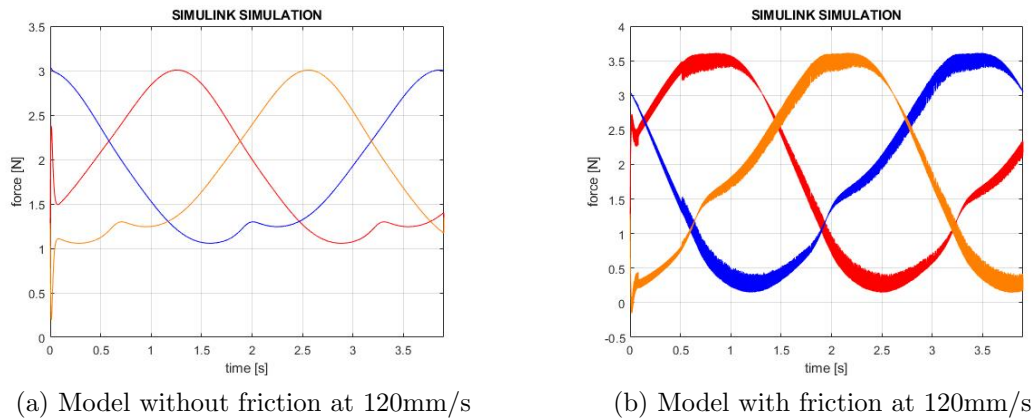


Figure 8.8: Friction effects on carriage's force.

8.1.2 Timing pulley

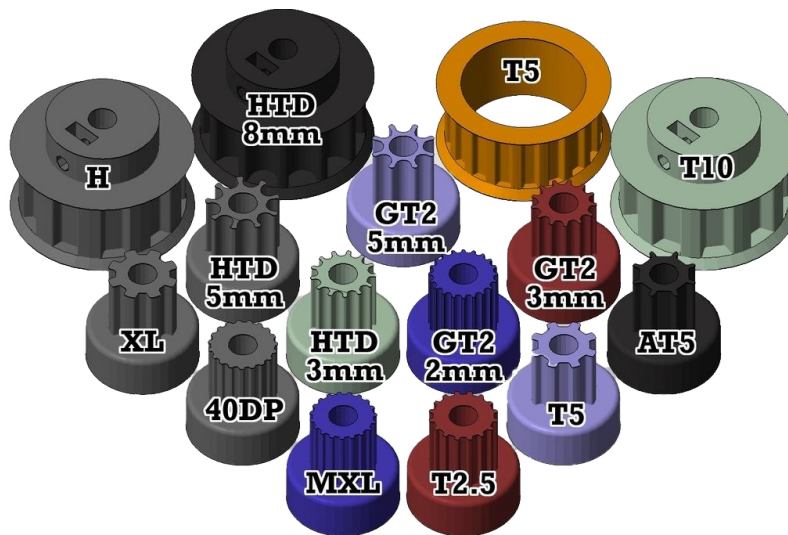


Figure 8.9: Standard timing pulleys

The timing pulley is a component as important as the motor. In general, but in particular for 3D printers, the Contitech Synchroflex ⁷ tooth profile is recommended by RepRap ⁸ for its high power transmission capability. For this reason HTD, H and TXX profiles have been excluded from this analysis.

⁷<https://www.contitech.de/en-GL/Solutions/Power-Transmission/Mechanical-engineering/Drive-Belts/Timing-belts/Products/Product-range/CONTI-SYNCHROFLEX-GEN3>

⁸<https://reprap.org/wiki/Belt>

S2M and S3M profiles have been excluded because they belong to Japanese standard and are quite costly in Europe.

On the internet there are harsh discussion about the T series and in particular the T2.5 and T5 timing belts that some believe may cause backlash ⁹.

The most common are the GTx series of pulleys, where the x symbolize the pitch in mm.

Due to the high number of degree of freedom between motors and pulley, only GT2 series will be taken into account.

Tooth Profile Availability

# TEETH	12	14	15	16	18	20	21	22	24	28	30	32	36	40	48	56	60	72	80	90	120	
2MR	X	X	X	X	X	X	X	X	X	X	X	X	X	X	X	X	X	X	X	X	X	X
3MR				X	X	X	X	X	X	X	X	X	X	X	X	X	X	X	X	X	X	X
5MR					X	X	X	X	X	X	X	X	X	X	X	X	X	X	X	X	X	X

Figure 8.10: GT2 and GT3 pulley

This series spaces from 12 up to 120 teeth as reported into the table fig. 8.10 ¹⁰.

Pulleys will be taken into account considering them as solid cylinder of aluminium. For the different pulley, will be choose a mean height of the pulley of 10 mm so that the inertia will be a function of the radius.

$$I_{pulley} = \frac{1}{2} \cdot m \cdot r^2 = \frac{1}{2} \cdot \pi \cdot r^4 \cdot height \cdot \rho$$

$$\rho_{aluminium} = 2.70 \cdot 10^3 \left[\frac{Kg}{m^3} \right]$$

$$I_{total} = I_{motor} + I_{pulley}$$

8.1.3 Stepper motors size

Stepper motors are essentially divided by size. The National Electrical Manufacturers Association, an US standardization institute, classify them by dimension of the faceplate. A NEMA 14 motor has an overall dimension of 1.4 x 1.4 inch (35.6 x 35.6 mm). Its size is only a coarse indication of its power.

⁹<https://reprap.org/forum/read.php?4,128202,128243#msg-128243>

¹⁰<https://www.torquetrans.com/gt2-pulleys>

The most used motors are stepper NEMA 17 in hobbyists - low - mid-end market.

The Nema 17 size has a

Holding torque = 22 to 65 [N · cm]

Rotor inertia = 34 to 102 [g · cm²]

To consider the two extreme case of highest

$$T_{max} = (I_{motor_{max}} + I_{pulley}) \cdot \frac{\ddot{q}_i}{r} + F_{pulley} \cdot r$$

$$T_{min} = (I_{motor_{min}} + I_{pulley}) \cdot \frac{\ddot{q}_i}{r} + F_{pulley} \cdot r$$

Using a pitch of 2.5 mm and changing the radius of the pulley, the sequent graph was obtained.

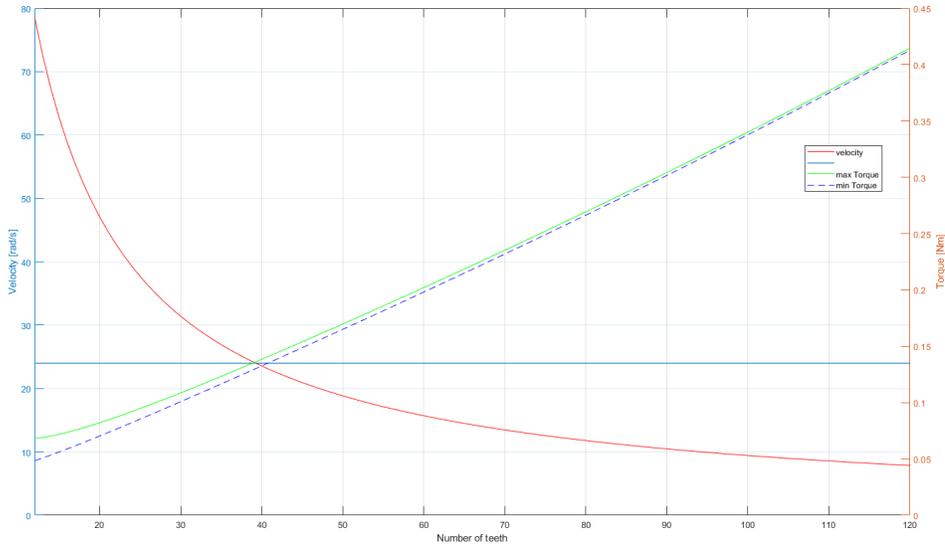


Figure 8.11: Torque and velocity varying the number of teeth

The intersection of torque and velocity curves is obtained with 40 teeth pulley. In this case the maximum torque required (without considering friction forces) is about 0.15Nm and when the printer is running at 120 $\frac{mm}{s}$ the motor would spin at 24 $\frac{rad}{s}$.

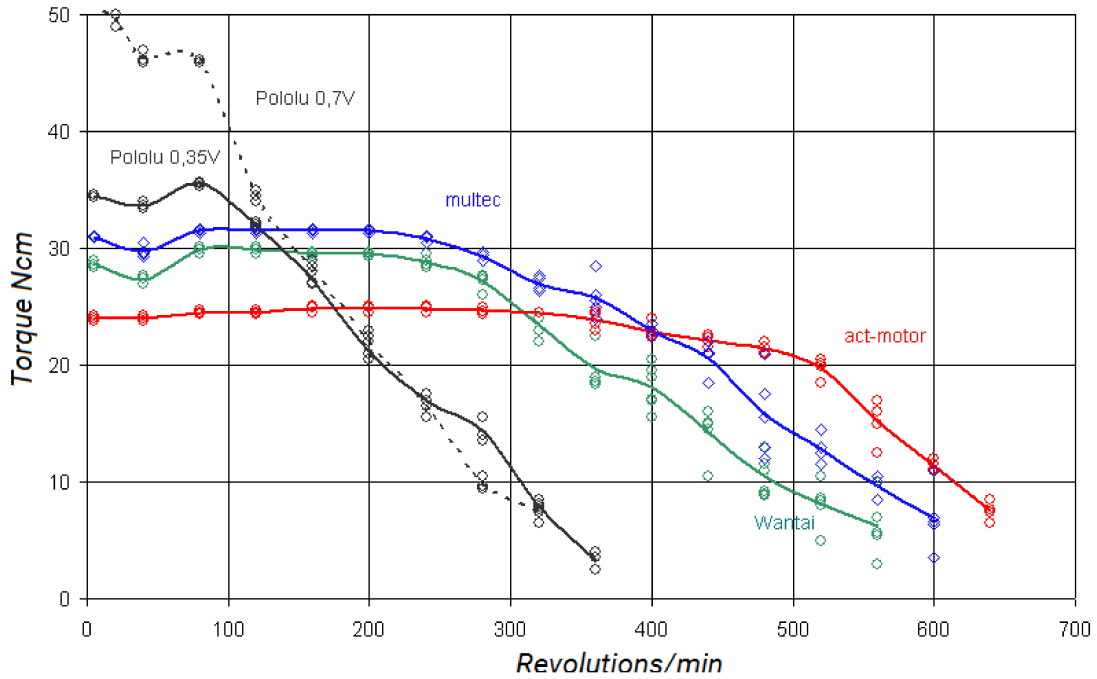


Figure 8.12: Motors-drivers characteristic

$24 \frac{rad}{s} \simeq 230 \frac{rev}{min}$. This is the maximum speed at whom the machine will work. Using a multec, Wantai or Act-motor¹¹ like a 42BYGHW609 (step of 1.8° , holding torque of $4.0 \frac{Kg}{cm}$) would guarantee a constant torque in all the speed range.

¹¹https://reprap.org/wiki/Stepper_torque

Table of contents

Bibliography

- [8.1] J. Alcisto, A. Enriquez, H. Garcia, S. Hinkson, T. Steelman, E. Silverman, P. Valdovino, H. Gigerenzer, J. Foyos, J. Ogren, J. Dorey, K. Karg, T. McDonald, and O.S. Es-Said, JMEP, 2011, 20(2), *Tensile Properties and Microstructures of Laser-Formed Ti-6Al-4V*, p 203212

- [8.2] Yong Huang, Ming C. Leu, Jyoti Mazumder, Alkan Donmez in “Additive Manufacturing: Current State, Future Potential, Gaps and Needs, and Recommendations”, *Strumenti Moderni*, Gaithersburg, MD 20899.

- [8.3] J.P. Merlet in “Parallel Robots”, INRIA, Sophia-Antipolis, France, Springer.

- [8.4] Bruno Siciliano, Oussama Khatib in “Handbook of Robotics”, Springer.

- [8.5] Sbastien Briot and Wisama Khalil in “Dynamics of Parallel Robots from Rigid Bodies to Flexible Elements”, 2015, Springer, France